School of Civil and Mechanical Engineering

Tribology Study on Elastomers

Ferial Hakami

This thesis is presented for the Degree of
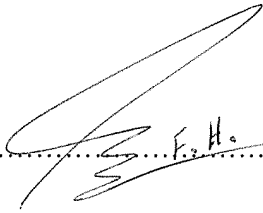**Doctor of Philosophy**
of
Curtin University

December 2018

Declaration

To the best of my knowledge and belief, this thesis contains no material previously published by any other person except where due acknowledgment has been made.

This thesis contains no material, which has been accepted for the award of any other degree or diploma in any university.

Signature: ....

Date: 14.12.2018

Acknowledgment

Abstract

This study aims to understand the tribological behaviour of elastomers by investigating effect of operating variables such as applied load and abrasive particle size and the elastomers' mechanical properties such as tensile strength, elongation at break, hardness, and tear strength by the experimental and analytical methods.

A DIN abrasion test machine (ISO 4649 standard) is used to perform the wear test and the friction test is conducted by a modified test machine, when the specimens including Natural rubbers (NRs), Styrene butadiene rubber (SBR), and Nitrile butadiene rubber (NBR) slide over abrasive paper with different sizes under variation of normal load. The worn surface and the generated wear debris are investigated by scanning electron microscope.

It has been observed that with increase of applied load and abrasive particle size, wear rate increases. The variation of wear mechanism while these parameters change depends on the elastomers' mechanical properties. The wear mechanism is mostly friction wear, which is mixed with fatigue wear abrading under higher applied loads or larger abrasives. Nevertheless, the wear mechanism of NBR and SBR, transfers from friction to abrasive wear. The formed ridges' space and wear debris' size also increase with increase of these factors.

Friction shows different trend compare to the wear with variation of operating variables. It decreases or increases with increase of normal load and abrasive particle size, which is affected by the contribution of adhesive friction and hysteresis to friction.

Comparison is drawn between wear rate and friction of different elastomers as measured experimentally under a range of test conditions. The tensile strength and elongation at break play a significant role when abrading under lower loads and fine abrasive, whereas hardness and tear strength are more pronounced at higher loads and coarser abrasives.

The second part of this study investigates the wear of the elastomers analytically, using the statistical methods. It is observed among the applied load, abrasive particle

size, and mechanical properties as input parameters, the abrasive particle size has the highest impact on the wear process, followed by the applied load.

Finally, by quantifying the contribution of operating variables and mechanical properties, a non-linear wear equation is developed to predict the wear rate.

Publication arising from this study

- Journal Papers:

1. **F. Hakami**, A. Pramanik, N. Ridgway, A. K. Basak, "Developments of rubber material wear in conveyor belt system", Tribology International, 111, 2017, 148-158.

2. **F. Hakami**, A. Pramanik, N. Islam, A. K. Basak, N. Ridgway, "Study of effective parameters on wear behaviour of rubbers based on statistical methods", Polymers for advanced technologies, 30, 2019, 1415-1426.

3. **F. Hakami**, A. Pramanik, A. K. Basak, N. Ridgway, "Elastomers' wear: Comparison of theory with experiment", Tribology International, 135, 2019, 46-54.

4. **F. Hakami**, A. Pramanik, A. K. Basak, N. Ridgway, N. Islam, "Effect of abrasive particle size on tribological behavior of elastomers", Part J: Journal of Engineering Tribology, (Under review, 2018).

- Conference paper:

F. Hakami, A. Pramanik, A. K. Basak, N. Ridgway, "Effect of abrasive particle size on tribological behavior of rubbers", The 18th Nordic Symposium on Tribology – NORDTRIB 2018, 18-21 June 2018, Uppsala University, Uppsala, Sweden.

Awards

- Curtin International Postgraduate Research Scholarship (CIPRS) 2015
- Thesis Completion scholarship, 2018

Nomenclature

α	Counter face roughness
ANOVA	Analysis of variance
BR	Butadiene rubber
COF	Coefficient of friction
CNC	Computer numerical control
CR	Chloroprene
C_p	Specific heat
d	Abrasive particle size
DOE	Design of experiment
DV	Dimensionless variable
ε	Elongation at break
EDS	Energy-dispersive X-ray spectroscopy
EPDM	Ethylene Propylene Diene Monomer
φ	Mass of abrading particles
F	Applied force/load
F_k	Friction force
γ	Surface energy
H	Hardness
HNBR	Hydrogenated acrylonitrile-butadiene rubber
k	Thermal conductivity
K	Wear coefficient

Ω	Contribution of material properties
NBR	Acrylonitrile butadiene rubber
NR	Natural rubber
ρ	Density
PA	Polyamide
PAEK	Poly aryl ether ketone
PE	Polyethylene
PEEK	Polyether ether ketone
Pt	Platinum
PTFE	Polytetrafluoroethylene
PVC	Polyvinylchloride
Ra	Arithmetic mean roughness
σ	Tensile strength
S	Sliding distance
S/N	Signal to noise ratio
SBR	Styrene-butadiene rubber
SEM	Secondary electron Microscopy
t	Time
T	Tear Strength
TBU	Temperature build-up
μ	Coefficient of friction
v	Sliding velocity

V   Wear volume

XNBR   Carboxylated acrylonitrile butadiene rubber

WR   Wear rate

Table of contents

Table of Figures

XIII

XIV

XV

Table of Tables

Chapter 1. Introduction

1.1. Introduction

A special class of amorphous and elastic polymers composed of long, chain-like cross-linked molecules with high elastic memory, tensile strength, Poisson ratio, elongation at break, and low elastic modulus is known as elastomers. Various different types of elastomers are used in wide range of applications such as automotive industries (tyre, brake drum, piston, cylinder liners, etc.), mining (conveyor belts), seals, gaskets, hoses, and consumer products (Khan, 2008, Hakami et al., 2017). Natural rubber (NR), styrene butadiene rubber (SBR), acrylonitrile butadiene rubber (NBR), ethylene propylene diene monomer (EPDM), and chloroprene (CR) are among the frequently used elastomers in different industrial applications. The term "rubber" is often used interchangeably with the term "elastomer".

The elastomers suffer from abrasive or sliding wear and friction while are used in components that interact with other surfaces in relative motion (Zum Gahr, 1987, Molnar et al., 2014, Hakami et al., 2017). Owing to wear and friction between moving components, which result in costly repair and downtimes, failure would be unavoidable in a system (Petrica et al., 2013, Shen et al., 2016, Hakami et al., 2017).

Different parameters have effect on the wear and friction behaviour, for instance, working variables such as counterpart texture, sliding distance, sliding velocity, applied load, temperature, abrasives, and time of running (Stachowiak and Podsiadlo, 2001, Lv et al., 2015). Additionally, the physical and mechanical properties of the material such as hardness, tensile strength, and elongation at break also affect the tribology behavior of them (Archard, 1953, Lancaster, 1968).

1.2. Objective

The high demand for using elastomers in different industrial applications makes it necessary to improve their tribological behavior and prolong their lifetime. To fulfil these expectations, their behaviour under different operating conditions should be investigated in detail.

Tribology of elastomers represents a particularly interesting field of research since their wear mechanism and friction differ significantly under variable conditions due

to their viscoelastic nature. Furthermore, previous studies focused on abrasion; nevertheless, wear and friction occur while elastomers are sliding against abrasives. Accordingly, researches are shifted from abrasion towards sliding wear and friction, nowadays.

The influence of operating variables and mechanical properties on the wear and friction are well known, however, so far, there is not much work disclosed in the literature concerning the investigation of wear and friction behavior of different types of elastomers. Besides, the effect of abrasive particle size is unknown on wear and friction of elastomers. It is not clear yet how variation of operating variables and mechanical properties of elastomers affect wear, friction, and associated mechanism during sliding.

In this context, the main aim of the present work is to investigate effect of applied load, abrasive particle size, and mechanical properties of different types of elastomer on wear and friction. To provide a better understanding of wear mechanism by new approaches. Furthermore, to determine the contribution of these parameters on tribological behaviour during two-body wear with statistical methods. Finally, to develop a model to find a relation between the operating variables, mechanical properties and wear rate of elastomers.

1.3. Scope of the work

To conduct this research, the thesis is structured as follows:

Chapter 2: A brief review is given, including a general background and detailed literature review on tribology behavior of elastomers. The various types of wear, wear mechanism, friction of polymers and elastomers, and the effective parameters (operating variables and the material properties) on the wear and friction are presented. Furthermore, the basic analytical available models for predicting the wear behavior of elastomers and polymers are presented. Finally, the known information and gaps in current researches are found out and considered for this investigation.

Chapter 3: A detailed description of the instruments and experimental design used in this work are provided. This chapter also presents instruments and methods to

analyze and characterize the results with emphasis on the determination of the wear rate, wear mechanism, and friction.

Chapter 4: It is difficult to generalize wear behavior of elastomers because of varying conditions. The effect of the applied load on the wear rate, mechanism, and friction of elastomers against an abrasive paper is investigated in this chapter. Thus, the relation between the tribological behavior of elastomers and mechanical properties at varied load are explained in details.

Chapter 5: The influence of the abrasive particle size on the wear and friction is studied to prolong the service life of elastomers in industrial applications. A better understanding of the tribological behavior of rubber for varied size of abrasive particles is provided in this chapter.

Chapter 6: The effect of parameters such as operating variables and mechanical properties on tribology behavior of different elastomer is analysed by using statistical method to identify the contribution of different input parameters on the output parameters. The obtained results ease selection of the proper elastomer type according to its application.

Chapter 7: Considering the high demand to use elastomers in industrial applications, a basic knowledge is required to control and predict the material removal rate. Due to the various behavior of elastomers and polymers under different operating conditions, there is not any good wear model. Thus, a wear model is presented to predict the wear rate of elastomers by quantifying the contribution of operating parameters and material properties.

Chapter 8: The key findings of this research are summarized. Further, some ideas for ongoing and future works are presented.

Chapter 2. General background

2.1. Elastomers

Elastomers are long hydrocarbon loose chain polymers that are connected to each other by chemical bonds, resulting in highly elastic behavior above the glass transition temperature. These materials return to their original shape after stretching. In another words, under stress, they can endure strain without significant deformation and show both elastic and viscous characteristics (Felhös, 2008, Wu, 2016). Fig. 2. 1 illustrates the schematic of the elastomer chain before and after deformation.

Fig. 2. 1. Reversible extension of cross-linked elastomer chain: (a) undeformed, (b) deformed.

The most common types of elastomers, which widely used in engineering applications, are rubbers such as Natural rubber (NR), Styrene-butadiene rubber (SBR), and Nitrile butadiene rubber (NBR).

2.1.1. Natural Rubber

NR is highly non-saturated elastomers with a long chain and high molecular weight, which is derived from the sap of the rubber tree. Generally, it has an outstanding tensile strength, fatigue behavior, and good abrasion resistance.

2.1.2. Styrene Butadiene Rubber

SBR, a copolymer of styrene and butadiene, is the most commonly used rubber. It is derived from petroleum oil. It has high resistance to abrasion, thermal degradation, and crack growth that makes them suitable to be used in the automotive industry and tyre production (Liang, 2007, Wu, 2016).

2.1.3. Acrylonitrile Butadiene Rubber

NBR is a copolymer of acrylonitrile and butadiene. Due to its high resistance to the oil and fluids, it is mostly used as seals, tubes, oil resistance conveyor belts, and automotive parts.

2.2. Tribology of polymers

2.2.1. Wear

Due to wear and friction, systems in which counterparts are sliding against each other, failure and eventually downtimes and costly repairs would be inevitable (Petrica et al., 2013, Shen et al., 2016, Hakami et al., 2017).

Wear is defined as the loss of material from the solid's surface in moving contacts, which decreases the mechanical performance of the materials in industrial application.

Owing to the variety of wear mechanisms and their interrelation, it is hard to classify the wear processes, though; the most common types for the polymers are abrasion, fatigue, adhesion, and roll formation (Briscoe and Sinha, 2002, Myshkin et al., 2005, Pal et al., 2009).

2.2.1.1. Abrasive wear

Abrasive wear, characterized as displacement of materials from the surface due to the protuberance of hard abrasive particles and friction between sliding parts, is the most destructive type of the wear (Zum Gahr, 1987, Stachowiak and Batchelor, 2002, Williams, 2005, Petrica et al., 2013, Ratia et al., 2014, Hakami et al., 2017).

Generally, abrasive wear is divided to two-body, three-body, or a combination of them (Voss and Friedrich, 1987, Petrica et al., 2013, Molnar et al., 2014). The projection of a hard surface to the softer one, while sliding against each other causes two-body wear. It is called three-body abrasive wear if the interfacial or external particles such as wear debris or sand penetrate the softer material (polymer) (Harsha and Tewari, 2003). Fig. 2. 2 demonstrates a schematic of two-body and three-body abrasive wear.
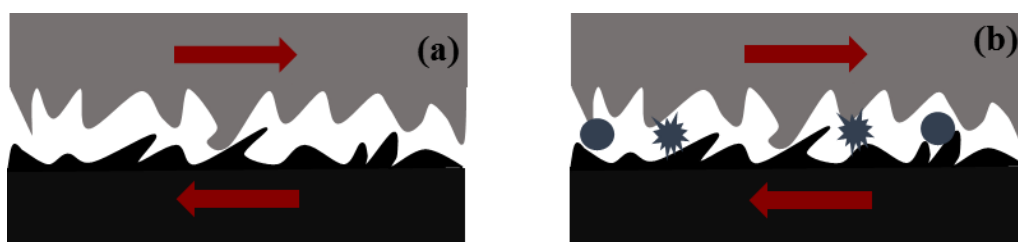
Fig. 2. 2. Schematic of abrasive wear: (a) two-body, (b) three-body.

Abrasive wear happens because of micro-cutting or ploughing (also known as grooving) and on the worn surface scratches, gouges, and scoring marks are observed. Plastic deformation occurs due to material removal from surface and forming wear debris or material displacement to the sides and forming the ridges by abrasives. The former one is called cutting, and the latter ploughing (Muhr and Roberts, 1992, Myshkin et al., 2005).

2.2.1.2. Adhesive wear

Adhesive wear also known as, "friction wear" is associated with the shearing of the friction's junctions. In this wear process; fracture occurs when the materials transfer between the surfaces exposed to the friction. Fig. 2. 3 illustrates schematic of adhesive wear. However, the materials' transfer effect on the wear rate could be different. For instance, if wear debris or film of soft materials (polymers) is transferred from the softer surface to the harder one, the wear rate does not show much difference. On the other hand, if the transferred debris or film is removed from the harder surface, then the wear rate increases. Other wear types, such as fatigue and abrasive typically are accompanied by adhesive wear, which is almost seen for all kinds of materials (metals, polymers, and ceramics) (Myshkin et al., 2005).
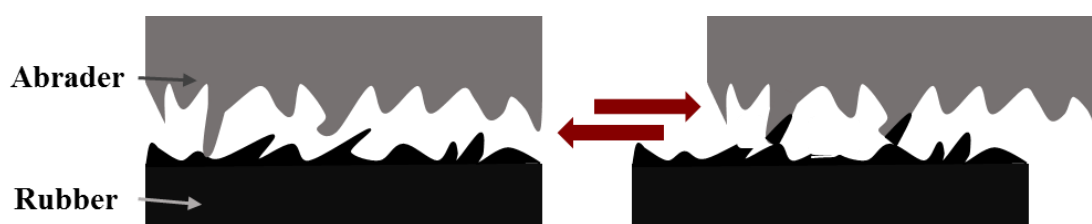
Fig. 2. 3. Schematic of adhesive wear.

2.2.1.3. Fatigue wear

When polymers slide against blunt abrasives, the stress concentrations applied by the cyclic load on the surface are not enough to remove particles, instead, cause pitting and cavitation on the surface that generates cracks, leading to the progressive fracture (Tangudom et al., 2014). The schematic of crack initiation and fatigue wear is shown in Fig. 2. 4. It is a continuous mechanism with a mild intensity. Defects on the surface such as dots, marks, scratches, and pits accelerate the crack initiation and growth.

Two phases are observed during the fatigue wear: initiation and steady state. Initially, the wear pattern propagates and wear rate increases until reaching a critical size, where the ridge space and wear rate achieve a constant value (Gent and Pulford, 1983).
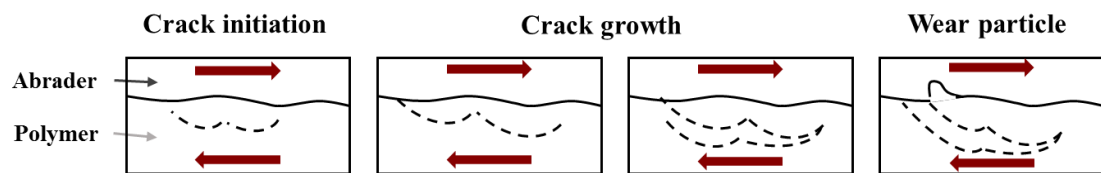
Fig. 2. 4. Schematic of fatigue wear.

2.2.1.4. Roll formation

On the smooth surface of polymers, wear by roll formation takes place when the formed waves adhere to the abrader. Thus, the contact area and height of the wave's tongue will increase with the further moving of the abrader. While the abrader moves forward, polymer detaches from the surface and forms a roll shape particle on the surface. Fig. 2. 5 shows schematic of wear by roll formation. This mode mostly happens when tear strength of the material is low (Hakami et al., 2017).

Fig. 2. 5. Schematic of roll formation.

2.2.2. Friction

In moving contacts, in addition to the wear, friction desired or not is present in the system. In dry conditions, two main factors contribute to the polymers friction; adhesive and hysteresis (deformation). Adhesive friction results from the adhesion between the counterpart's surfaces place when the junctions are formed and ruptured between surfaces while moving against each other and deformation is caused by micro elastic energy dissipation (Liang, 2007). Barquins et al. (Barquins and Roberts, 1986) studied friction of rubber and claimed that the attraction between the substrate and the elastomer's chain leads to physical or chemical interaction. By applying force the adhered chain would be detached, thus with network deformation, some energy is elastically stored. The energy would be released and the chain would retract freely by reaching a critical force for chain detachment.

When the applied pressure is more than the shear strength of the softer material the deformation happens that is governing by the contact of sliding surfaces' asperities. It is continuous and could be elastic, plastic, or viscoelastic (Myshkin et al., 2005).

In the presence of lubricants and wear, viscous friction and cohesion friction also participate to the friction force. The former one is attributed to the shearing of the fluid at the interface, and the latter is due to crack initiation and wear leading to the additional energy loss (Gabriel, 2010).

The texture of the contact surface affects the contribution of adhesion and hysteresis. For the smooth surfaces, adhesion is the dominant factor, in contrast with the rough surfaces that deformation dominates the friction. For instance, Persson (Persson, 2001) claimed the adhesive friction's effect on rough surfaces, like tyre/road contact is insignificant.

2.2.3. Friction and wear mechanism

Different displacement modes and mechanisms participate in elastomers and polymers' wear and friction, which depend on the viscoelastic properties of them and the topography of the surface (Schallamach, 1963).

2.2.3.1. Stick-slip motion

At high sliding speeds, when the static friction is higher than the dynamic friction, the stick-slip motion occurs on the rough surfaces. The stick happens when the contact area between the abrader and the elastomer increases and the sliding speed almost becomes zero. If the tangential force shears the junction between the contact points, slip occurs. In other words, the stick-slip motion is caused by the repeated attachment and detachment of two surfaces (Liang, 2007).

2.2.3.2. Wear pattern

The first attempt to study the wear mechanism of the elastomer is done by Schallamach (Schallamach, 1958). He investigated the rubber's wear by applying a needle that scratches the surface and reported the propagation of microcracks on the surface.

Gent et al. (Gent and Pulford, 1983) categorized the abrasive wear process into two stages; first, the cracks are generated as a detachment of the small particles. Then, the formed cracks under the cyclic stress create larger debris leading to the wear.

During the abrasion, a series of parallel-ridged pattern perpendicular to the sliding direction termed as "abrasion pattern" also known as Schallamach waves are formed. The formed wear pattern of ethylene propylene diene monomer (EPDM) is shown in Fig. 2. 6. These patterns are generated on the surface due to the adhesive force, where the vertical contact spots are formed on the edge of the contact zone from front to back (Fukahori and Yamazaki, 1994, Tangudom et al., 2014). With passing the abrader over the rubber's surface, produced compression-tension strain folds the rubber forward, followed by the rubber relaxation that results in turning back of the folds owing to the viscoelastic nature of the rubber. However, it does not get back exactly to its original position, therefore, waves are formed and wear rate increases.
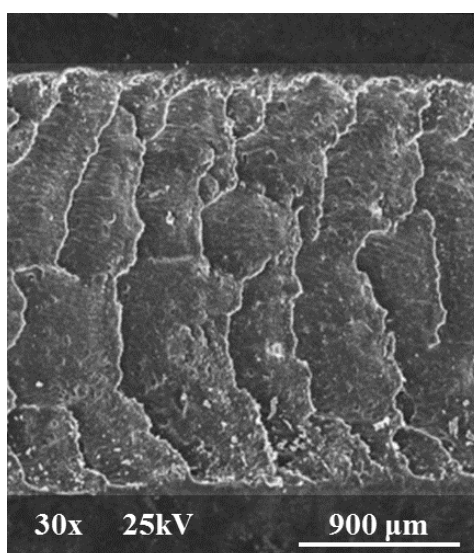
Fig. 2. 6. SEM image of wear pattern EPDM (Gatos et al., 2007).

Schallamach (Schallamach, 1958) who studied the abrasive pattern of the elastomer suggested that at the contact spots between the abrader and the elastomer the stress concentration is high, leading to the stick-slip motion and propagation of the lateral cracks into the surface. Moreover, the formed abrasion pattern's spacing is, directly and indirectly, proportional to the cube root of normal load and elastic modulus, respectively (Schallamach, 1954).

Further study is done by Fukahori et al. (Fukahori and Yamazaki, 1994) and convey et al. (Coveney and Menger, 1999). They proposed a mechanism to explain the relationship between the friction and formation of abrasion pattern by using the stick-slip motion and micro-vibration. Initiation and propagation of the cracks occur at the slip and stick region, respectively. The driving force for initiating a crack is provided by the micro-vibration; as a result, small particles are generated. The large particles are produced by the stick-slip motion.

2.2.4. Effective parameters on the wear and friction

It has been reported that variation of wear and friction is influenced by the interfacial conditions such as normal load, sliding velocity, time of running, temperature, counterpart texture, and abrasives (Petrica et al., 2013, Ratia et al., 2014, Lv et al., 2015, Popov et al., 2018). In addition to these parameters, type of the material

and its properties such as hardness, Young's modulus, tensile strength, and elongation at break also influence wear and friction (Archard, 1953, Lancaster, 1968).

2.2.4.1. Applied load

Among the effective parameters, the applied load plays an important role in the tribological behaviour of materials (Suresha et al., 2008, Ravi Kumar et al., 2009, Bhattacharya and Bhowmick, 2010).

Previous studies have shown that wear rate is directly proportional to the normal load. For instance, Archard's equation (Archard, 1953), which shows the relationship between the wear volume (V), applied load (F), sliding distance (d), and hardness (H) is used to describe adhesive wear of metals.

$$V = K \frac{Fd}{H} \qquad (2.1)$$

This equation does not hold good correlation for polymers owing to the variation of mechanical properties with applied load, sliding velocity, and temperature (Zum Gahr, 1987, Hakami et al., 2017).

For friction behaviour of metals, the Coulomb friction law (Eq. 3) states the friction force (F_k) is linearly proportional to the applied load (F) (Braun et al., 2016).

$$F_k = \mu F \qquad (2.2)$$

However, friction of elastomers and polymers do not follow the classical law, attributed to the variation of the real contact area with increase of the applied load for polymers and elastomers that affects the frictional force (Schallamach, 1952, Quaglini et al., 2009, Braun et al., 2016). Hence, the effect of load on wear and friction of polymers and elastomers should be studied separately.

During three-body wear of SBR against hard rocks, Thavamani et al. (Thavamani et al., 1993) observed with increase of the applied load, wear mechanism has changed from fatigue wear to wear by ploughing.

Harsha et al. (Harsha and Tewari, 2003) reported an increase in wear rate along with an increase of the load during two-body and three-body wear of Poly aryl ether ketone (PAEK), while the maximum load was 12N.

Further studies on the wear of NR, XNBR, and NBR and their composites by Pal et al. and LV et al., respectively (Pal et al., 2010a, Lv et al., 2015) are done by applying load ranged between 4 to 13.5N against the rocks. The obtained results showed an increase in the wear rate, in addition to the variation of the wear mechanism with increase of the load. The relation between wear rate and load is also observed in a wet environment (Wu et al., 2016).

The wear rate's increase is due to the further penetration of hard asperities to the softer material and increase of the real contact area, leading to increase of deformation and fracture of asperities (Unal et al., 2004, Suresha et al., 2009).

An equation is proposed by Fukahori et al. (Fukahori and Yamazaki, 1995), which shows wear volume is indirectly proportional to normal load for rubbers.

$$V = KF^{\alpha} \qquad (2.3)$$

Where K and α are constant. The compound and sharpness of wear tracks affect the value of α. Fig. 2. 7 indicates the relation between wear volume and applied load.
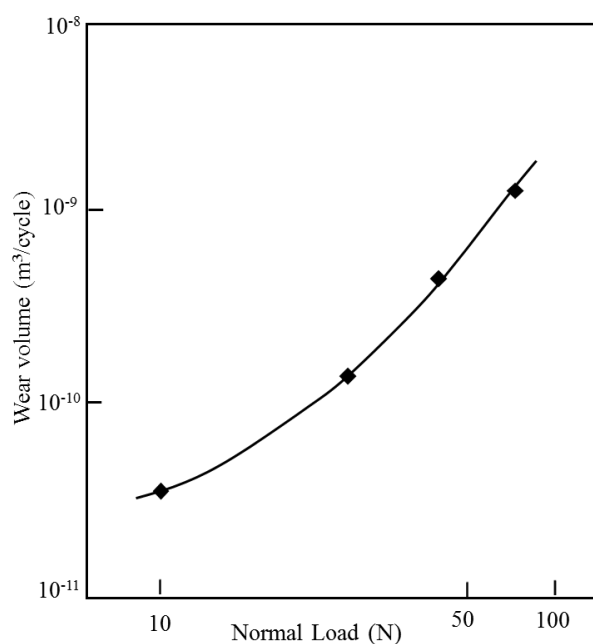
Fig. 2. 7. The relation between wear volume and load (Fukahori and Yamazaki, 1995).

According to the theoretical equation (see Eq. 2.2), the friction force is proportional to the normal load, which is just fulfilled for some polymers under specific conditions. The pioneering studies of the normal load's effect on the friction of different polymers such as polytetrafluoroethylene (PTFE), polyvinylchloride (PVC), and polyethylene (PE) showed at load range of 2-100 N, the friction is independent of the applied load (Myshkin et al., 2005).

On the one hand, other authors who studied the relationship between the friction and load (low load range) reported that the friction force decreases with the increase of the load. It could be due to elastic deformation of asperities under pressure, wear and material properties (Myshkin et al., 2005, Gustafsson, 2013). But on the other hand, further studies by Quaglini (Quaglini et al., 2009) on some polymers shows with increase of normal load, real contact area and coefficient of friction increase. This apparent contrast could be explained by a change in adhesive and hysteresis friction's contribution to the friction force and the transition from elastic to plastic deformation of the asperities.

2.2.4.2. Effect of sliding speed and sliding distance

Sliding speed and distance are two other external factors that influence wear and friction. The obtained results by different authors (Unal and Mimaroglu, 2003, Unal et al., 2005, El-Tayeb and Nasir, 2007, Tangudom et al., 2014), who studied the effect of these parameters on tribology behavior of polymers and elastomers show that wear rate is increased with different trends with increase of sliding speed and distance. Owing to a higher rate of thermal degradation and continued wear weight loss. Nevertheless, the variation of the friction coefficient is different; it could be constant, increasing, or decreasing with accelerating speed and distance (Schallamach, 1953, Schallamach, 1968, Myshkin et al., 2005, Thongsang et al., 2012). Due to the viscoelastic nature of the polymer, the sliding velocity affects its friction behavior through two mechanisms: viscoelasticity and frictional heat. At low sliding velocities, the variation of the surface temperature is insignificant; thus, the friction force is independent of sliding speed. At higher sliding velocities, the value of the friction force depends on the contribution of adhesive friction and hysteresis friction. If the viscous resistance increases, the friction force increases. On the contrary, if the elastic

behavior dominates at the contact zone, the friction force decreases. According to the polymer type, with an increase of the sliding velocity, the frictional heating increases resulting in rising of the surface temperature, which melts the polymer at the counter face and adhesive bonds break, so friction force drops.

With the increase of sliding distance, the wear mechanism varies from fatigue and friction to abrasion by ploughing and cutting. Therefore, the real contact area reduces, leading to decrease of the friction force.

2.2.4.3. Effect of abrasives

Displacement of the material from the surface known as abrasive wear occurs due to the protuberance of hard abrasives, which could be the harder surface or foreign particles, such as abrasives suspended in a fluid, generated wear debris, or dust (Williams, 2005, Woldman et al., 2013).

The abrasive's properties such as shape, hardness, size, and roughness affects friction and wear rate; and associated wear mechanisms of different materials (Schallamach, 1968, Stachowiak and Stachowiak, 2001, Harsha and Tewari, 2003, De Pellegrin et al., 2009a, Coronado and Sinatora, 2011, Hamid et al., 2013). The effect of the abrasives on tribological behavior of metals has been studied comprehensively. The results indicate that wear rate and friction coefficient increase linearly until reaching a critical size, then it becomes constant, decreases or increases (Xie and Bhushan, 1996, Gåhlin and Jacobson, 1999, Coronado and Sinatora, 2011, Coronado, 2015). Fig. 2. 8 demonstrates the schematic variation of wear rate and coefficient of friction with abrasive particle size.

The effect of the abrasives' hardness on three body abrasion wear of rubber has been studied by Pal et al. (Pal et al., 2010a). An increase in wear rate and COF has been observed with the increase of the abrasives' hardness.

The shape of the abrasives (rounded or sharp) also influences the wear mechanism. The wear by blunt or sharp asperities leads to fatigue or abrasive wear mechanism, respectively (Schallamach, 1968, Gent and Pulford, 1983).
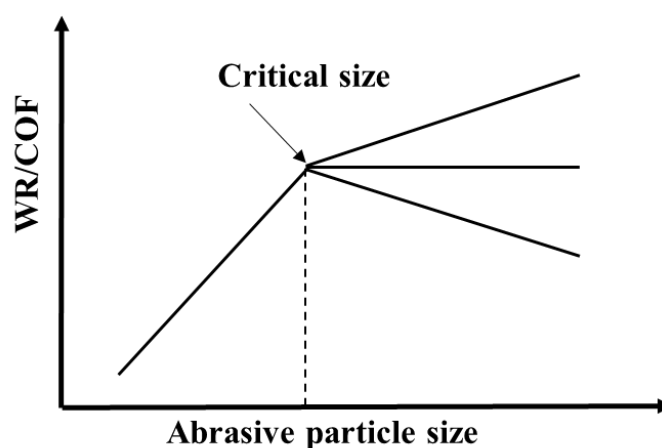
Fig. 2. 8. Variation of the wear rate or coefficient of friction as a function of abrasive particle size.

Quaglini et al. (Quaglini et al., 2009) investigated the effect of roughness on friction of polymers used in bearing technology and showed there is an optimum value for the surface roughness of the abrader, where the friction is minimum. Further studies by Feng et al. and Padenko et al. (Feng et al., 2016, Padenko et al., 2016) on the influence of abrasives' roughness on NBR and HNBR, respectively. Wear rate and COF increase with raising of the roughness since the height of abrasives increases resulting in deep penetration of hard surface. The wear mechanism also changed from fatigue and roll formation to the abrasion by cutting.

A recent study on abrasive size's effect on wear and friction of NBR showed that higher abrasive size results in higher wear rate. It is due to wear mechanism's change from adhesive wear to the abrasive wear, which also explains the reduction of friction coefficient to a minimum value and increasing of it with further increase of the abrasives' size (Shen et al., 2016).

2.2.4.4. Effect of Temperature

Elastomers are viscoelastic materials, thus their behavior depends on temperature, which could be the ambient temperature or the generated temperature at the surface by the frictional heating. It affects the strength of the elastomers' mechanical properties, wear and friction resistant of them. When two materials slide against each other because of friction, the mechanical energy converts to the heat, therefore at the

counter face, particularly at the contact spots, the temperature is higher than the bulk. The frictional heating is attributed to the plastic deformation, hysteresis, dispersion, and viscous flow. Besides, it might be due to the breakdown of adhesive bonds. This temperature is known as flash temperature or temperature built up (TBU) (Myshkin et al., 2005, Persson, 2006, Tangudom et al., 2014).

Gent et al. (Gent and Pulford, 1983) carried out abrasion test of filled and unfilled elastomers at two different working temperature (25 and 100 °C) and reported that the temperature has an insignificant effect on the wear rate of the specimens.

The finding of Gent et al. contradicts with the pioneering study done by Grosch et al. (Grosch, 1963), who investigated the effect of temperature ranged from -15 °C to 85 °C and sliding velocity on friction coefficient of rubbers. The obtained results are presented as a master curve illustrated in Fig. 2. 9. Further studies (Schallamach, 1963, Myshkin et al., 2005, Lorenz et al., 2011) also confirm the obtained results by Grosch, which mean the COF's behavior with a variation of temperature depends on dominant friction mechanism. If the adhesive friction dominates, the COF drops with an increase of ambient temperature.
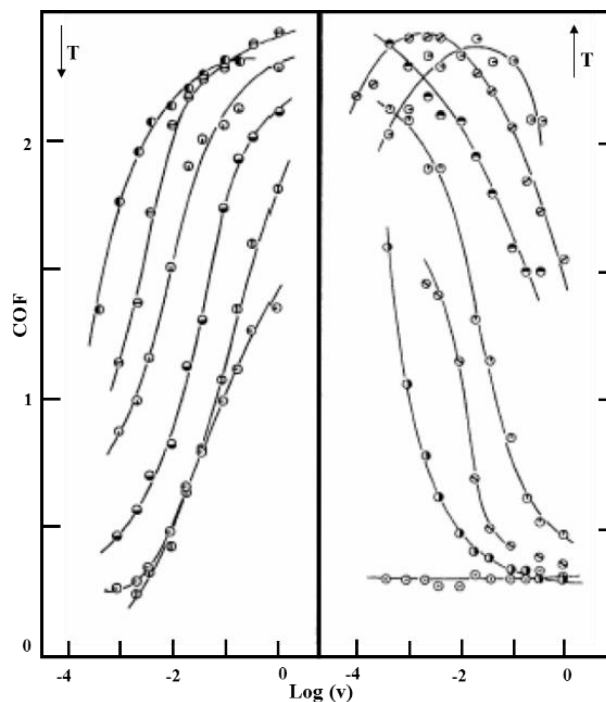
Fig. 2. 9. COF as a function of sliding velocity as different temperature (Grosch, 1963).

Investigation of the effect of TBU on the friction of the natural rubber and its composite showed (Persson, 2006, Bhattacharya and Bhowmick, 2010) that the friction coefficient drops with an increase of the TBU. The effect of TBU on friction increases with the increase of the applied load, however, it has insignificant effect at low sliding speeds.

2.2.4.5. Effect of mechanical properties

In addition to the external parameters, the mechanical properties of the material such as Young's modulus, hardness, tensile strength, and elongation at break affect wear and friction and control the wear mechanism.

The classic relationship between wear and hardness of metals (see Eq. 2.1) states that wear is inversely proportional to the hardness. It means the wear rate decreases with increase of the hardness. The practical studies, though, showed the relation for polymers and elastomers is more complicated. Lancaster (Lancaster, 1968) suggested that wear rate is inversely proportional to the product of tensile strength and elongation at break of polymers. They reported polymers with higher hardness, elongation at break, and tensile strength show higher wear resistance at room temperature. The abrasion wear test of some polymer composites (Harsha et al., 2003) and SBR blends (Molnar et al., 2014) exhibits materials with higher hardness and modulus of elasticity have better resistance against protuberance of hard abrasives, but the relationship is not linear. Besides, for some polymers, the combination of $(\sigma.\varepsilon)$ shows a stronger correlation compare to the individual mechanical properties (Alajmi and Shalwan, 2015). Further investigation show this relation is not general, for instance, Budinski (Budinski, 1997) did not observe any correlation between the wear rate and hardness of examined 21 different polymers. The obtained wear rate is less than the predicted one by the equation, however, the wear rate correlates with the inverse value of $(\sigma.\varepsilon)$ (Shipway and Ngao, 2003). This contrast could be explained by different wear mechanisms, which take place during the abrasion and transfer of polymer film to the counterface. Moreover, the mechanical properties differ at contact points with variation of applied load (Myshkin et al., 2005).

These mechanical properties also play an important role in friction behavior of composite polymers, the higher tensile strength, and elongation at break result in lower

COF. In comparison with hardness, the influence of the modulus of elasticity on COF is more significant (Alajmi and Shalwan, 2015).

2.2.5. Prediction of wear in polymers

To better understanding, the wear behaviour of polymers, the prediction of wear is desirable under different operating conditions and material properties. It can be done with the help of laboratory experiments, mathematical models, and computer simulations (Abdelbary, 2014).

Meng et al. (Meng and Ludema, 1995) have comprehensively analyzed a wide range of available wear equations, however, they concluded there is not a general equation for predicting wear behavior of all materials. In comparison with metals, there are limited models for prediction of wear behavior of polymers. Followings are some of these studies, which attempted to find a relationship between the wear rate of polymers and the operating variables (such as applied load, sliding velocity, distance, and time of running) and material properties (such as hardness, elasticity modulus, tensile strength, and elongation at break). The findings in the literature are presented in Table 2. 1.

In order to explain the correlation between the wear rate and mechanical properties of the polymer, Lancaster and Ratner (Lancaster, 1968) proposed equation 2.4. It shows wear volume is directly proportional to the normal load and friction coefficient and inversely proportional to hardness, tensile strength, and elongation at break. Nevertheless, it did not hold good correlations for all polymers and their composites (Budinski, 1997), though a linear trend has been reported in some cases (Harsha et al., 2003). Lewis and Rhee (Rhee, 1970) proposed non-linear wear equations (2.5) and (2.6), respectively, which presented the adhesive wear of polymer sliding on metallic surfaces as a function of applied load, sliding speed, and time.

Few papers used the dimensional analysis method to quantify the contribution of operating variables and mechanical properties. For instance, Kar et al. (Kar and Bahadur, 1974) developed a non-linear equation (see Eq. 2.7) including normal load, sliding velocity, surface energy, elastic modulus, temperature, and specific heat. It did not include any counter face parameter, consequently, Viswanath et al. (Viswanath

and Bellow, 1995) proposed an equation (see Eq. 2.9) by adding the counter face roughness as an additional parameter. By involving the friction coefficient and breaking strength, in addition to operating factors an equation (see Eq. 2.8) has been developed by Burr (Burr and Marshek, 1982). It relates the wear volume of O-ring materials to the frictional work. The majority of proposed equations are applicable for adhesive wear behavior of polymers. Hence, Rajesh et al. (Rajesh and Bijwe, 2005) analyzed the abrasive wear of polyamides (PAs) and developed an empirical model (see Eq. 2.10) including the fracture properties (critical crack length and fracture stress), which controls the failure of the material after cracks' generation. Similarly, Fukahori et al. (Fukahori and Yamazaki, 1995) represented a relation for abrasive wear of natural rubber (see Eq. 2.11), which shows the volume loss is indirectly proportional to the applied load. It has been also suggested that the volume loss could be related indirectly to the frictional work by Pal et al. (Pal et al., 2010b).

Table 2. 1. Some wear equations for wear of polymers/composites.

Author	Equation	Where
Ratner (Lancaster, 1968)	$V = \dfrac{\mu F}{H \sigma \varepsilon}$ (2.4)	μ is coefficient of friction, F is applied load, H is hardness, σ is tensile strength, and ε is elongation at break
Lewis (Rhee, 1970)	$V = KFvt$ (2.5)	F is applied load, v is sliding speed, t is time of sliding
Rhee (Rhee, 1970)	$\Delta W = KF^a v^b t^c$ (2.6)	F is applied load, v is sliding speed, t is time of sliding
Kar (Kar and Bahadur, 1974)	$V = 1.5K \dfrac{\gamma^{1.775}}{E^{3.225}} F^{1.47} S^{1.25}$ (2.7)	γ is surface energy, E is elastic modulus, k is thermal conductivity, C_p is specific heat, S is sliding distance
Burr (Burr and Marshek, 1982)	$V = K \mu^{-0.025} F^{1.325} S^{0.35} \sigma^{-1.325}$ (2.8)	μ is coefficient of friction, F is applied load, S is sliding distance, σ is breaking strength
Viswanath (Viswanath and Bellow, 1995)	$V = 3.59 \times 10^{-18} F^{1.711} v^{1.711} T^{1.024} \alpha^{0.728} F^{0.463} \gamma^{-2.861} \left(\dfrac{C_p}{K} \right)^{-0.687}$ (2.9)	α is counterface roughness
Rajesh (Rajesh and Bijwe, 2005)	$V = KF^{1.157} \emptyset^{0.458} \Omega$ (2.10)	Φ is mass of abrading particles, Ω contribution of material properties
Fukahori (Fukahori and Yamazaki, 1995)	$\bar{V} = k_4 F^\alpha$ (2.11)	k is a constant, F is normal load
Pal (Pal et al., 2010b)	$V = kF^n$ (2.12)	n and k are constant, F is frictional work

2.3. Summary and aim of this work

The basic knowledge of elastomers and tribology behavior of polymers is briefly reviewed in this chapter. Besides, a literature review of polymers' wear and friction is given.

As mentioned previously, most studies have focused on tribology behavior of polymers and their composites, while the wear and friction behaviour of elastomers and rubbers are more complex, since during dry sliding the surface is heated by frictional energy, and its wear mechanism differs significantly under variable conditions. Therefore, to address these issues it is important to know the parameters, which are controlling wear and friction, and understand the wear mechanism of elastomers during the sliding at the different operating condition. Furthermore, prediction of wear rate of a given tribological system is desirable.

The aim of this work is to investigate the effect of variation of normal load and abrasive particle size on wear and friction of various elastomers, in addition to determining the contribution of each parameter. The further target is to find a link between the operating variables and mechanical properties of elastomers with wear resistance of the elastomer to predict the lifespan of it in service.

It is expected that the obtained results will be addressed to the better understanding of elastomers wear in practice.

Chapter 3. Materials and Methodology

3.1. Introduction

The purpose of this chapter is to describe the materials, methods, and instruments used to run the experiments and analysis of the obtained results.

Experiments have been carried out to investigate the influence applied load and abrasive particle size on wear and friction of the elastomers.

To predict wear durability of elastomers a variety of methods are available, for instance, Pico abrasion (ASTM D2228), NBS abrasion (ASTM D1630), DuPont abrasion (ASTM D394), Tabor abrasion (ASTM D3389), and DIN abrasion (DIN 53516/ ISO 4649), which the wear test has been conducted according to DIN abrasion test to study sliding wear. Friction experiments are made on a customized machine. Surface roughness of the worn surface and surface temperature are also measured.

3.2. Materials

3.2.1. Elastomers

Commercially used elastomers, namely natural rubber (NR), styrene butadiene rubber (SBR), and nitrile butadiene rubber (NBR) are studied in the present research. Table 3. 1 shows the suppliers of different elastomers and Fig. 3.1 depicts the molecular structure of these elastomers.

Tables 3.2 and 3.3 show the mechanical properties and chemical composition of them, respectively. The mechanical properties are provided by the suppliers (see table 3.1) and chemical compositions are obtained by Energy-dispersive X-ray spectroscopy (EDS) analysis.

Table 3. 1. Elastomers and suppliers.

Elastomer	Supplier	Elastomer	Supplier
NR1	Industrial Rubber Supplies	NR7	Rudex Australia
NR2	Rema Tip Top	NR8	Reglin Rubber
NR4	Reglin Rubber	SBR	Complete Rubber Pty. Ltd.
NR6	Reglin Rubber	NBR	Complete Rubber Pty. Ltd.
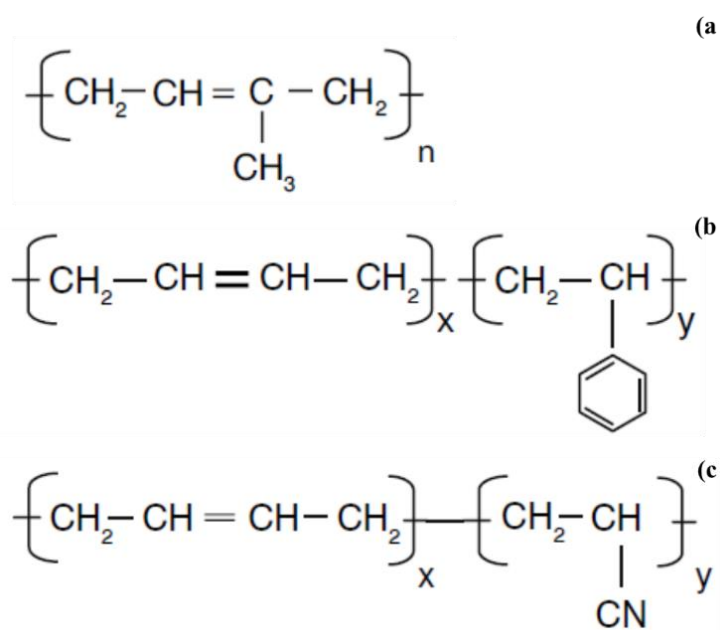
Fig. 3. 1. Structure of elastomer unit: (a) NR, (b) SBR, (c) NBR.

3.2.2. Abrasives

The corundum (aluminium oxide) sandpaper is used as the abrasive medium, supplied by Abrasive Industrial Distributors. Fig. 3. 2 shows the scanning electron microscope (SEM) image of abrasive paper's surface before running the test.

Table 3. 2. Mechanical properties of the elastomers.

	Hardness (Shore A)	Tensile Strength (MPa)	Tear Strength (N/mm)	Elongation at Break (%)
NR1	40	18	30	600
NR2	34±5	14	8	750
NR4	38±5	19	60	650
NR6	38±5	19	60	650
NR7	35±5	25	35	800
NR8	38 ± 5	19	60	650
SBR	65 ± 5	3.5	12	250
NBR	65 ± 5	14	40	400

Table 3. 3. The chemical composition of the elastomers.

	C (%)	S (%)	Si (%)	Zn (%)	Ca (%)	Na (%)
NR1	79.31	2.66	1.53	-	-	-
NR2	71.66	5.42	0.93	-	-	-
NR4	80.73	2.16	3.41	1.73	0.60	1.26
NR6	74.45	3.26	4.00	4.65	0.55	3.00
NR7	72.37	1.85	6.31	-	-	-
NR8	88.41	2.98	0.24	2.10	0.07	-
SBR	60.47	-	-	5.79	10.46	1.26
NBR	76.38	2.59	2.67	10.4	-	-
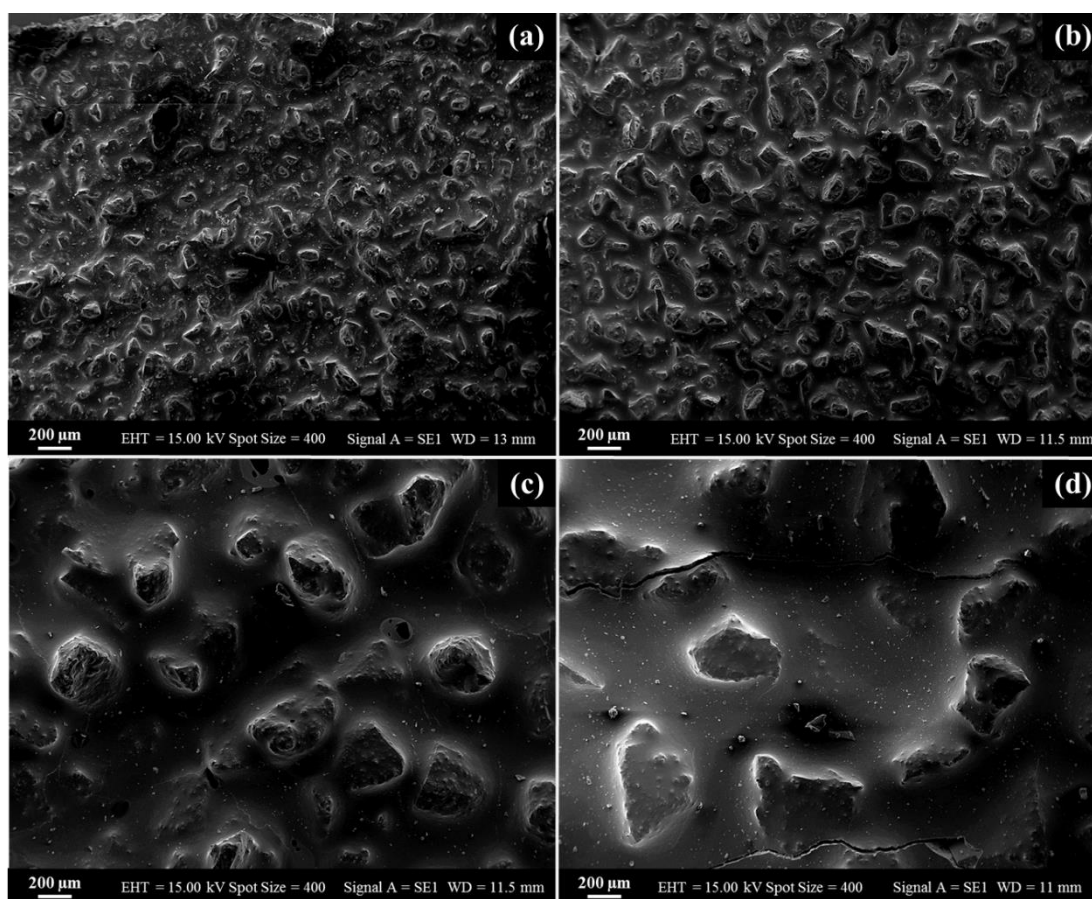
Fig. 3. 2. SEM images of abrasive paper: (a) 82 µm, (b) 125 µm, (c) 269 µm, (d) 425 µm.

3.3. Tribotests

3.3.1. Two body wear test

The wear test has been conducted according to ISO 4649 standard with a DIN abrasion test machine as shown in Fig. 3. 3. This machine consists of a rotating cylinder and a loading arm with the specimen holder normal to the cylinder. Specimens have a cylindrical shape with 16 mm diameter and 6 mm thickness that are placed in the holder in contact with corundum paper, which is utilized as the abrasive medium, resulting in two-body abrasion wear. Normal load is applied via a dead weight system. The test parameters are as followings:

- Sliding distance: 40 m
- Sliding velocity: 0.32 m/s

- Applied normal load: 2.5, 5, 7.5, 10, 12.5, 15, 17.5, and 20 N
- Abrasive particle size: 82, 125, 269, and 425 μm

After each experiment, the abrasive paper is cleaned with a brush to remove the generated particles/wear debris. The specimens are weighed before and after the wear test in a chemical balance with an accuracy of 10^{-4} g. To find out the wear rate (WR), weight loss method is used according to equations 3.1 and 3.2:

$$\Delta V = \frac{\Delta m}{\rho} \ (mm^3) \qquad (3.\ 1)$$

$$WR = \frac{\Delta V}{S} \ \left(mm^3/m\right) \qquad (3.\ 2)$$

Where ΔV is the volume loss of the specimen due to wear, Δm is mass loss, ρ is experimental density, and S is abrading distance.
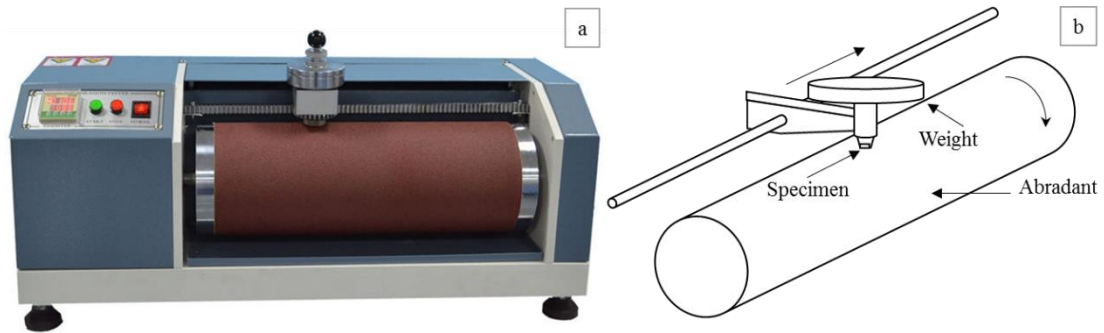
Fig. 3. 3. Wear test equipment (a) Image, (b) Schematic.

3.3.2. Friction test

The friction tests are conducted with the help of a modified Computer numerical control (CNC) machine while applying a static normal load, friction force has been measured by a dynamometer, under variable sliding speeds, where corundum paper is used as an abrasive medium, elastomers specimens are held by a holder. The actual normal load acting at the elastomers-abrasive paper interface is obtained from a prepared calibration chart for different weights. During the tests, specimens slide

against the abrasive paper, linearly. The output is a graph that demonstrates F_x, F_y, and F_z as a function of time. F_y and F_z represent the tangential (friction) force and normal force (the applied load), respectively. For calculating the coefficient of friction (COF), Amontons' laws of friction is used according to equation 3.3:

$$COF = \mu = \frac{F_y}{F_z} = \frac{F_k}{F} \qquad (3.\,3)$$

Where μ is the coefficient of friction, F is the applied load, and F_k is the friction force (measured tangential force).

All the tests were performed at room temperature with similar relative humidity. Fig. 3. 4 shows the customized equipment used for the friction test. The test parameters are as follows:

- Sliding distance: 10 cm
- Sliding velocity: 0.25, 0.5, and 1 m/min
- Applied force: 5, 7.5, 10, 12.5, 15, 17.5, and 20 N
- Abrasive particle size: 82, 125, 269, 425 μm
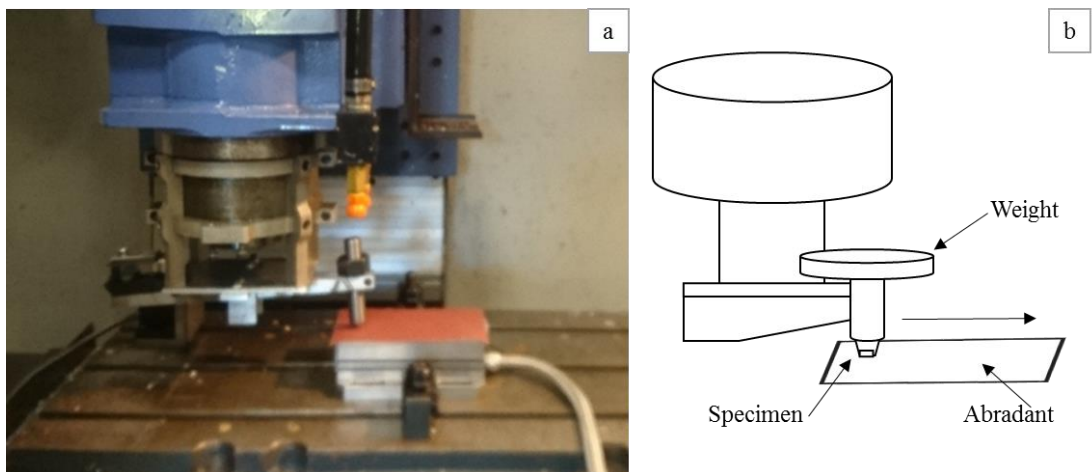
Fig. 3. 4. Test equipment used for the friction test (a) Image, (b) Schematic.

3.4. Micro-structural characterization

The morphology of worn surface of tested specimens are inspected by scanning electron microscope (Zeiss Evo 40XVP), demonstrated in Fig. 3. 5. Prior to SEM investigation, the specimens are coated with Pt (Platinum).

 ImageJ software is used for analysis of SEM images (calculating the average value of ridge spacing and size of wear debris). All the experiments are repeated minimum three times under the same condition to ensure repeatability and the average values of the data is reported for analysis purpose.

Fig. 3. 5. Image of scanning electron microscope.

3.5. Measurement of surface roughness and surface temperature

A surftest profilometer (SJ- 201P, Mitutoyo, Japan) is used to measure the surface roughness Ra (Arithmetic mean roughness) of the worn samples. The machine consists of a driving unit, a detector, and a diamond stylus. At the end of the detector, the diamond stylus is mounted, which is in contact with the surface. The machine is calibrated by measuring the surface roughness of a reference specimen. The average of eight roughness measurement readings is reported.

A dual laser infrared thermometer (Model DT-8868) is used to measure initial and final rubber's surface temperature.

3.6. Summary

In this chapter, a detailed description of used materials, instruments, and methods for analysis and characterization of the results are provided.

Chapter 4. Effect of the applied load

4.1. Introduction

As stated in chapter 2 different parameters have effect on the caused wear and friction in the system, when two materials slide against each other. It could be external parameters such as sliding distance, sliding velocity, working temperature, time, and the applied load (Lv et al., 2015, Wu et al., 2016). In addition to operating variables the material properties, for example, hardness, tensile strength, elongation at break also influence wear and friction (Archard, 1953, Lancaster, 1968).

The applied load's influence on the wear rate of materials and their composites are confirmed by other researchers (see chapter 2). The results show that increase of load results in enhancing of wear rate by deeper penetration of hard asperities to the softer surface (Unal et al., 2004, Suresha et al., 2009).

Moreover, it is known that applied load has a significant effect on friction of materials. However, the frictional behaviour of elastomers is more complicated than metals and composites; the friction could be constant, decreasing, or increasing by increase of normal load (Popov et al., 2018).

Elastomers' surface, due to their mechanical properties and molecular structure, changes with mechanical stresses, temperature, and chemical reactions (Myshkin et al., 2005). Despite several attempts to investigate a relationship between the mechanical and tribological properties of polymers, still, there is not a specific correlation between the materials' mechanical properties and their tribological behavior.

In general, there are difficulties to generalize the obtained results by others for all polymers and elastomers since the relation differs from polymer to polymer under specific conditions. Consequently, the effect of normal load on tribological behavior of elastomers is not clearly understood yet; therefore, in this chapter effect of applied load is studied on wear rate, mechanism, and friction of elastomers against an abrasive paper. In order to get a clear understanding of the relation between the tribological behavior of elastomers with mechanical properties, while the applied load changes.

4.2. Method

For these experiments, eight different elastomers as specimen, wear test machine, friction test rig, and secondary electron microscope described in chapter 3 are used. The wear test parameters are: abrasive particle size 269 μm, sliding speed 0.32 m/s, sliding distance 40 m, and applied load 2.5, 5, 7.5, 10, 12.5, 15, 17.5, and 20N. The friction test parameters are: abrasive particle size 269 μm, sliding speed 0.5 m/min, sliding distance 10 cm, and applied load 5, 7.5, 10, 12.5, 15, 17.5, and 20N.

4.3. Results

Fig. 4. 1 shows the effect of the applied load on the wear rate of different elastomers. For all specimens, the wear rate enhances with different slopes as normal load increases from 2.5 to 20 N. The variation of wear rate with applied load is ascending, however, it is not linear. Fig. 4. 2 indicates a comparison of the elastomers' wear rate when the different normal load is applied. NR8 has the lowest wear rate. NR7 and NR6 have the highest wear rate value at low and high loads, respectively.

Figures 4.3-4.10 demonstrate SEM images (magnification is 100) of worn surface of rubbers after wear under varying applied load. Generally, ridges and furrows are formed on the surface of elastomers because of rolling, sliding, tearing and cutting; that cause material displacement.

Table 4. 1 shows the average size of the ridge's space evaluated from SEM images. The ridge space of formed abrasion pattern grows with increase of the applied load causing higher wear rate until it achieves to a critical size. In this case, the ridge space of NR4 and NR6 do not change significantly with the increase of applied load from 15N to 20N. It is known that the ridge space of abrasion pattern is proportional to the cube root of the normal load (see section 2.2.3.2). This relation is represented in Fig. 4. 11. As seen, the ridge's space grows with increase of the applied load.
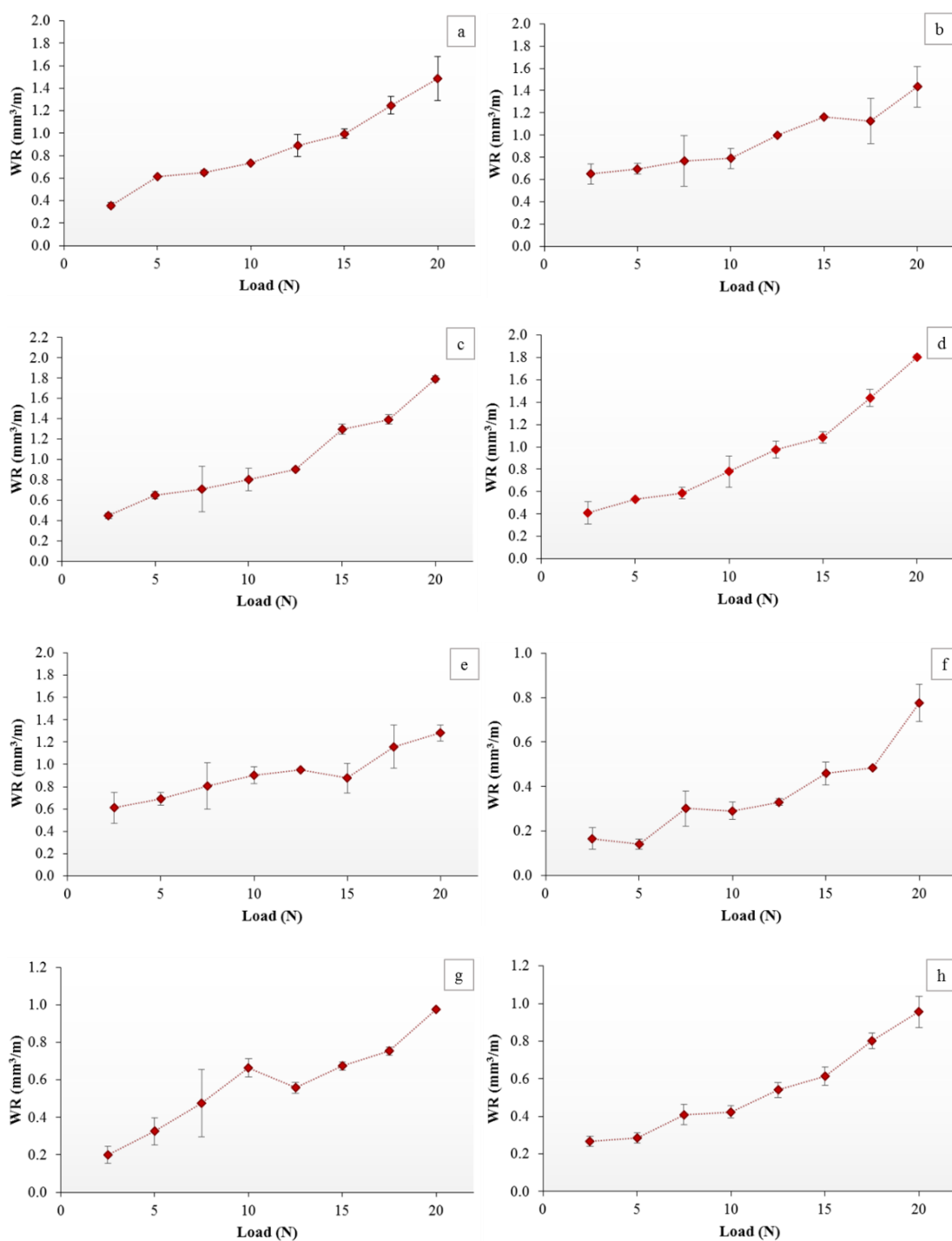
Fig. 4. 1. Wear rate as a function of normal load: (a) NR1, (b) NR2, (c) NR4, (d) NR6, (e) NR7, (f) NR8, (g) SBR, (h) NBR.
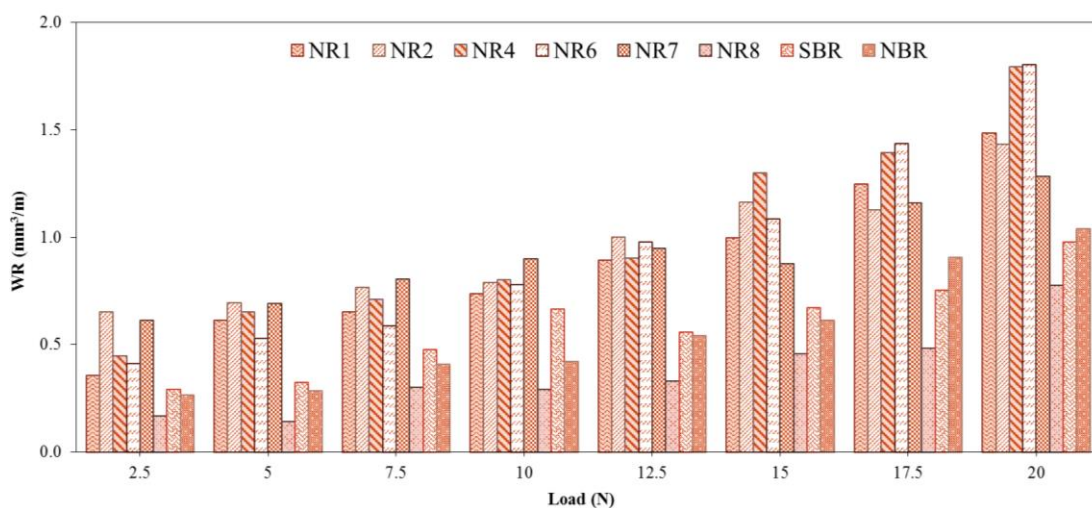
Fig. 4. 2. Wear rate as a function of normal load.
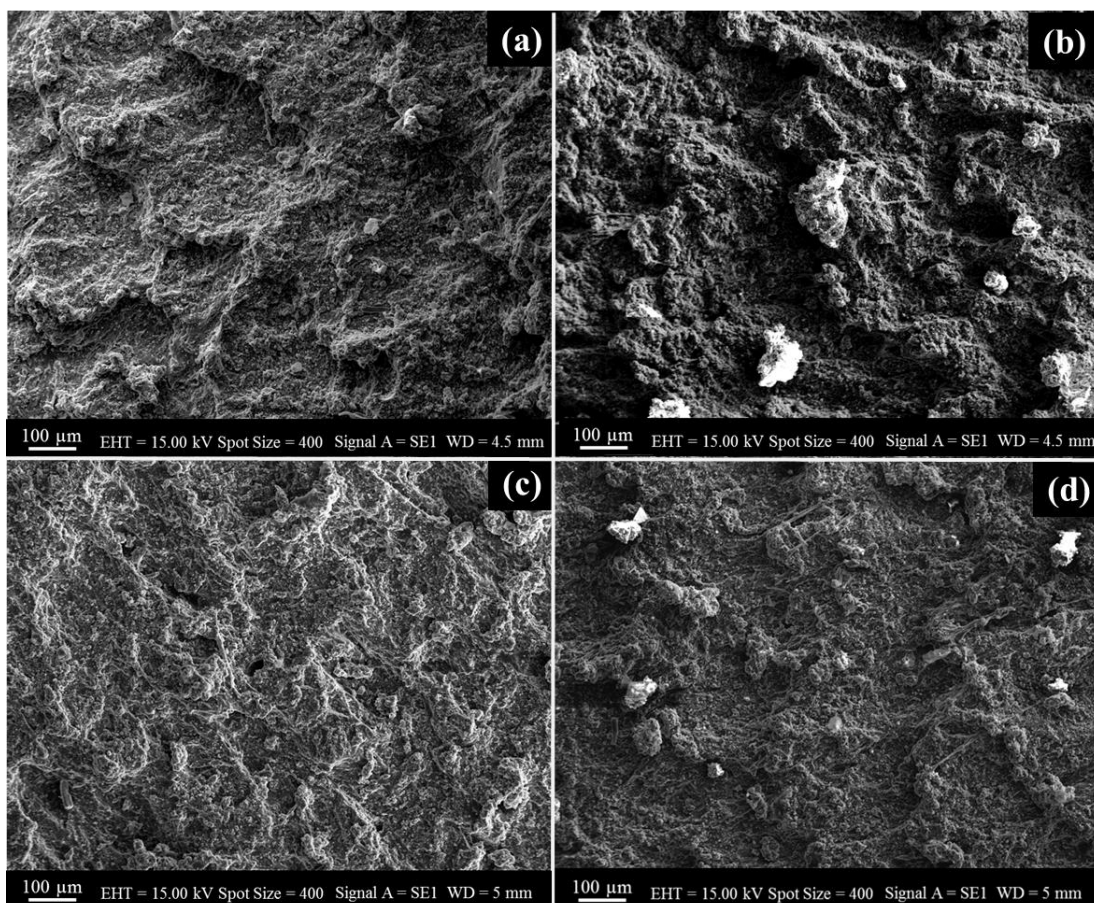
Fig. 4. 3. SEM images of NR1 after abrasion tests with different applied loads: (a) 5N, (b) 10N, (c) 15N, (d) 20N.
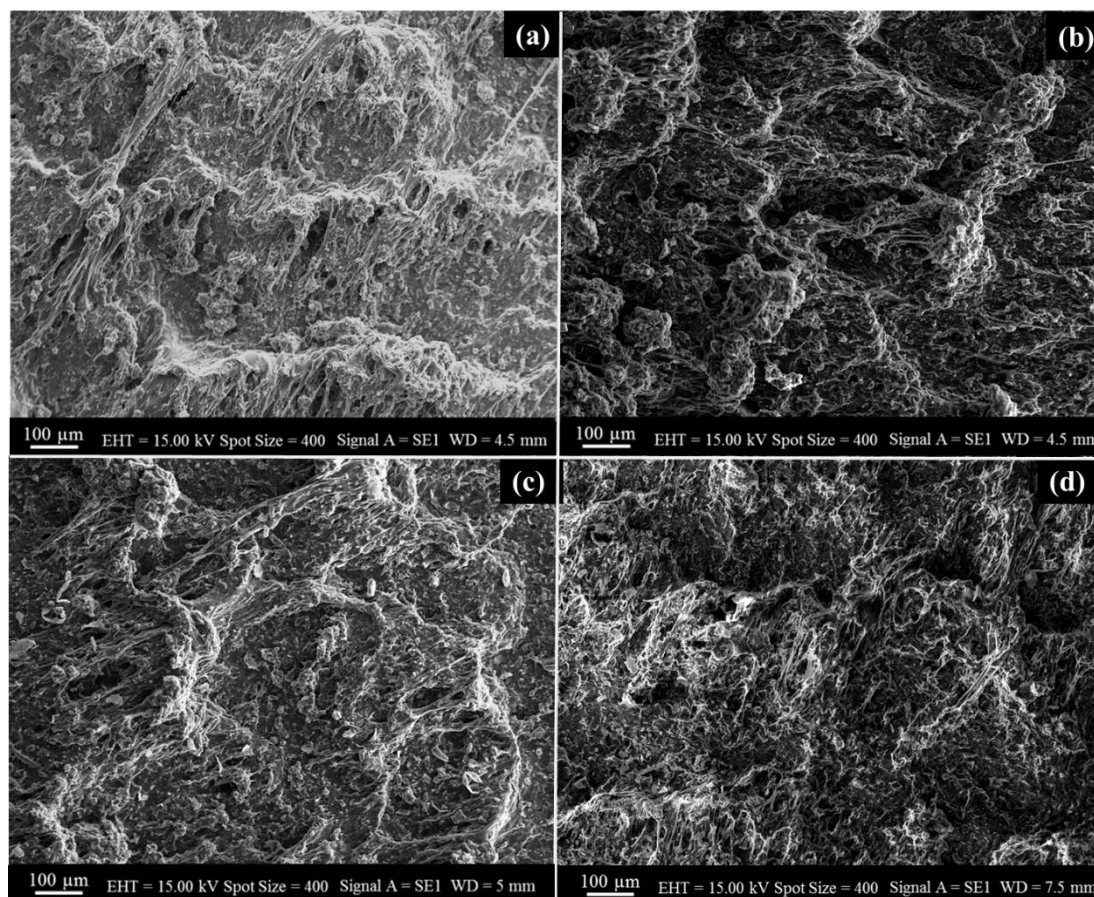
Fig. 4. 4. SEM images of NR2 after abrasion tests with different applied loads: (a) 5N, (b) 10N, (c) 15N, (d) 20N.
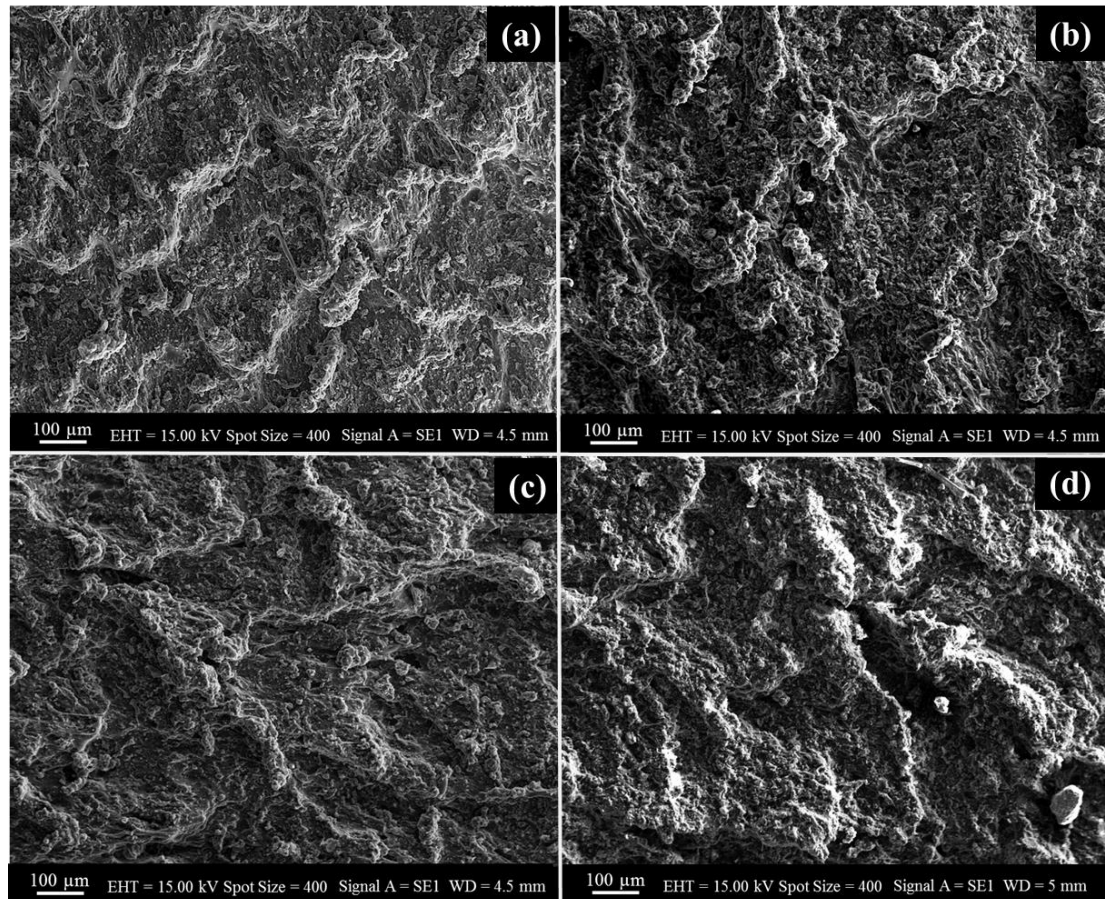
Fig. 4. 5. SEM images of NR4 after abrasion tests with different applied loads: (a) 5N, (b) 10N, (c) 15N, (d) 20N.
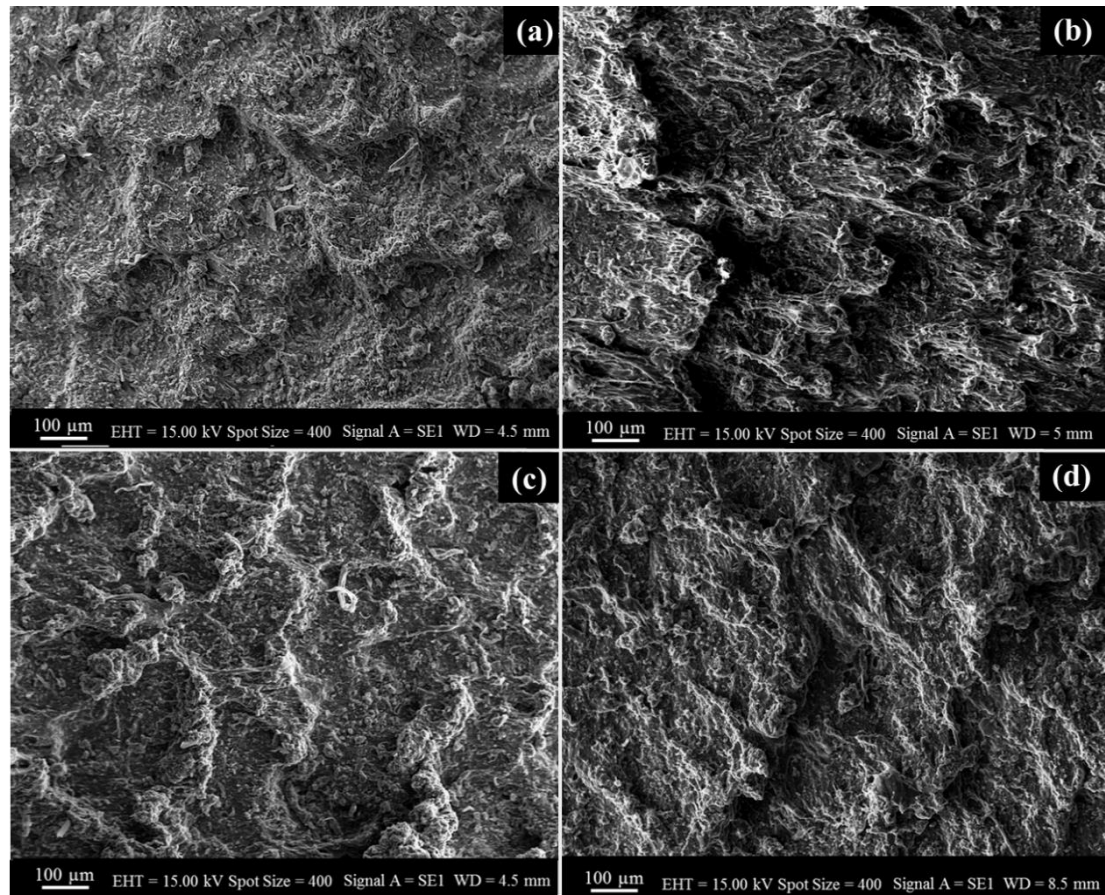
Fig. 4. 6. SEM images of NR6 after abrasion tests with different applied loads: (a) 5N, (b) 10N, (c) 15N, (d) 20N.
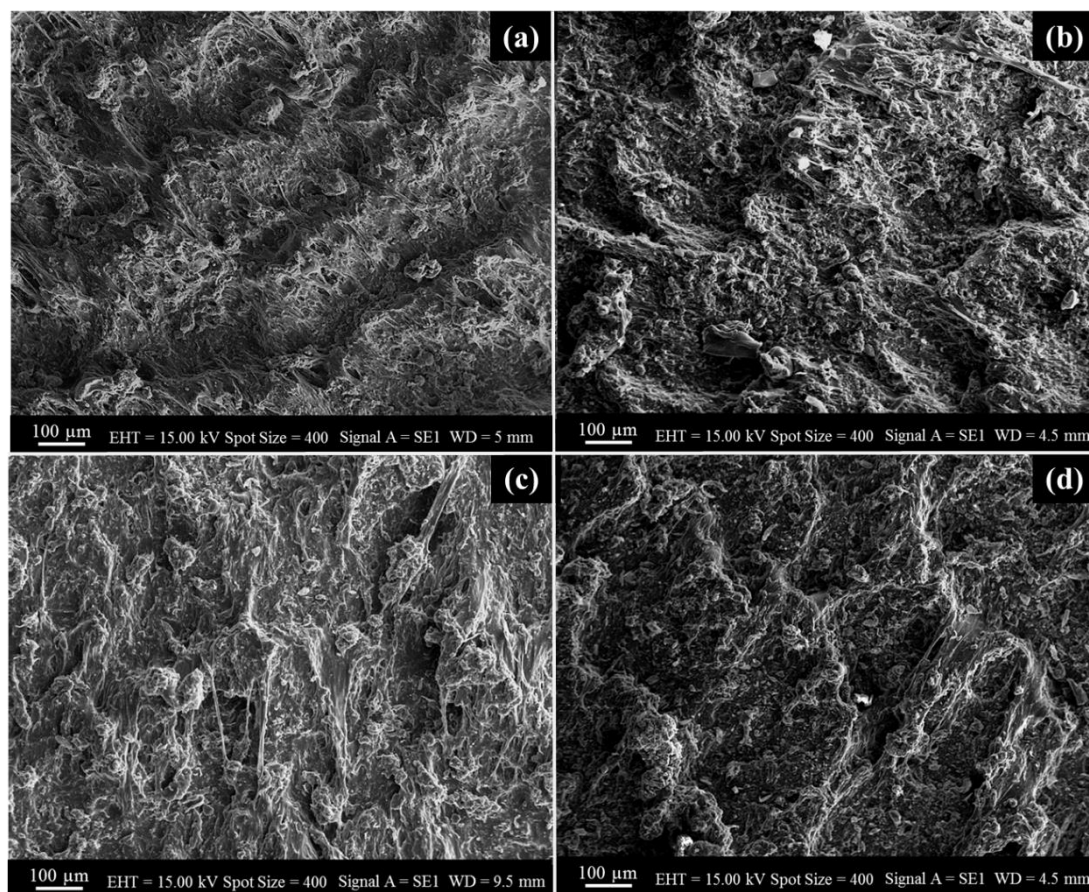
Fig. 4. 7. SEM images of NR7 after abrasion tests with different applied loads: (a) 5N, (b) 10N, (c) 15N, (d) 20N.
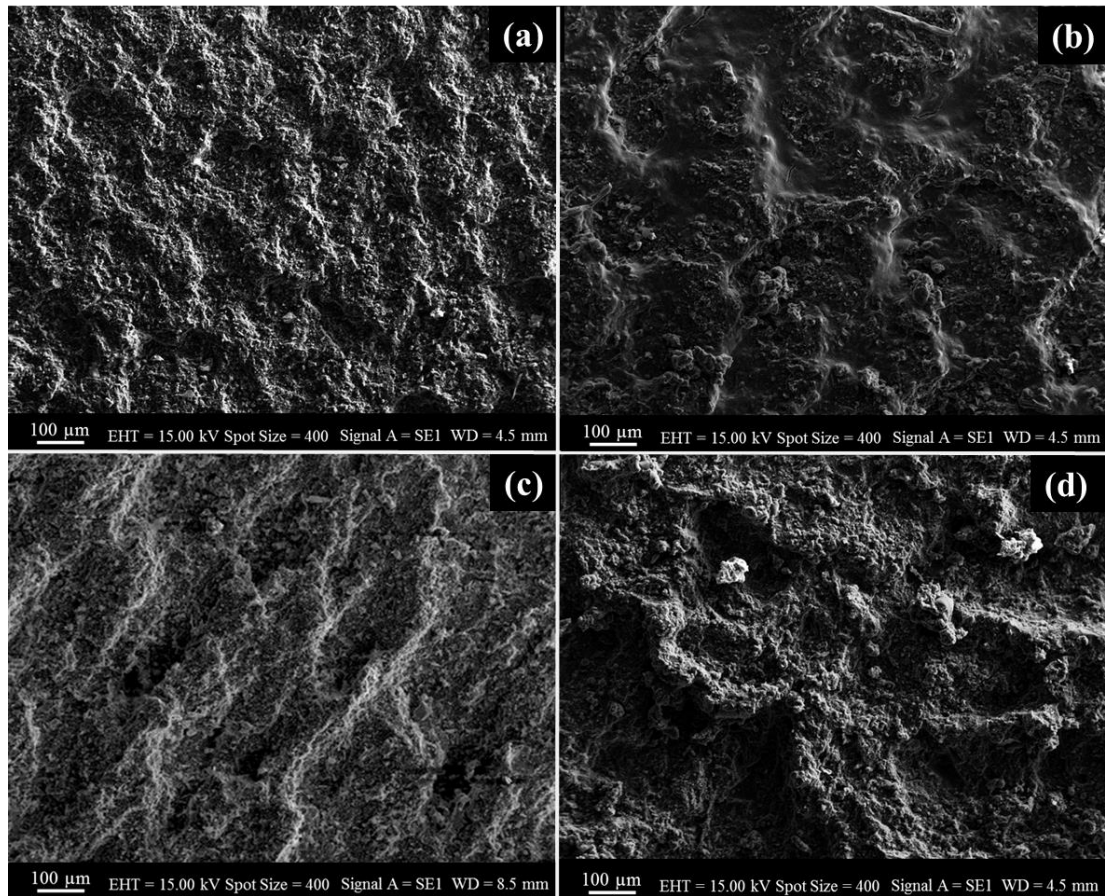
Fig. 4. 8. SEM images of NR8 after abrasion tests with different applied loads: (a) 5N, (b) 10N, (c) 15N, (d) 20N.
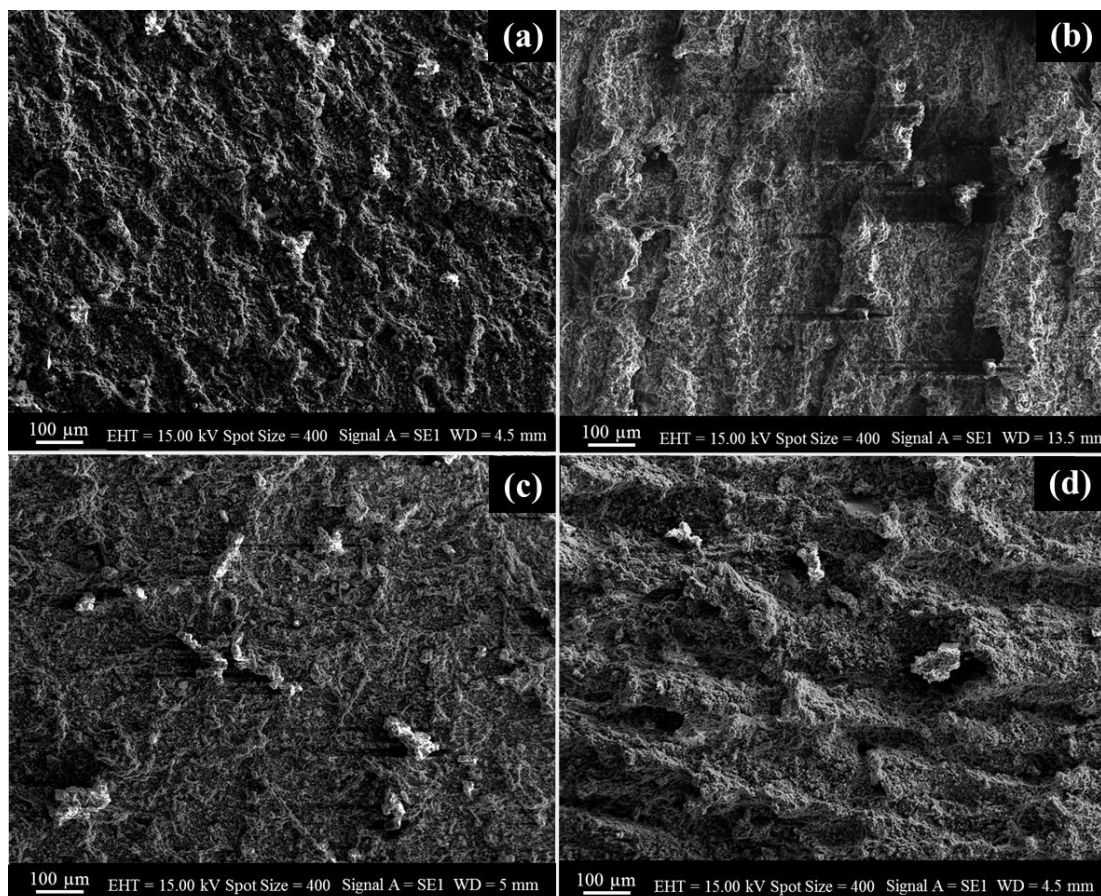
Fig. 4. 9. SEM images of SBR after abrasion tests with different applied loads: (a) 5N, (b) 10N, (c) 15N, (d) 20N.
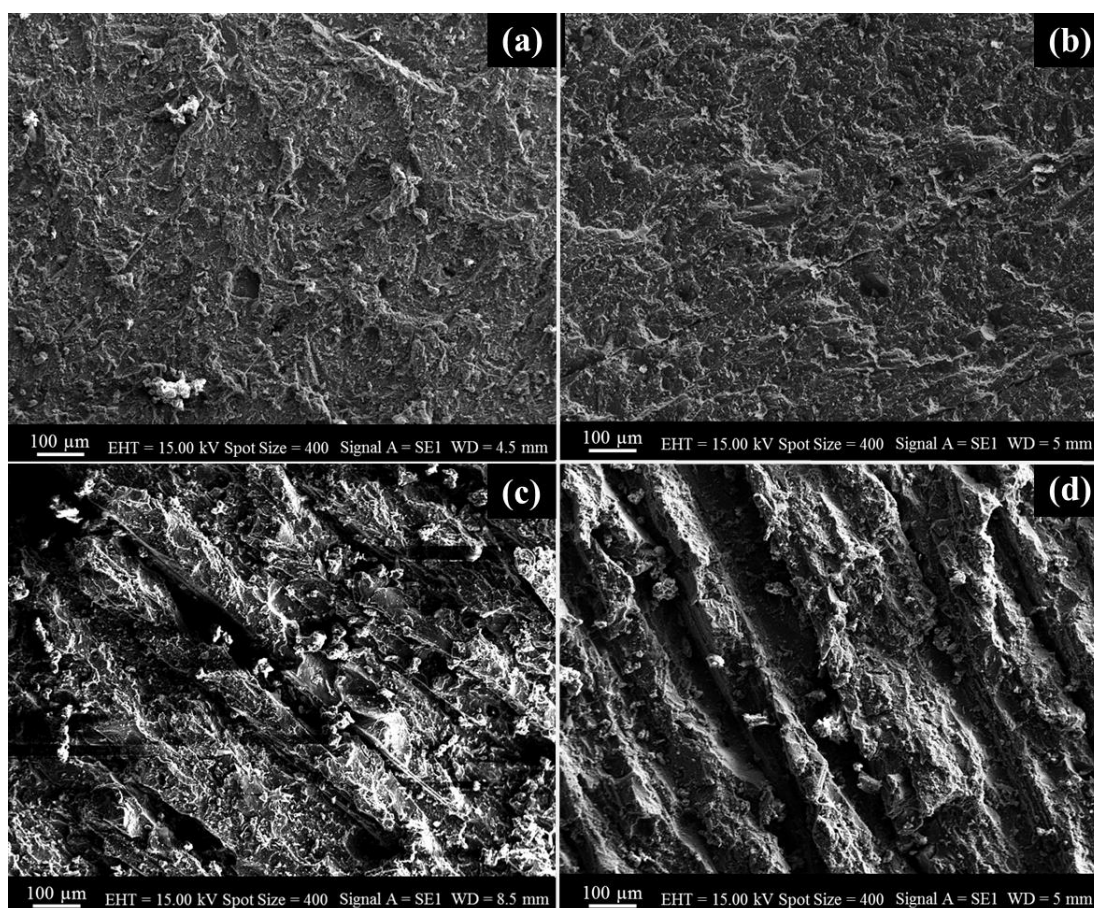
Fig. 4. 10. SEM images of NBR after abrasion tests with different applied loads: (a) 5N, (b) 10N, (c) 15N, (d) 20N.

Table 4. 1. The average size of ridge space evaluated from SEM images.

Applied Load (N)	Ridge Space (μm)					
	NR1	NR2	NR4	NR6	NR7	NR8
5	307.52±6.65	357.540±9.73	266.91±5.88	299.24±12.21	298.94±9.74	166.013±5.33
10	333.45±6.96	394.46±8.93	294.58±13.00	302.11±13.94	405.55±10.71	271.44±15.24
15	336.99±13.44	390.27±8.57	347.24±10.67	333.05±8.94	408.20±13.83	324.59±16.52
20	333.86±8.48	427.40±7.36	351.43±7.56	356.23±14.39	406.76±6.04	338.11±12.42
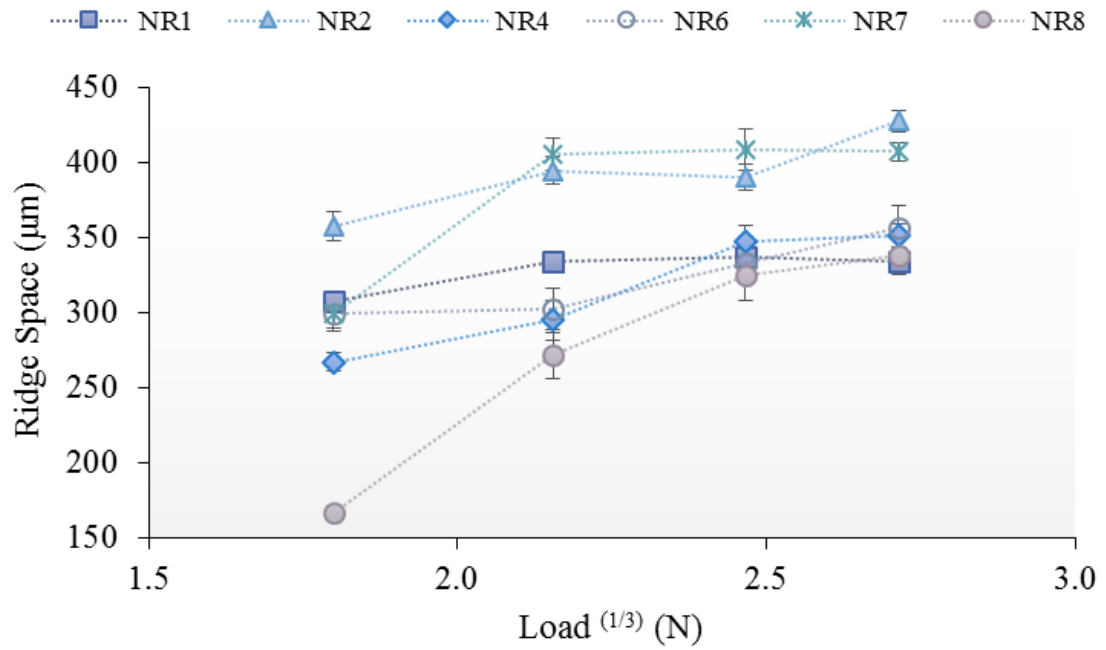
Fig. 4. 11. The ridge's space vs. normal load.

The SEM image of the collected wear debris during the two-body abrasive wear test, when the applied load is 5, 10, 15, and 20 N are shown in figures 4.12- 4.19. Table 4. 2 shows the average size of generated wear debris, which has increased with the increase of applied load. The largest change in the size of wear debris is observed for NR2.
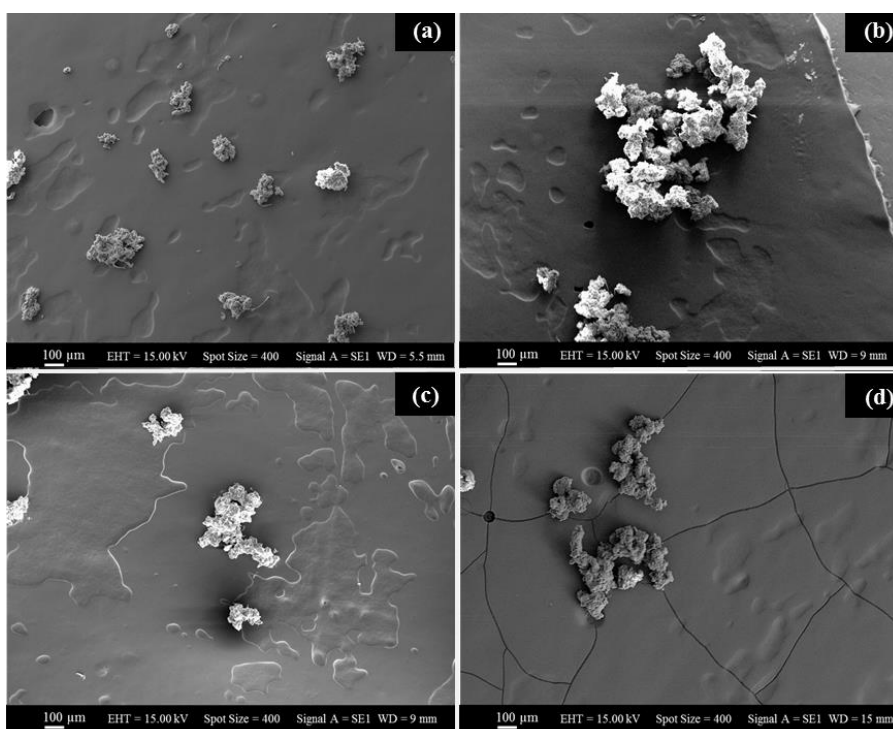
Fig. 4. 12. SEM images of NR1's debris after abrasion tests with different applied loads: (a) 5N, (b) 10N, (c) 15N, (d) 20N.
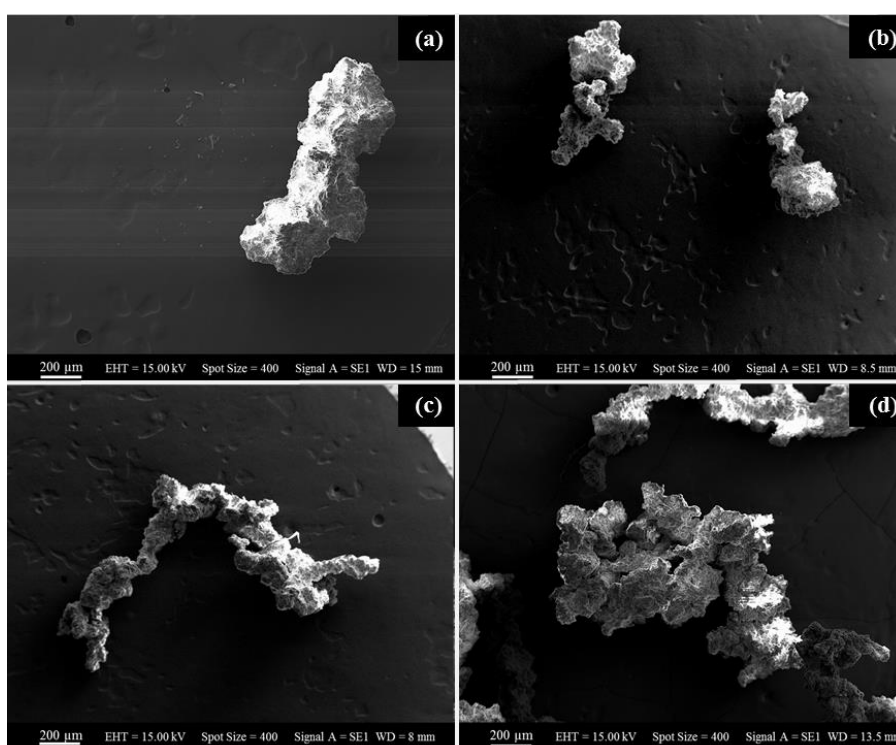
Fig. 4. 13. SEM images of NR2's debris after abrasion tests with different applied loads: (a) 5N, (b) 10N, (c) 15N, (d) 20N.
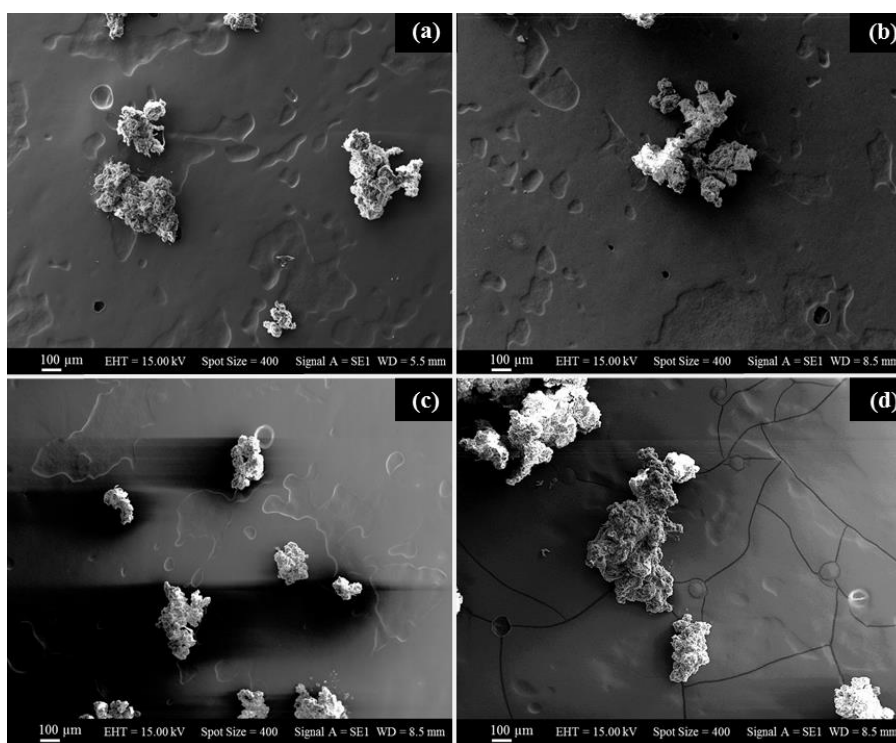
Fig. 4. 14. SEM images of NR4's debris after abrasion tests with different applied loads: (a) 5N, (b) 10N, (c) 15N, (d) 20N.
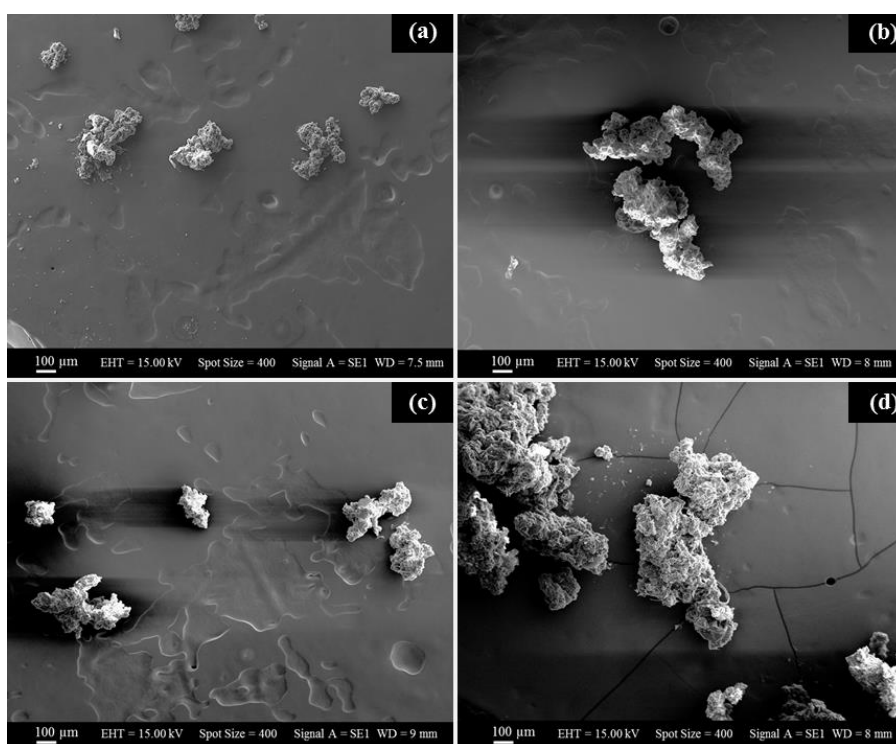
Fig. 4. 15. SEM images of NR6's debris after abrasion tests with different applied loads: (a) 5N, (b) 10N, (c) 15N, (d) 20N.
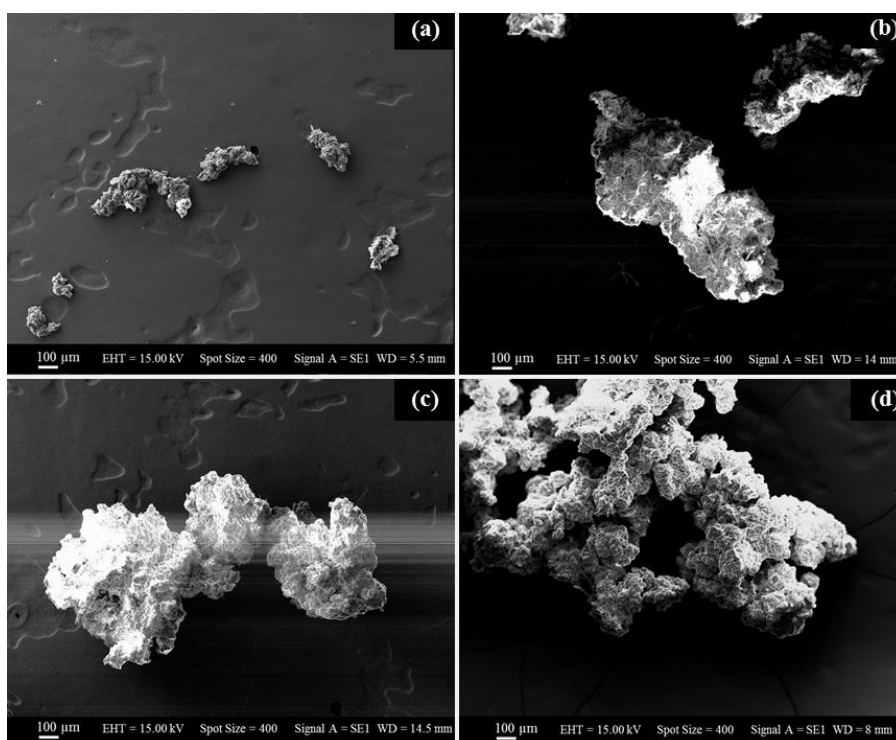
Fig. 4. 16. SEM images of NR7's debris after abrasion tests with different applied loads: (a) 5N, (b) 10N, (c) 15N, (d) 20N.
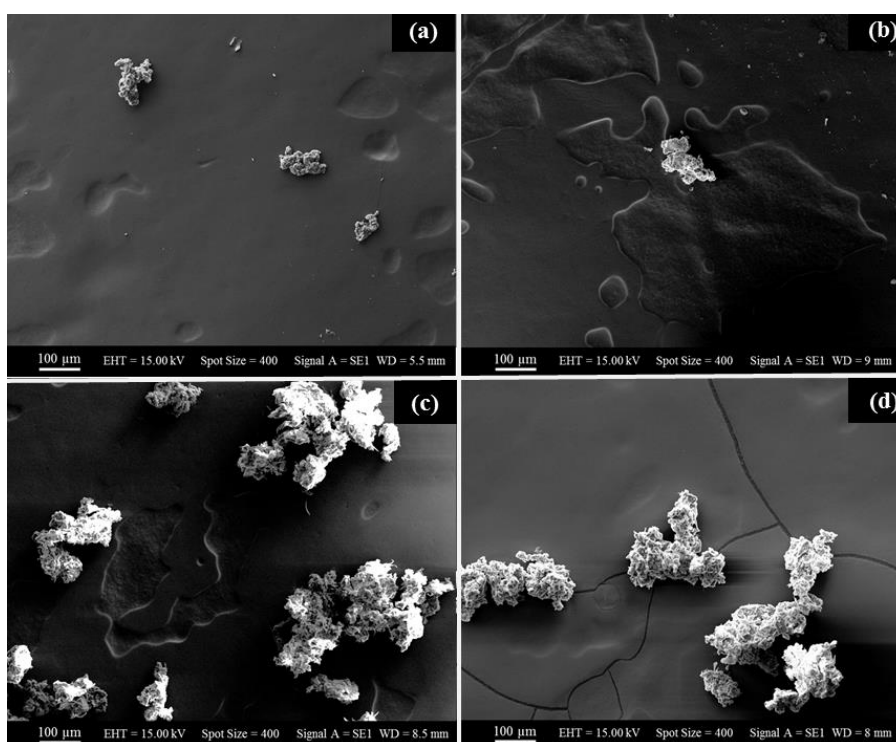
Fig. 4. 17. SEM images of NR8's debris after abrasion tests with different applied loads: (a) 5N, (b) 10N, (c) 15N, (d) 20N.
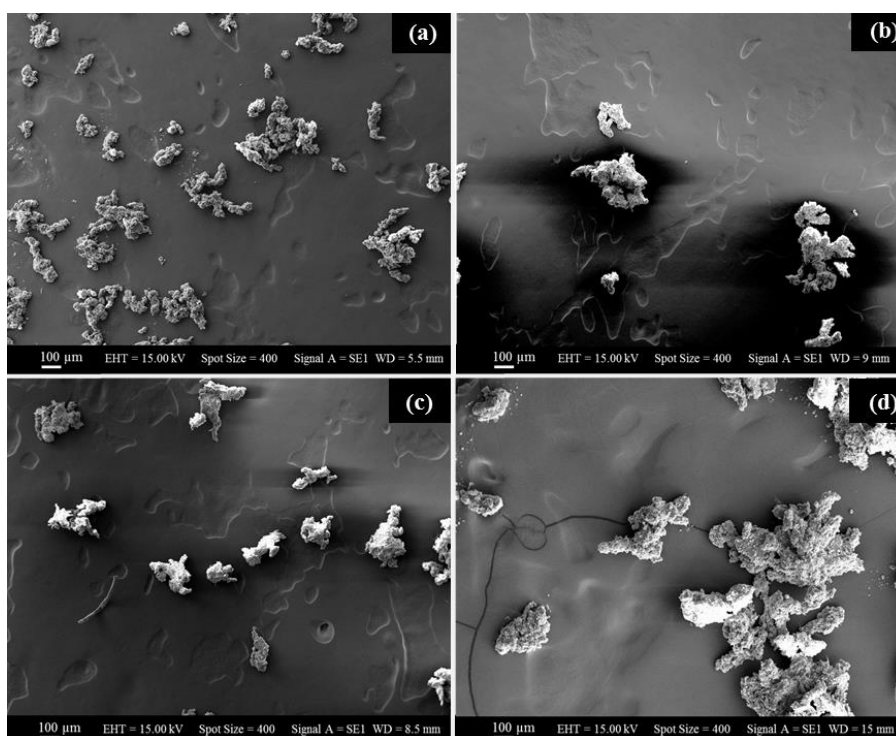
Fig. 4. 18. SEM images of SBR's debris after abrasion tests with different applied loads: (a) 5N, (b) 10N, (c) 15N, (d) 20N.
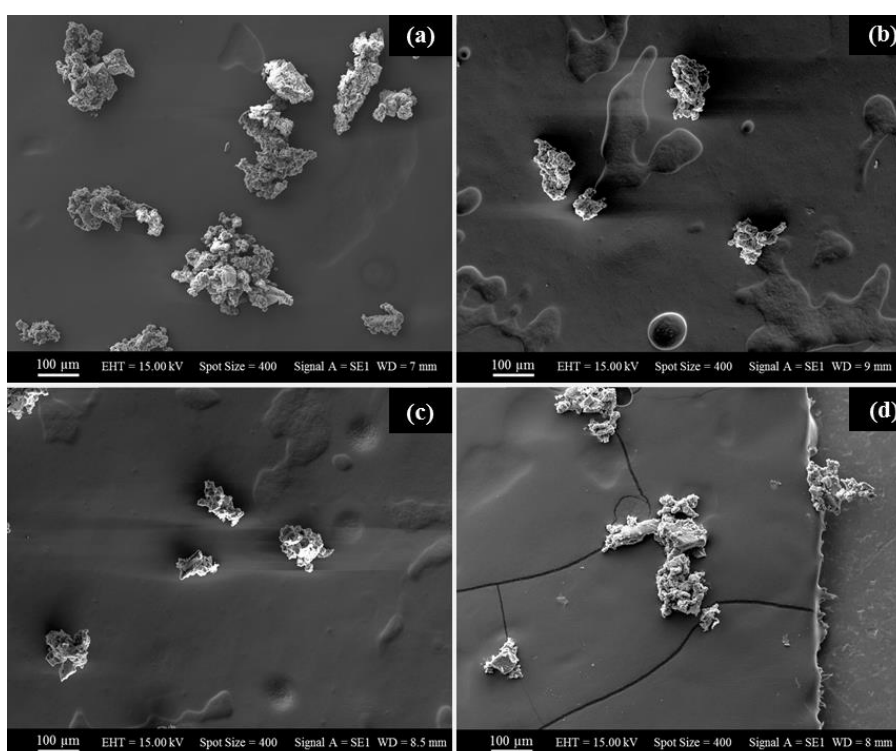
Fig. 4. 19. SEM images of NBR's debris after abrasion tests with different applied loads: (a) 5N, (b) 10N, (c) 15N, (d) 20N.

Table 4. 2. The average size of wear debris evaluated from SEM images.

Applied Load (N)	The average size of wear debris (μm)							
	NR1	NR2	NR4	NR6	NR7	NR8	SBR	NBR
5	113.39±6.68	577.55±1.48	189.73±8.48	186.08±8.12	155.08±8.77	107.42±6.51	120.26±4.57	127.71±4.24
10	137.50±4.95	571.42±9.46	252.26±9.63	250.58±9.65	661.69±11.91	113.41±6.84	124.86±2.13	131.94±6.84
15	186.72±9.21	1410.99±25.04	262.68±10.27	262.09±4.43	805.90±13.47	126.15±3.95	174.56±10.44	129.17±5.95
20	206.64±21.57	1539.60±45.23	472.40±7.61	402.37±10.65	659.54±14.04	247.05±10.99	165.63±7.83	137.88±5.27

Fig. 4. 20 indicates variation of coefficient of friction as a function normal load when the sliding speed is 0.5 m/min. COF of natural rubbers decrease with different rates as normal load increases from 5 to 20 N. On the contrary, COF of NBR increases with the increase of applied load. Fig. 4. 21 and Fig. 4. 22 demonstrate elastomers' COF as a function of normal load and WR, respectively, which descends with increase of wear rate except for NBR.
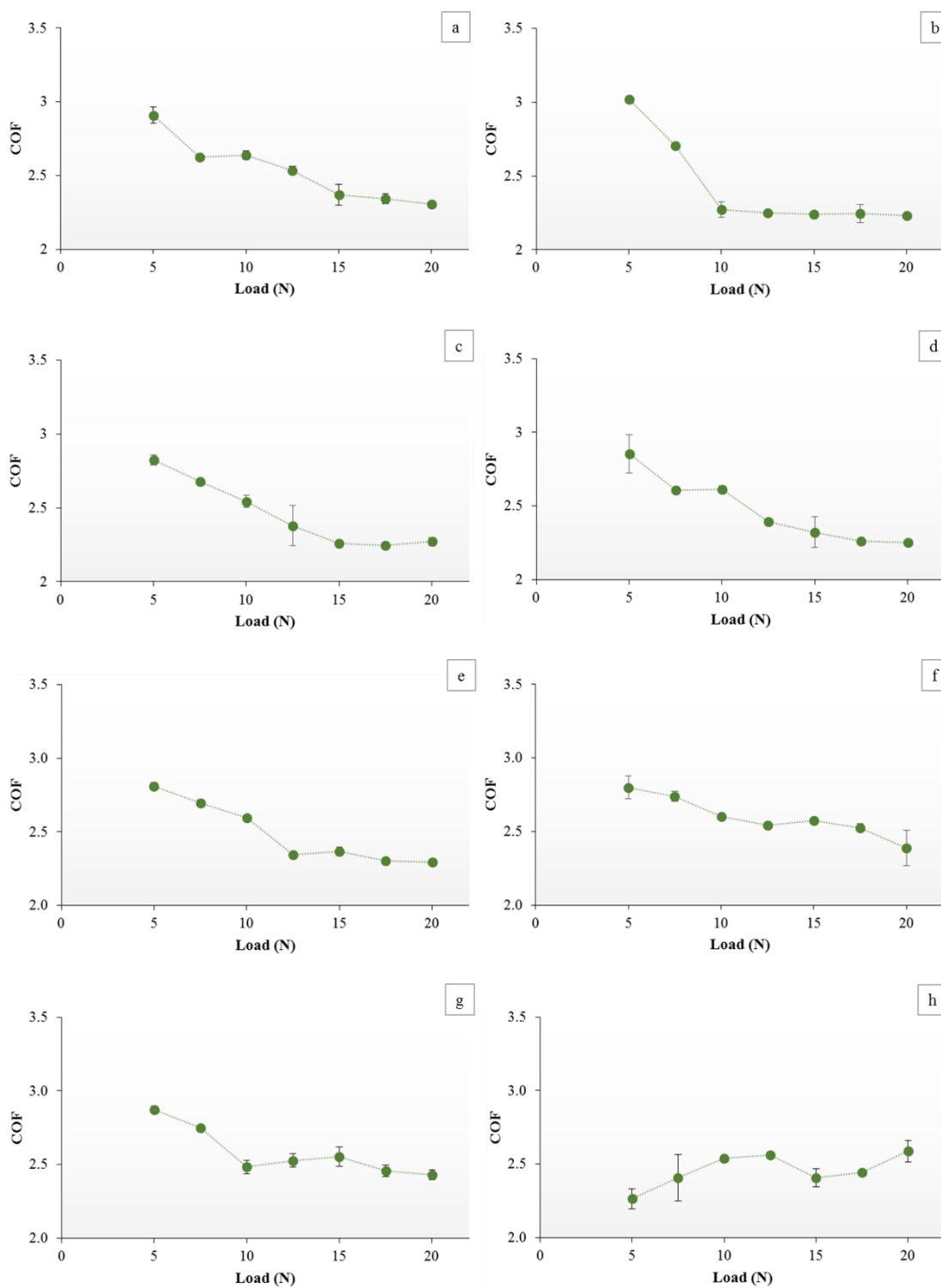
Fig. 4. 20. COF as a function of applied load (a) NR1, (b) NR2, (c) NR4, (d) NR6, (e) NR7, (f) NR8, (g) SBR, (h) NBR.

Fig. 4. 21. COF as a function of normal load
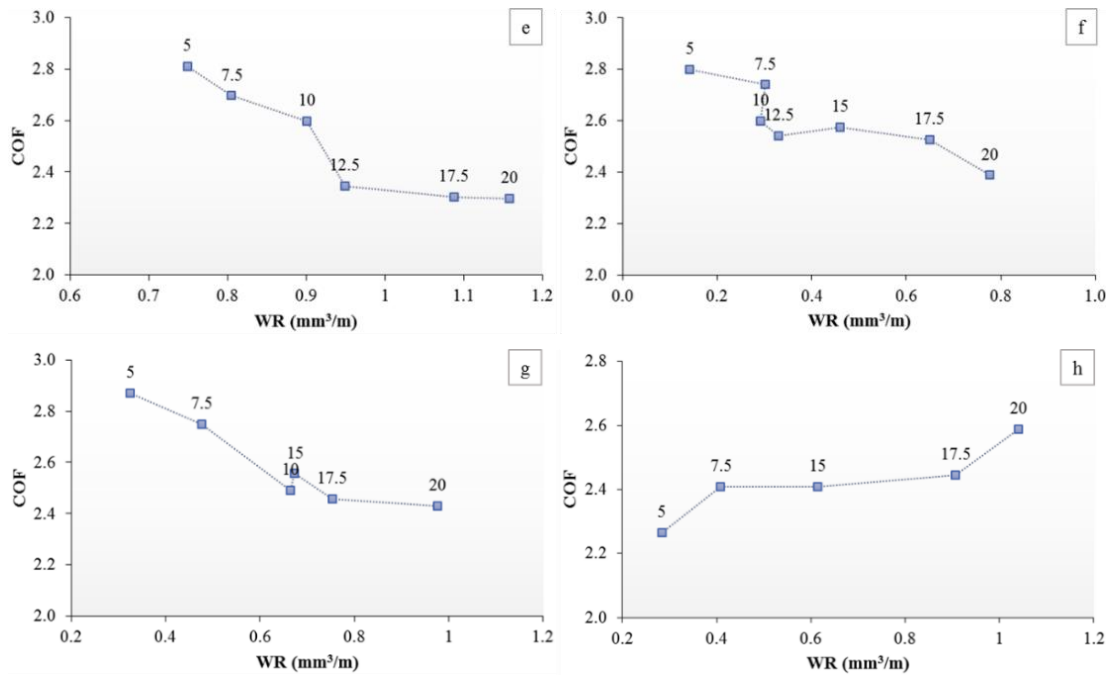
Fig. 4. 22. COF as a function of WR: (a) NR1, (b) NR2, (c) NR4, (d) NR6, (e) NR7, (f) NR8, (g) SBR, (h) NBR.

4.4. Discussion

4.4.1. Effect of the applied load on wear

4.4.1.1. Wear Rate

Under abrasive condition, with the increase of applied load, elastomers' wear rate escalates (see Fig. 4. 1), due to the higher protuberance of abrasives into the surface. It causes higher depth of penetration and greater contact area that removes materials from the surface by ploughing, micro cutting, and tearing. Therefore, the wear rate increases with the increase of the applied load. In contrast with previous findings by Harsha et. al. and Shen et. al. (Harsha and Tewari, 2003, Shen et al., 2016), who reported a linear relationship between the wear volume and load, here the relationship between wear rate and applied load is not linear, that could be attributed to the sliding velocity and generated heat. When the sliding speed is low (under 0.1 m/s), similar to their experiments' test condition the generated heat because of the friction is negligible. Nevertheless, at higher sliding speed, the produced heat during sliding influences the load and wear rate's proportion, thus the energy dissipates since the

deformation of elastomers is not entirely plastic anymore (Lancaster, 1969, Moore, 1978). Besides, the generated wear particles are trapped between the specimen and abrasive paper that leads to clogging effect and variation of the real contact area. Consequently, the increase of the wear rate with load is not linear.

The wear rate's ascending trend varies with the increase of the applied load especially for SBR and NBR (Fig. 4. 1. g and h) because of change in wear mechanism, which is observed by other researchers, too (Lancaster, 1969, Thavamani et al., 1993, Bhattacharya and Bhowmick, 2010). It is discussed in detail in section 4.4.1.2.

In addition to testing parameters, mechanical properties such as hardness (H), tensile strength (σ), elongation at break (e) and tear strength (T) have effect on the tribological behavior of the rubbers. In some cases, it is reported that wear rate is proportional to $(1/H.\sigma.\varepsilon)$ (Lancaster, 1969, Briscoe et al., 1986, Shipway and Ngao, 2003). At low temperatures and single pass tests relation between the wear rate and $(1/H.\sigma.\varepsilon)$ could be linear (Tewari and Bijwe, 1991).

At the present work, all the mechanical parameters are examined, but the product of them shows a better correlation with the wear rate rather than the individual one. For comparison, the polynomial regression (ax^2-bx+c) is applied between wear rate and the mechanical properties. The fitted lines and coefficient of determination are shown in Fig. 4. 23. At low loads, between the wear rate and $(1/\sigma.\varepsilon)$, there is a good correlation of determination ($R^2 > 0.80$); however, the relationship is not linear opposed to the findings of Lancaster et al. (Lancaster, 1968). At the initial stage of wear, when the applied load is low a limited number of abrasives are in contact with the surface of the rubber. The caused stress on the surface by the abrasives is not sufficient to remove the elastomer from the surface and it mostly deforms it. Hence, tensile strength, elongation at break, and hardness have more influence on the wear rate of the elastomers.

With the increase of the applied load, more abrasives are in contact with the surface and penetrate deeper, so hardness that hinders abrasives' penetration plays an important role. Besides, the formed cracks at initial stages grow faster and wear particles are torn off, which results in the formation of wear debris and increase of the wear rate. Thus, it could be said that hardness and tear strength are the most effective

mechanical parameters at higher loads. To support this, a graph of wear rate as a function of (1/H.T) is plotted in Fig. 4. 24. As it is observed when the regression is applied, a good coefficient of determination ($R^2 > 0.85$) is reached between wear rate and (1/H.T) at the higher applied loads.
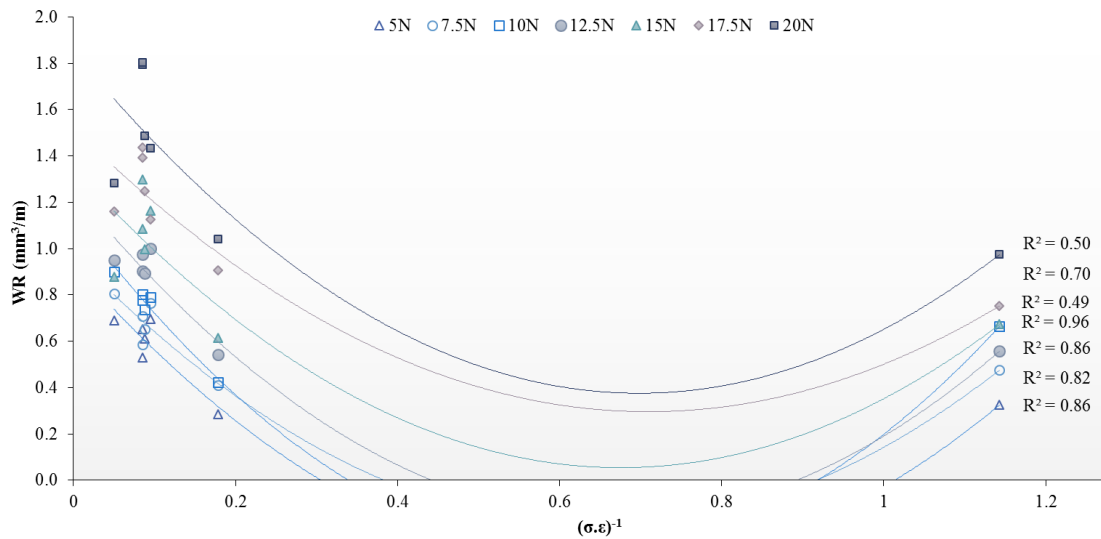
Fig. 4. 23. Wear rate vs. $(\sigma.\varepsilon)^{-1}$.
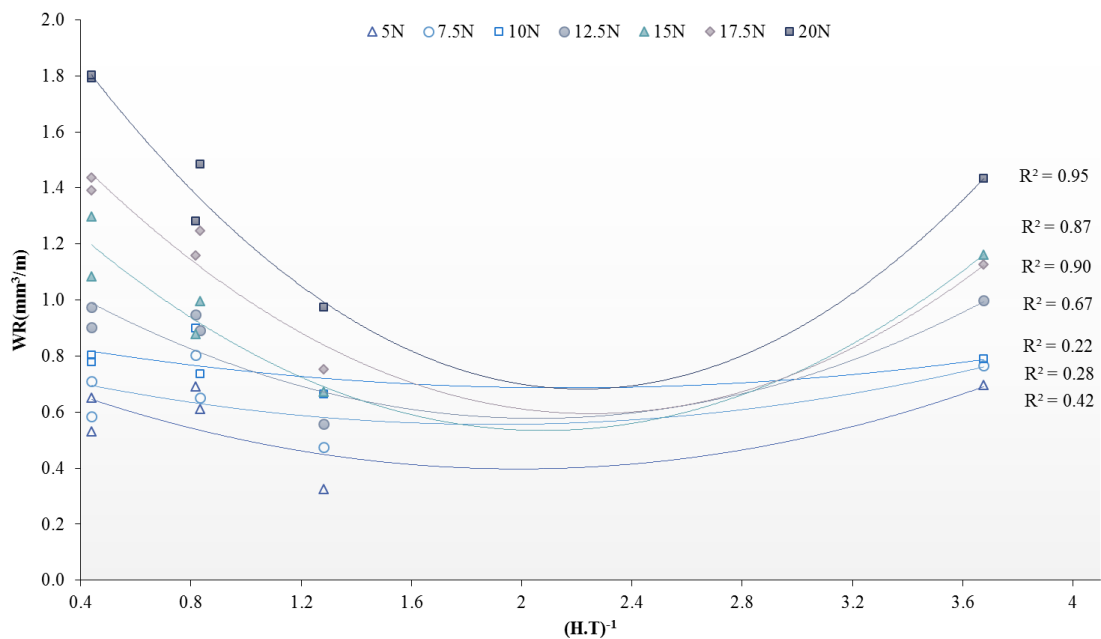
Fig. 4. 24. Wear rate vs. $(H.T)^{-1}$.

Accordingly, at low loads, the tensile strength and elongation at break are dominant mechanical properties since elastomers under low pressure mostly deform. On the other hand, with increase of the load the chance of cutting of materials increases, thus, the most influential mechanical properties are hardness and tear strength, which affect the resistance of the elastomer against the abrasives under stress.

NRs with a linear chain structure (shown in Fig. 3. 1) when are sliding against a rough surface under a range of loads show low resistance and deform more easily. Nonetheless, the molecular chain of NBR and SBR have an attached bulky group, which restricts the chain movement, as result, they resist more to deform. Besides, previous studies on the effect of tensile strength and elongation at break on wear durability of materials showed that reduction of the product of ($\sigma.\varepsilon$) results in wear resistant deterioration (Harsha and Tewari, 2003). The weakest mechanical properties belong to SBR followed by NBR compare to the other available elastomers, even though, they show better wear resistance. The comparison of the obtained results at different loads presented in Fig. 4. 2. shows that the wear rate does not follow the order and there are some exceptions. Therefore, in addition to the mechanical properties and the molecular structure other factors also play an important role on wear durability of elastomers.

As seen in Fig. 4. 23, when the elastomer slides over the rough surface under low normal load the caused stress on the surface is not enough to detach the material, thus deformation plays a pivotal role in wear. The high hardness of SBR and NBR prohibits penetration of the abrasives into the surface leading to the formation of the smaller real contact area compared to NRs. Moreover, their low tensile strength results in formation of smaller asperities and wear particles under pressure that causes low COF. Since, one of the effective factors on the wear resistant of rubber is coefficient of friction (Vaziri et al., 1988, Harsha and Tewari, 2003), low friction results in lower wear rate. It is known that tear strength affects the growth of fatigue crack, as it becomes lower, the initiated crack grows faster (Liang et al., 2010). Additionally, SBR has low tensile strength and elongation at break, thus when the force is increased, it deforms easier and cracks grow faster. Consequently, particles are rapidly torn off from the surface leading to the formation of a shorter tongue and change of the strain

level. Besides, at the crack's root, the release rate of the stored energy required to derive the wear process reduces (Liang et al., 2010), with reduction of the tear strength. These factors dominate during wear of SBR and NBR; therefore, they release less strain energy hence the wear rate is lower.

A similar case happened when Fukahori et al. (Liang et al., 2010) investigated the abrasion wear of rubbers by calculating the stored energy release. In contrast to the model's prediction, they observed that butadiene rubber (BR) with the weakest mechanical properties show the minimum wear rate. They explained that it is attributed to the asperities' geometry that affects the caused strain level on the surface and as a result the fracture resistance of the BR.

Moreover, the low wear resistant of NRs during the abrasion wear is due to their strain-induced crystallization, which is suppressed by very rapid loading rates that are encountered on the surface. At the root of NRs' asperity, the tearing energy is high so the abrasion is higher (Liang et al., 2010). In other words, the speed of loading is fast enough to beat the crystallization rate during the wear.

It is known that the wear process involves a small scale tearing process that is similar to the failure of materials under single stress or cracks growth under frequent stress, which is correlated to the tensile stress and elongation at break (Bhattacharya and Bhowmick, 2010). Among NRs with similar molecular structure, those with a higher elongation at break (NR2 and NR7) show higher wear durability under severe wear conditions. They have the ability to deform plastically before wear particles detach from the surface. Thus, at high loads, the generation of wear debris is prohibited; the formed ridges fold over the worn area and protect the weak area from further wear, thus the accelerating rate of wear lowers. While wear debris is generated easily due to cracking in elastomers with low tear strength and elongation at break, the volume loss increases. At higher loads, the determining factor is tearing; however, at lower loads, the crack growth rate and deformation control the wear. Thus, tensile strength is more influential and the lowest wear resistance belongs to NR2. This change in wear rate ranking sequence is due to the differences in the strength of rubbers that causes a change in wear mechanism.

NR4, NR6, and NR8 have similar mechanical properties, though; NR8 shows significantly high wear resistance compare to NR4 and NR6 (see Fig. 4. 2). This apparent paradox could be explained by their difference in chemical composition and geometry. The EDS analysis results (see Table 3. 3) show that there is high amount of silica (Si) and low amount of carbon (C) in NR4 and NR6 compared to NR8. Increased Si content reduces wear resistant of NR (Tangudom et al., 2014, Padenko et al., 2016). It is also reported by Wu (Wu, 2016) that fillers especially Si because of the higher surface area agglomerates at the tip of the crack, which results in weakening of the material in that direction due to the strain induced anisotropy, thus the crack growth rate for NRs with a higher amount of silica is higher. Besides, the size of the formed wear debris of NR8 is smaller than NR4 and NR6 (see Table 4. 2) thus, the abrasive paper is covered by debris and the counter face becomes smooth, hence rubber slides at ease, as a result, the volume loss is lower. The other effective parameter is the geometry of NR8 (CN bonding layer at the bottom), which results in lower strain rate and consequently low wear rate. The different wear behaviour of elastomers with same mechanical properties and molecular chain shows the importance of the asperity geometry and elastomers' chemical composition, and their effect on crack growth rate and size of formed debris.

4.4.1.2. Wear mechanism

As can be seen from figures 4-3 to 4-8, a series of ridges are formed on the abraded surface of NRs. These features are termed as wear pattern (Schallamach waves) and formed because of nucleation and developments of micro-cracks in elastomers when sliding under stress. Their geometry (size and shape) characterize the wear process (Liang et al., 2010). The formed ridges are well defined and equally spaced. By further increase of load and sliding the formed cracks at the root of the wear become deeper and the protruding flap tears off (Fukahori and Yamazaki, 1994), thus the wear debris is formed on the surface.

The formed parallel ridges, stretched particles, and small voids are observed on the worn surface of NRs, which are characteristic of the frictional wear mechanism. Hence, the wear mechanism is adhesive or frictional wear under the low applied load. With the increase of applied load, on the surface dimples, pitting marks, and voids

become more obvious (see Fig. 4. 8), which are the characteristic of fatigue wear (Thavamani et al., 1993), the wear mechanism changes from frictional wear to fatigue wear resulting in a slight change of wear graphs' slope (see Fig. 4. 1). The accelerating rate of fatigue wear is lower than the friction wear. Besides, the presence of stretched particles and voids are more obvious in SEM images of NR2 (Fig. 4. 4) and NR7 (Fig. 4. 7), natural rubbers with high elongation at the break, they severely deform before material removal.

At low applied load, SEM images of the worn surface of SBR and NBR (Fig. 4. 9. a and Fig. 4. 10. a) show formation of the ridges caused by deformation. However, the ridges are shallow with little or no pattern. The wear mechanism is adhesive wear.

With increase of the applied load from 10 N to 15 N and 20 N, rolled debris (Fig. 4. 9. c), fractured ridges, and grooves (Fig. 4. 9.d) are evident, respectively on the worn surface of SBR. At high loads, the wear mechanism shifts from frictional wear to abrasion by ploughing.

After abrasion under 10 N, ridges are not evident obviously in SEM images of NBR; instead, parallel grooves and scratches are formed as result of high pressure (Fig. 4. 10. b), indicating the plastic flow of materials or abrasion caused by ploughing (Lancaster, 1969, Muhr and Roberts, 1992). The material removal is because of the formation and propagation of micro-cracks. With the increase of the applied load to 15 N and 20 N, ploughing becomes deeper and scratches are more obvious. Fading of the ridges and presence of grooves and scratches confirm wear mechanism alters from frictional wear to abrasive wear. When the deformation changes from elastic to plastic, because of the low flexibility of elastomer the score lines (see Fig. 4. 10. b) are seen on the worn surface (Junkong et al., 2015).

On the worn surface of NRs, the average formed ridge's space (see Table 4. 1) is increased by raising of the applied load. The ridge's space and its height grow with lowering wear resistance. After reaching a critical size, the geometry of ridges remains constant (Fukahori and Yamazaki, 1994). As seen for NR4 and NR6, the ridges' space remains constant after reaching a critical size around 356 μm when the load is 15 N. The ridge space of NR7 is almost constant after reaching a critical size at 10 N.

As seen in Fig. 4. 25, the wear rate increases when the ridge's space increases until reaching a critical value. Then the material removal and wear particles' formation dominate the wear. The ridge's space correlates linearly (the coefficient of determination (R^2) is over 0.8 with the wear rate at different applied load ranged between 5 to 20N in contrast to findings of Medalia et al. (Medalia et al., 1992), who reported that there is not any correlation between the ridge's space and wear rate.
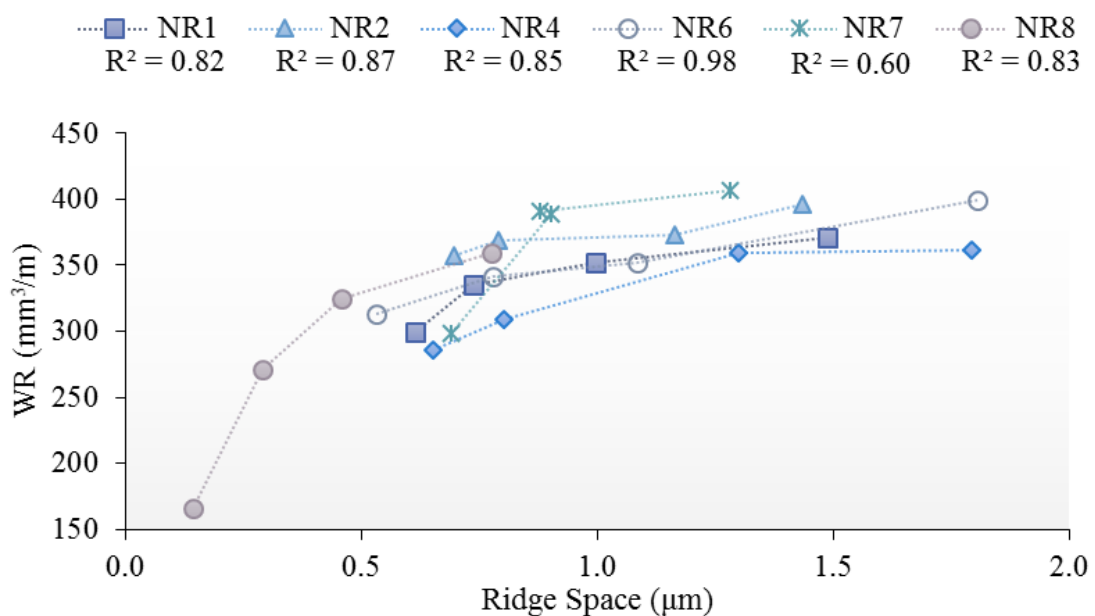
Fig. 4. 25. The average ridge's space vs. wear rate of NRs.

An average value of ridge spacing as a function of ($1/H.\sigma.\epsilon$) is plotted in Fig. 4. 26. It shows that the mechanical properties (tensile strength, elongation at break, and hardness) of NRs affect the ridge's spacing similar to the wear rate. The ridge's space is proportional inversely to the mechanical properties. To put it differently, NRs with high mechanical properties have higher wear resistant and lower ridge's space when the wear mechanism is friction or fatigue.
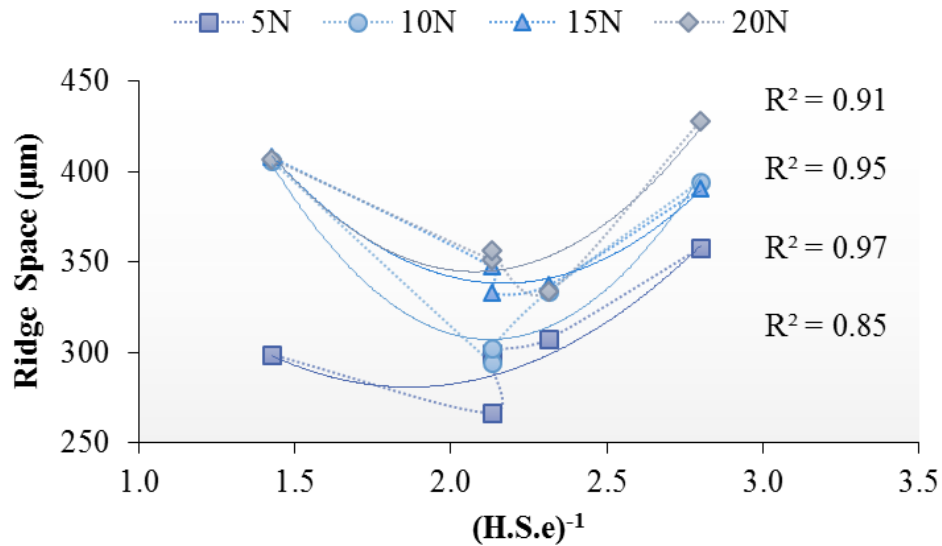
Fig. 4. 26. The average ridge's space vs. $(H.\sigma.\varepsilon)^{-1}$ of NRs.

4.4.1.3. Wear debris

According to Bhattacharya et al. (Bhattacharya and Bhowmick, 2010), there are two major types of generated wear particles during the wear: intrinsic and aggregates. The growth of microflaws and tearing of micro asperities result in the formation of intrinsic particles, which their detachment leads to the abrasion pattern's formation. The aggregates particles originate from the adhesive interaction during the slip-induced process or periodic tearing off the formed ridge's tongue. It has been reported that increase of the frictional work results in increase of the aggregates' particle size, nevertheless, it does not have any effect on the size of intrinsic particles (Bhattacharya and Bhowmick, 2010).

The SEM images (see Fig. 4. 12 to Fig. 4. 19) of the generated wear debris show intrinsic and aggregate wear debris are formed when the applied load is low (5 and 10 N) and high (15 and 20 N), respectively. However, the wear debris of SBR and NBR is also intrinsic at higher load, since instead of the ridges that act as source of the aggregates particle formation, the grooves and scratches are present on the surface (see Fig. 4. 9 and Fig. 4. 10). The generated wear particles of elastomers with the highest elongation at break (NR2 and NR7) are continuous and elongated. The wear debris of other elastomers is deformed and discontinued.

The average size of wear debris increases with the increase of the normal load (see Table 4. 2). At low loads, the wear debris is loose and granular, which becomes agglomerated abrading under the higher applied loads.

The wear debris of NBR and SBR is small, due to their high hardness. Among the NRs with similar hardness, NR2 and NR7 have the longest wear debris since the deformability of the elastomer is high and its frictional work increases, resulting in the formation of the aggregate particles.

4.4.2. Effect of the applied load on the friction

As mentioned in chapter 2 (Persson et al., 2008, Braun et al., 2016), there are two major effective parameters that contribute to the friction during the sliding of the elastomers against a rough surface: adhesion and deformation (hysteresis). Adhesion between the elastomer and abrasive causes adhesive friction and the hysteresis friction is caused by the energy loss resulted from plastic deformation of the elastomer and wear debris formation (Liang, 2007, Coronado, 2015).

The average COF of NRs and SBR is reduced with the increase of normal load shown in Fig. 4. 20. When the applied load is low, the adhesion is the dominant factor that contributes to the friction. As it is known, in addition to the applied load, the surface roughness affects the adhesion friction (Zsidai et al., 2002). Thus, the COF reduction could be due to increase of the surface roughness (see Fig. 6. 4), which reduces the real contact area (Braun, Steenwyk et al. 2016). Moreover, as reported by Basak et al. (Basak et al., 2014) the coefficient of friction varies with load that transfers from the counter-body to the interface of tribo-contacts in both soft and hard surfaces. In case of the relatively soft surface (Basak et al., 2010), part of the normal load became absorbed in the materials due to their predominant elastic behaviours, which in turn reduces the effective normal load and thus change the effective load scale.

Apparently, there is a contrast with previous studies (Myshkin et al., 2005, Quaglini et al., 2009), which reported the real contact area increases with the increase of the load. Nevertheless, it should be considered that the relation between force and the real contact area is mostly for elastic or elastoplastic deformation contacts. By increase of applied load, the ridges and wear debris are formed on the surface of elastomers, due

to their mechanical properties, which results in increase of roughness and decrease of the real contact area. Thus, the COF decreases with the increase of normal load, when the dominant friction is adhesive.

In contrast with other specimens, COF of NBR enhances with increase of the applied load. Several factors affect this different trend. Firstly, since NBR has high hardness, deeper penetration of abrasives into elastomer requires higher tangential force to move on its hard surface. Then, the formed wear particles are so small (see Table 4. 2), therefore the real contact area grows because of embedded fine wear debris on the surface of rubber and abrasive paper (Boissonnet et al., 2012). The fine wear debris act as a transfer film that is formed when the wear mechanism is abrasion/ploughing, hence the friction turns to be between elastomer on elastomer that has a higher adhesion because the contact is between two material with same atomic composition and molecular structure. With the raise of the applied load, however, the formed layer's thickness reduces because of detaching of the loose particles and greater compaction (Zsidai et al., 2002), thus the adhesion friction's contribution to the friction declines resulting in decrease of COF and change of the slope with variation of the load (see Fig. 4. 20. h).

Comparison of COF of elastomers (see Fig. 4. 21) shows at low loads that the dominant factor is adhesive friction; the elastomer with high elongation at break (NR2) leading to high ridge's space and larger real contact area has the highest COF, followed by COF of SBR and NR1. Compared to other elastomers they have low tear strength, therefore a thin layer of particles is formed at the counterface leading to increase of the real contact area. Additionally, higher hardness of NBR results in the smaller contact area, at initial stages, thus its COF is the lowest.

With the increase of the applied load, the influence of adhesion friction and deformation friction on COF decreases and increases, respectively. In other words, the response of COF depends more on the surface deformation and the energy consumption. The major energy-consuming mechanism, which affects deformation friction is the formation of the wear debris. That is why the hardness and tear strength are important parameters and their effect on COF becomes more significant. NBR, SBR, NR8, and NR1 show higher COF in comparison with other rubbers. It is

attributed to their resistance to deformation, thus the required tangential force and the energy loss are increased resulting in increase of the deformation friction. Simultaneously, with increase of the applied load, the ridge space reaches to a constant value and does not change significantly that affects real contact area. Besides, the generation of wear particles acting as a third party reduces the real contact area (Mofidi, 2009). As a result, COF of other elastomers drops with further increase of the applied load. Moreover, NRs have a linear molecular chain with excellent flexibility, which easily deforms and show less resistance to the sliding, thus they have lower COF compare to SBR and NBR with an attached bulky group to their molecule structure. This attachment makes the sliding harder and movement of the molecular chain is restricted leading to the higher COF.

Consequently, the variation of coefficient of friction of elastomers with increase of the normal force depends on the wear mechanism, mechanical properties, and contribution of adhesive or deformation on friction, COF may increase or decrease.

Fig. 4. 22 indicates a correlation between COF and wear rate, under different applied load. As can be seen, wear rate responds in accordance with the friction behavior. It is observed that NRs, with lower wear rate, have higher COF, on contrary, NBR at low applied load has the lowest COF for the lowest wear rate. It supports the proposed equation (see Eq. 2.4) by Lancaster and Ratner (Lancaster, 1968) who claimed there is a relationship between the wear volume and coefficient of the friction. However, it shows this relation could be direct or inverse. As COF itself varies with the variation of the applied load and mechanical properties of the elastomer.

4.5. Summary

- Generally, the greater applied load results in higher wear rate, due to deeper penetration of abrasives, greater real contact area, and more energy input, thus the material reaches its critical fracture energy and tears quickly.
- The combination of several mechanical properties affects the wear rate and wear mechanism of elastomers. In addition to the mechanical properties, the geometry of rubber, molecular chain's structure, and chemical composition also have an effect on tribology behavior of them.

- The wear mechanism of elastomers under the pressure is friction wear, which is combined with fatigue wear with increase of load for NRs. However, the wear mechanism of SBR and NBR changes to abrasive wear by ploughing and cutting with increase of the applied load.

- Elastomers with the highest elongation at break have the longest wear debris. Those with higher hardness have the smaller debris.

- The COF of elastomer varies with increase of the applied load. It decreases for NRs and SBR and increases for NBR. The effective parameter is their mechanical properties, which influence adhesion and deformation friction by changing the participation of the real contact area and resistance to deformation. It depends on dominant parameter; COF could be ascending or descending.

- Mechanical properties and wear mechanism have effect on real contact area, third body formation, and deformation ability of the rubbers.

Chapter 5. Effect of the abrasive particle size

5.1. Introduction

Abrasive wear is one of the most common and destructive type of wear (Zum Gahr, 1987, Stachowiak and Batchelor, 2002, Williams, 2005, Petrica et al., 2013, Ratia et al., 2014, Hakami et al., 2017), which is defined as a displacement of materials from the surface due to the protuberance of the hard abrasive particles (Lancaster, 1969). Generally, abrasive wear is categorized into two types: (a) two-body and (b) three-body (Williams, 2005, Petrica et al., 2013). In both cases, the abrasives are harder surface or foreign particles such as sand and wear debris, which are present in the system and penetrate into the softer material (Williams, 2005, Woldman et al., 2013). The abrasive particles' properties such as hardness, shape, and size also influence the tribological behaviour of different materials (Stachowiak and Stachowiak, 2001, De Pellegrin et al., 2009a, Coronado and Sinatora, 2011, Hamid et al., 2013). The abrasive particles' size effect on the wear and friction of metals has widely investigated. Nevertheless, there are limited studies on the effect of abrasive particles' size on tribology behaviour of elastomers.

In this chapter, the effect of the abrasive particle size is investigated on wear and friction behaviour of elastomers. The results will lead to the better understanding of the tribological behaviour of elastomers used in industrial applications associated with size and nature of abrasive, controlling wear rate and thus prolonging the service life of them.

5.2. Methods

For these experiments, eight different elastomers as specimen, wear test machine, friction test rig, and secondary electron microscope, described in chapter 3 are used. The parameters for wear test are: abrasive particle size 82,125, 269, and 425 μm, sliding speed 0.32 m/s, sliding distance 40 m, and applied load 10N. The parameters for the friction test are: abrasive particle size 82,125, 269, and 425 μm, sliding speed 0.25, 0.5, and 1 m/min, sliding distance 10 cm, and applied load 10N.

5.3. Results

The wear rate as a function of the abrasive particle size is presented in Fig. 5. 1. With the increase of the abrasive particle size from 82 μm to 425 μm, the wear rate increases with different rates for each elastomer.
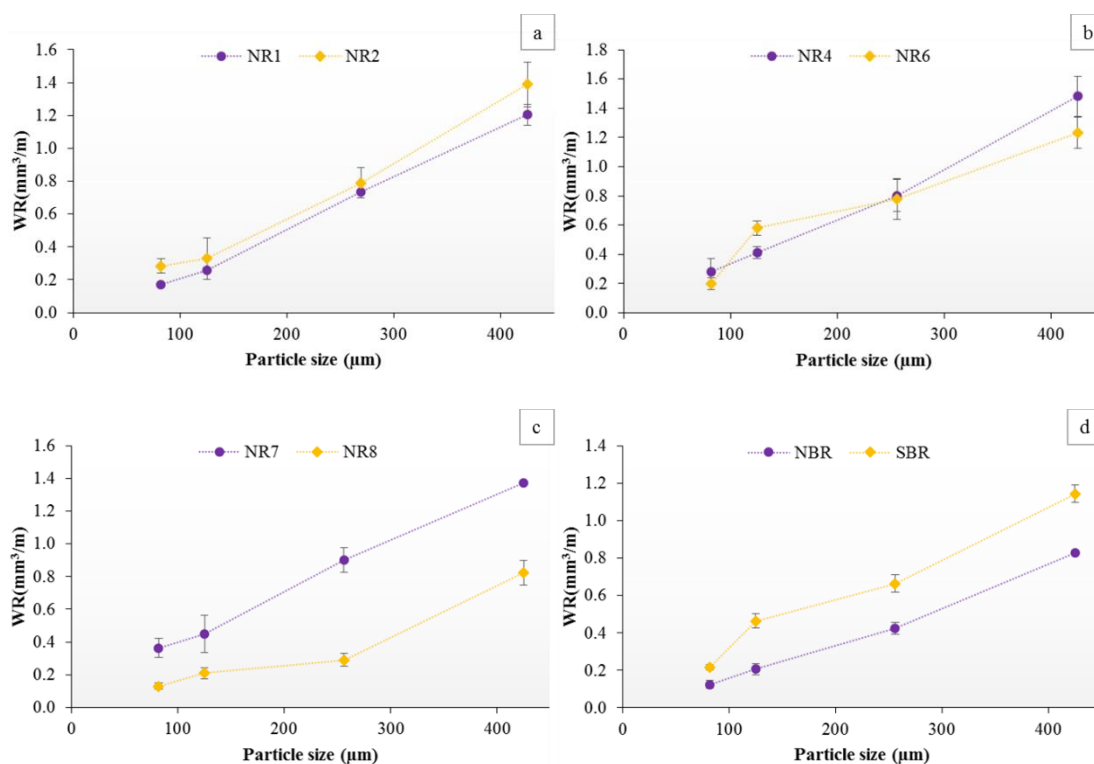
Fig. 5. 1. Wear rate as a function of abrasive particle size: (a) NR1 and NR2, (b) NR4 and NR6, (c) NR7 and NR8, (d) SBR and NBR.

The comparison of the elastomers' wear rate as a function of different abrasive particle size, demonstrated in Fig. 5. 2, shows NBR and NR8 have the lowest wear rate, whereas the highest wear rate values belong to NR7 and NR4.

SEM images of worn surfaces of abraded by different abrasive particle sizes are shown in figures 5.3-5.10. Generally, the displacement of the material in response to the tangential force is attributed to the rolling, sliding, tearing and cutting leading to the formation of the ridges and furrows. The formed ridges protect the surface from further abrasion by lowering the real contact area (Junkong et al., 2015). Table 5. 1

and Fig. 5. 11 show the average ridge's space measured by ImageJ software and the relation between the ridge's space and abrasive particle size, respectively.
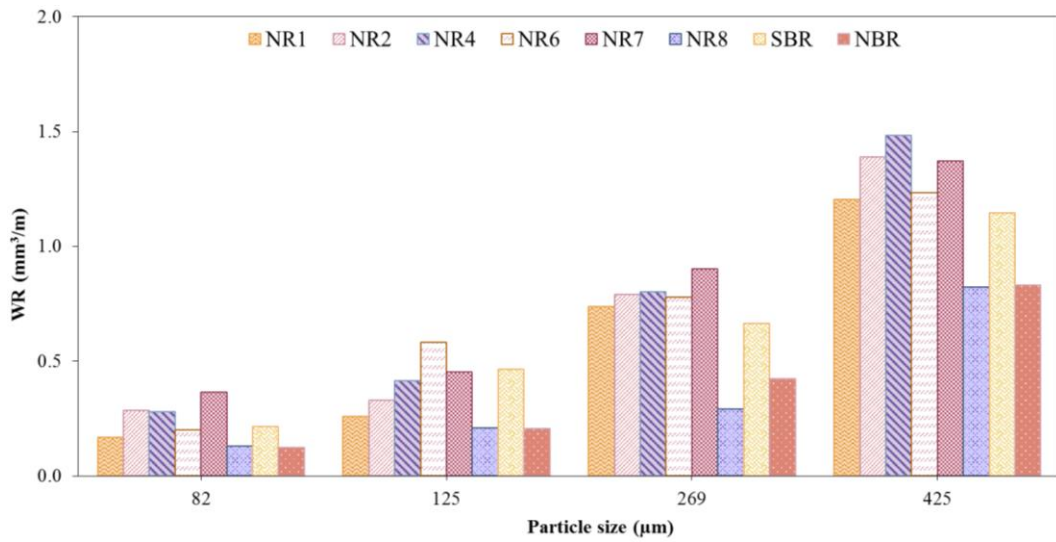
Fig. 5. 2. Wear rate as a function of abrasive particle size.
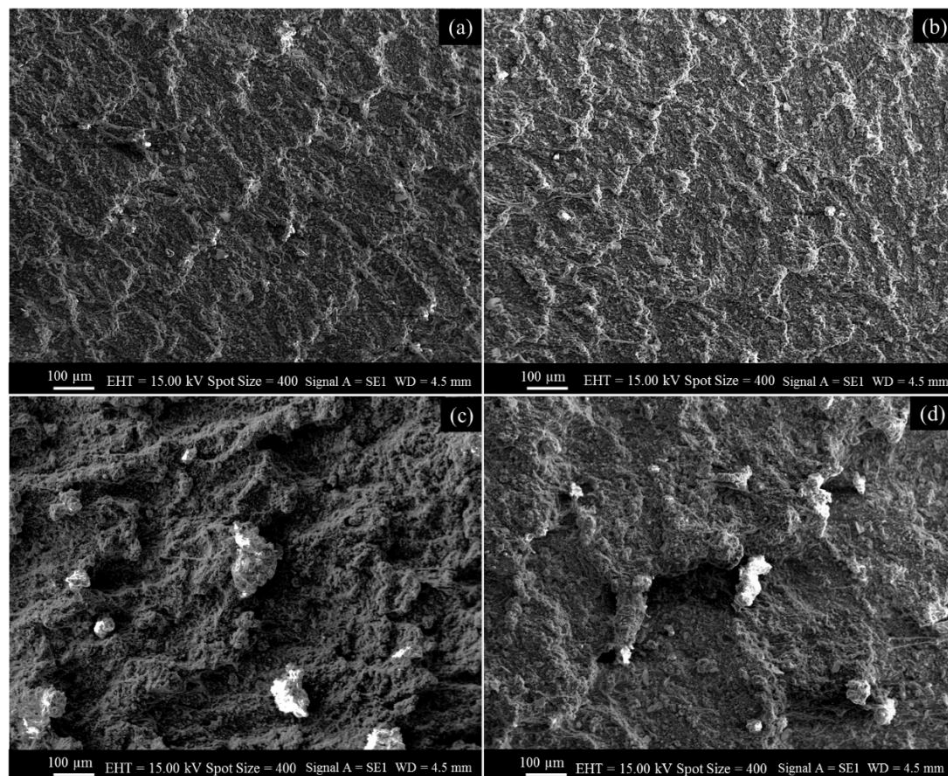
Fig. 5. 3. SEM images of NR1 after abrasion tests with different sized abrasive particles: (a) 82 µm, (b) 125 µm, (c) 269 µm, (d) 425 µm.
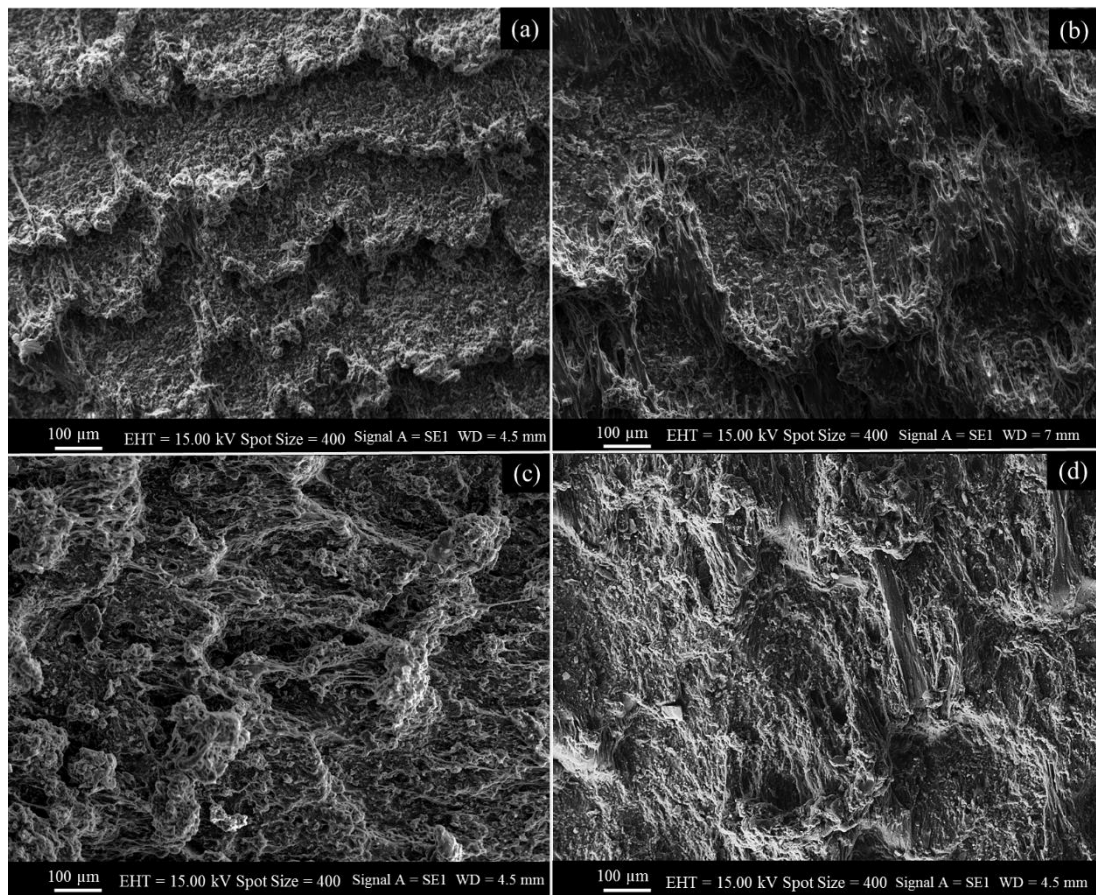
Fig. 5. 4. SEM images of NR2 after abrasion tests with different sized abrasive particles: (a) 82 μm, (b) 125 μm, (c) 269 μm, (d) 425 μm.
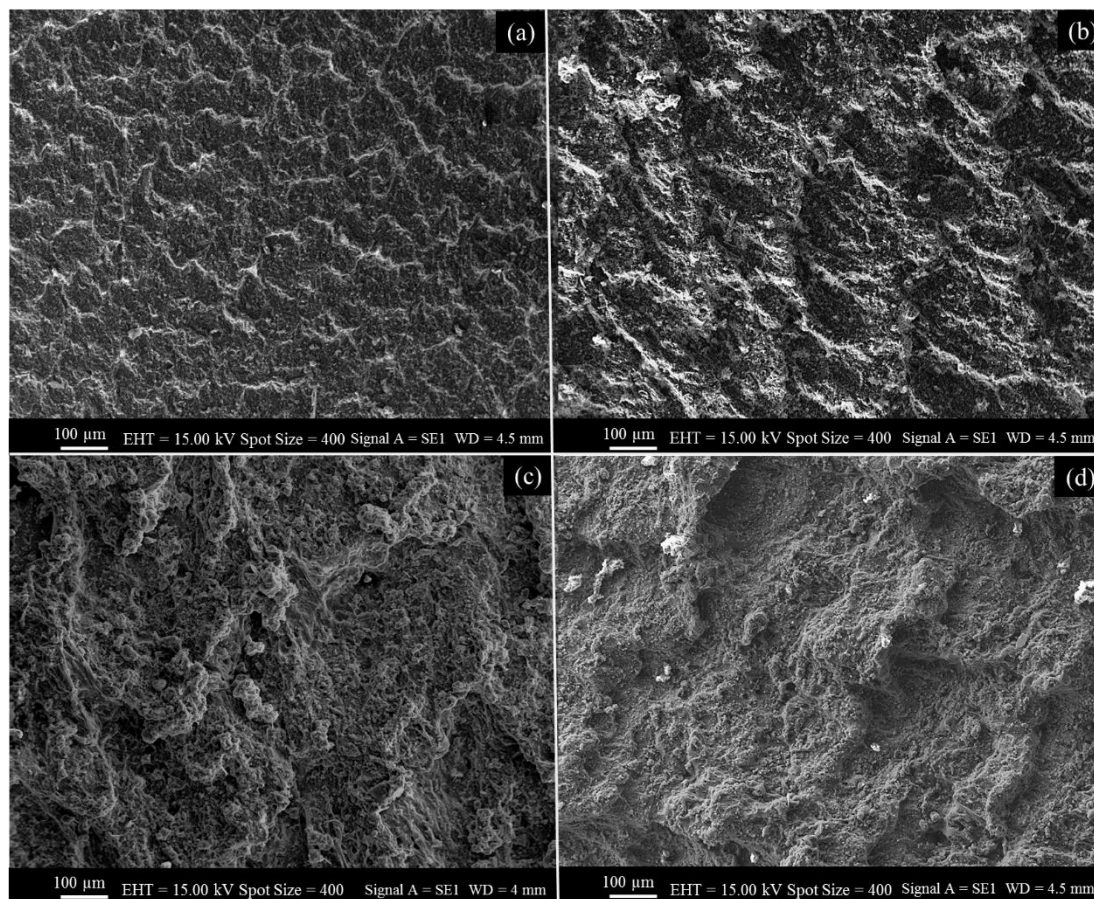
Fig. 5. 5. SEM images of NR4 after abrasion tests with different sized abrasive particles: (a) 82 µm, (b) 125 µm, (c) 269 µm, (d) 425 µm.
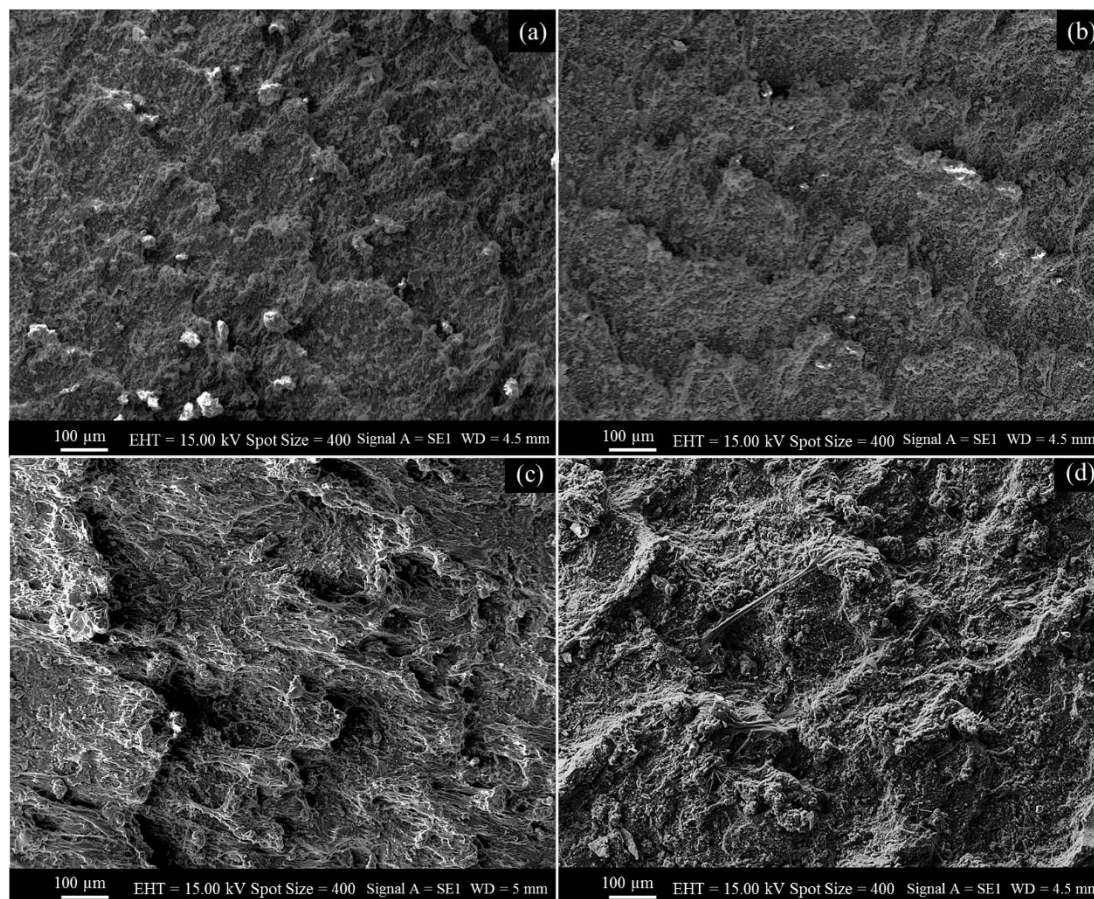
Fig. 5. 6. SEM images of NR6 after abrasion tests with different sized abrasive particles: (a) 82 µm, (b) 125 µm, (c) 269 µm, (d) 425 µm.
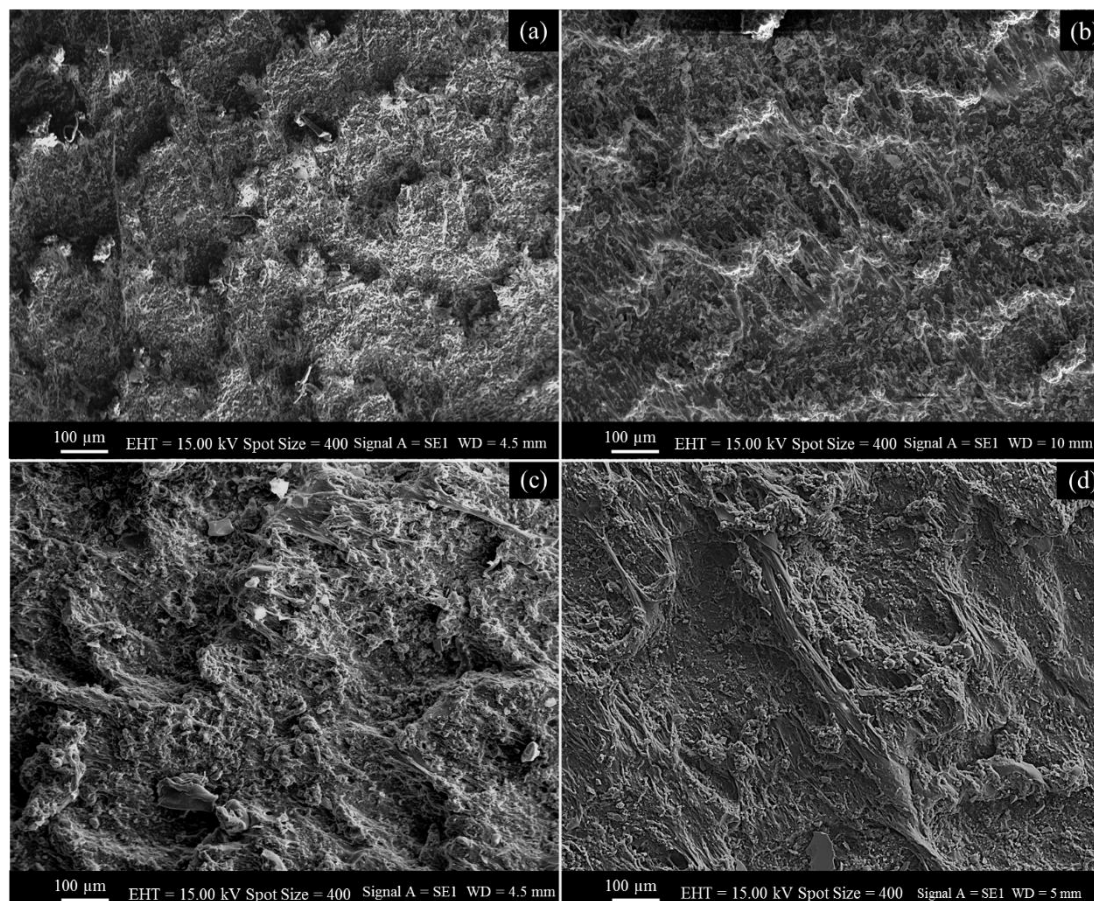
Fig. 5. 7. SEM images of NR7 after abrasion tests with different sized abrasive particles: (a) 82 µm, (b) 125 µm, (c) 269 µm, (d) 425 µm.
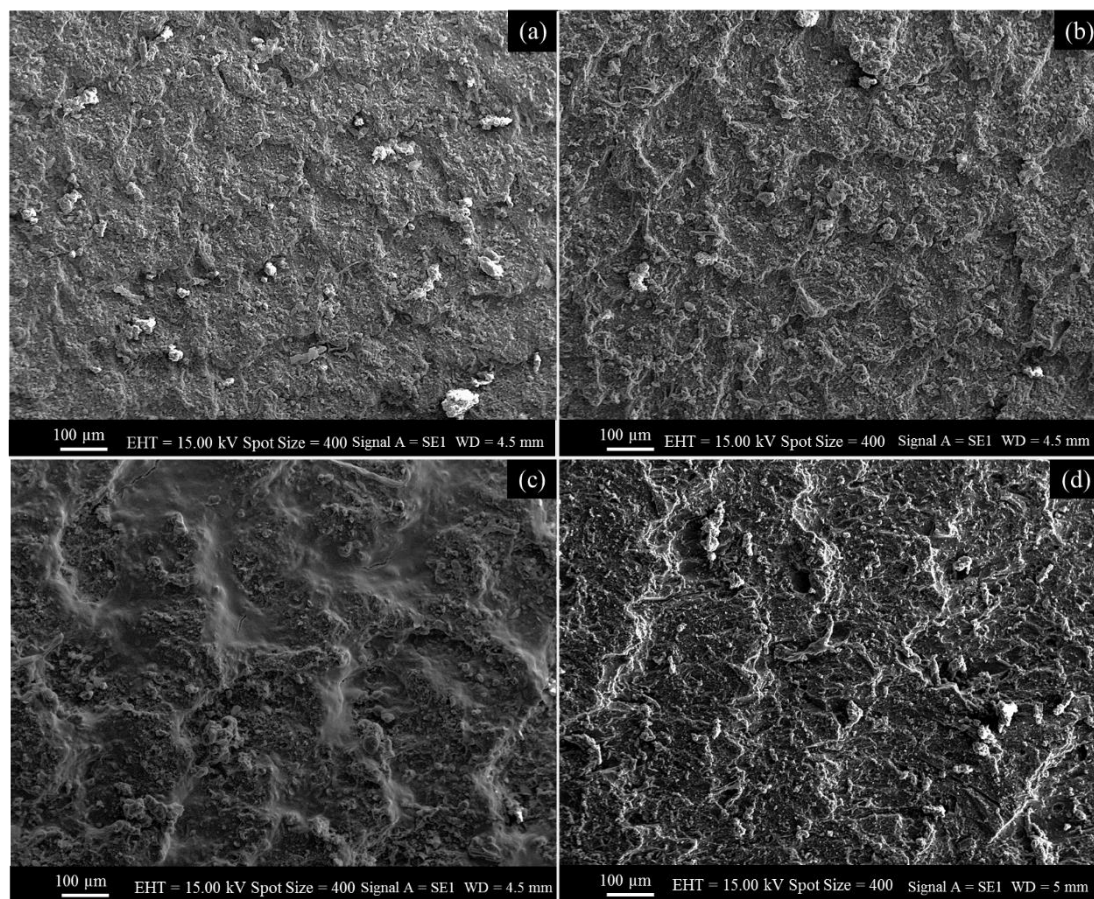
Fig. 5. 8. SEM images of NR8 after abrasion tests with different sized abrasive particles: (a) 82 µm, (b) 125 µm, (c) 269 µm, (d) 425 µm.
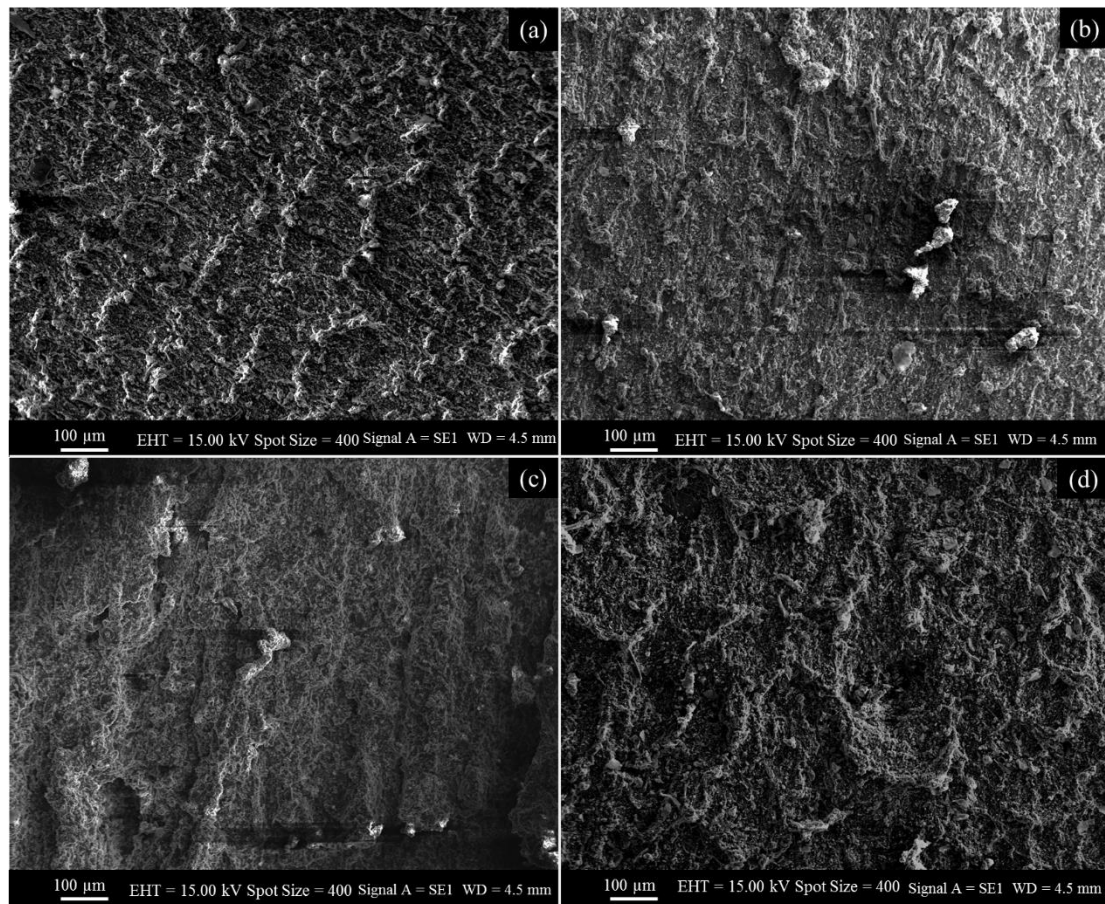
Fig. 5. 9. SEM images of SBR after abrasion tests with different sized abrasive particles: (a): 82 µm, (b) 125 µm, (c) 256 µm, (d) 425 µm.
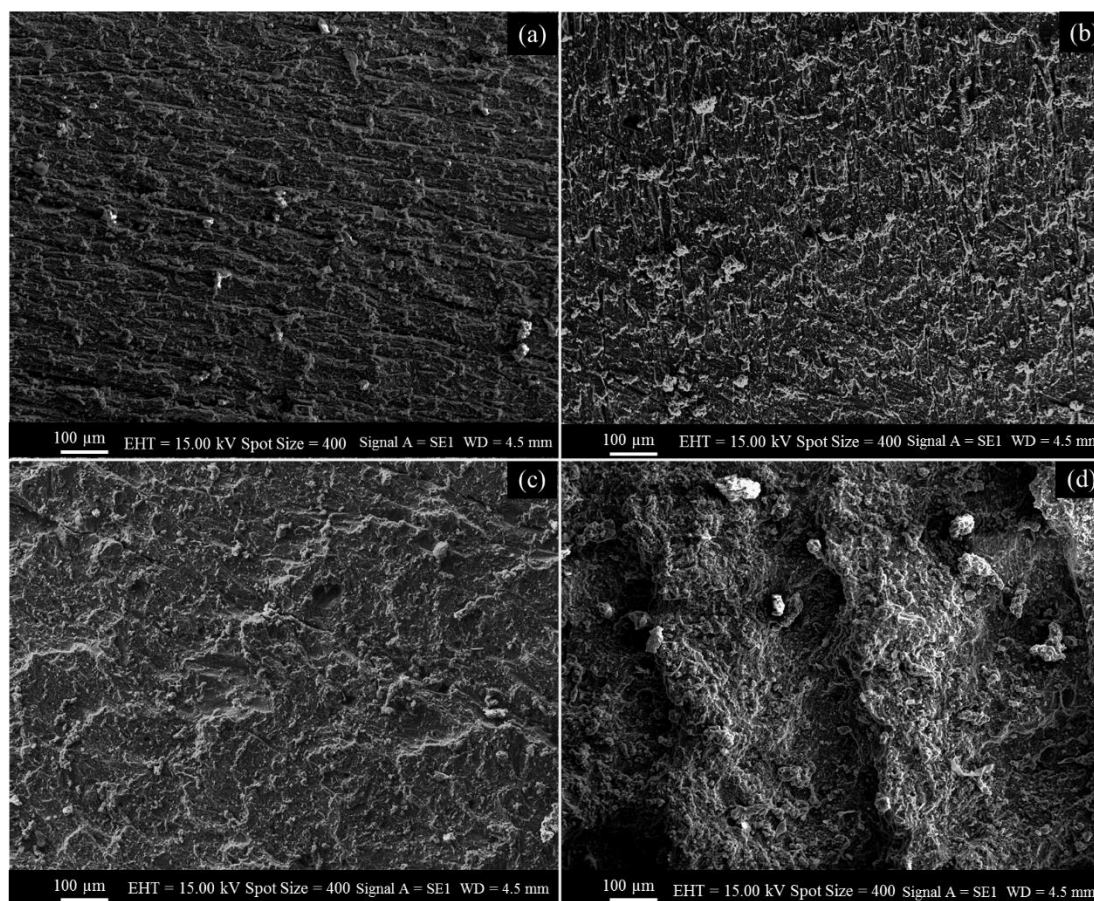
Fig. 5. 10. SEM images of NBR after abrasion tests with different sized abrasive particles: (a) 82 µm, (b) 125 µm, (c) 269 µm, (d) 425 µm.

Table 5. 1. Average size of ridge's space evaluated from SEM images.

Abrasive Particle size (µm)	Ridge Space (µm)					
	NR1	NR2	NR4	NR6	NR7	NR8
82	179.87±2.47	261.75± 8.45	169.22±8.27	165.30±1.24	251.70±4.39	176.08±2.66
125	223.22±7.29	358.87±8.09	209.2±1.95	215.92±10.84	298.65±10.14	188.20±4.10
256	333.45±6.96	394.46±8.93	294.58±13.00	302.11±13.94	405.55±10.71	271.44±15.24
425	409.52±13.73	510.88±6.94	417.32±4.23	417.43±2.90	541.98±5.84	273.87±5.94
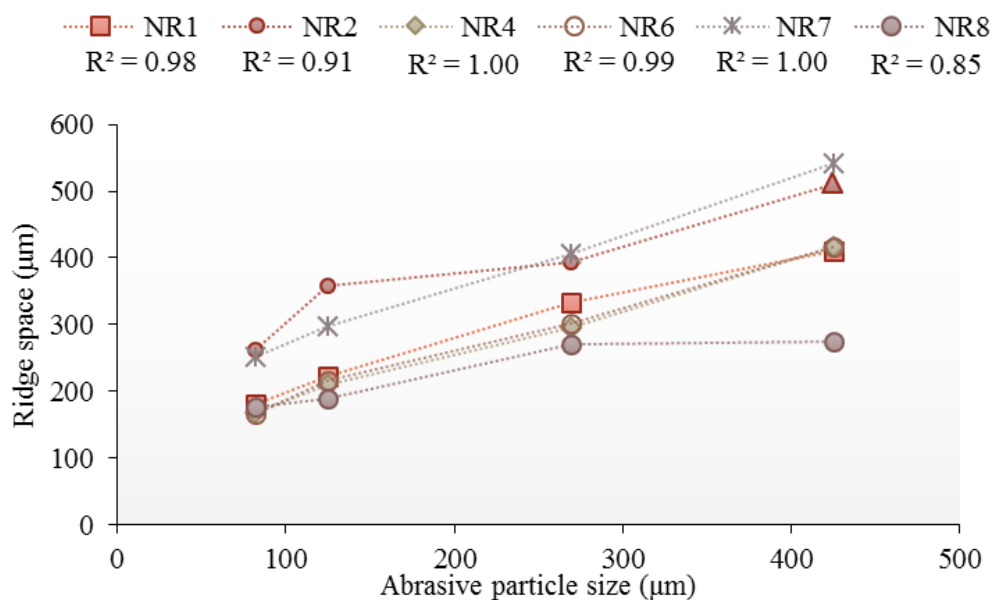
Fig. 5. 11. Ridge spacing vs. abrasive particle size.

Table 5. 2 shows the average size of generated wear debris, which has increased with the increase of the abrasive particle size. The largest wear debris size change is observed for NR2.

Table 5. 2. Average size of wear debris evaluated from SEM images.

Abrasive particle size (μm)	Size of wear debris (μm)							
	NR1	NR2	NR4	NR6	NR7	NR8	SBR	NBR
125	83.8 ± 4.2	264.6±4.4	91.8±2.9	153.2±6.2	179.2±4.8	68.4 ± 4.8	126.0 ± 5.9	63.5 ± 5.0
425	259.8 ± 2.0	1053.8±8.4	493.9±12.1	471.6±17.6	474.8±8.0	117.4 ± 1.6	255.4 ± 1.7	171.6 ± 7.3

Fig. 5. 12 and Fig. 5. 13 show the SEM image of collected wear debris during the two-body abrasive wear test when the abrasive particle size is 125 μm and 425 μm, respectively.
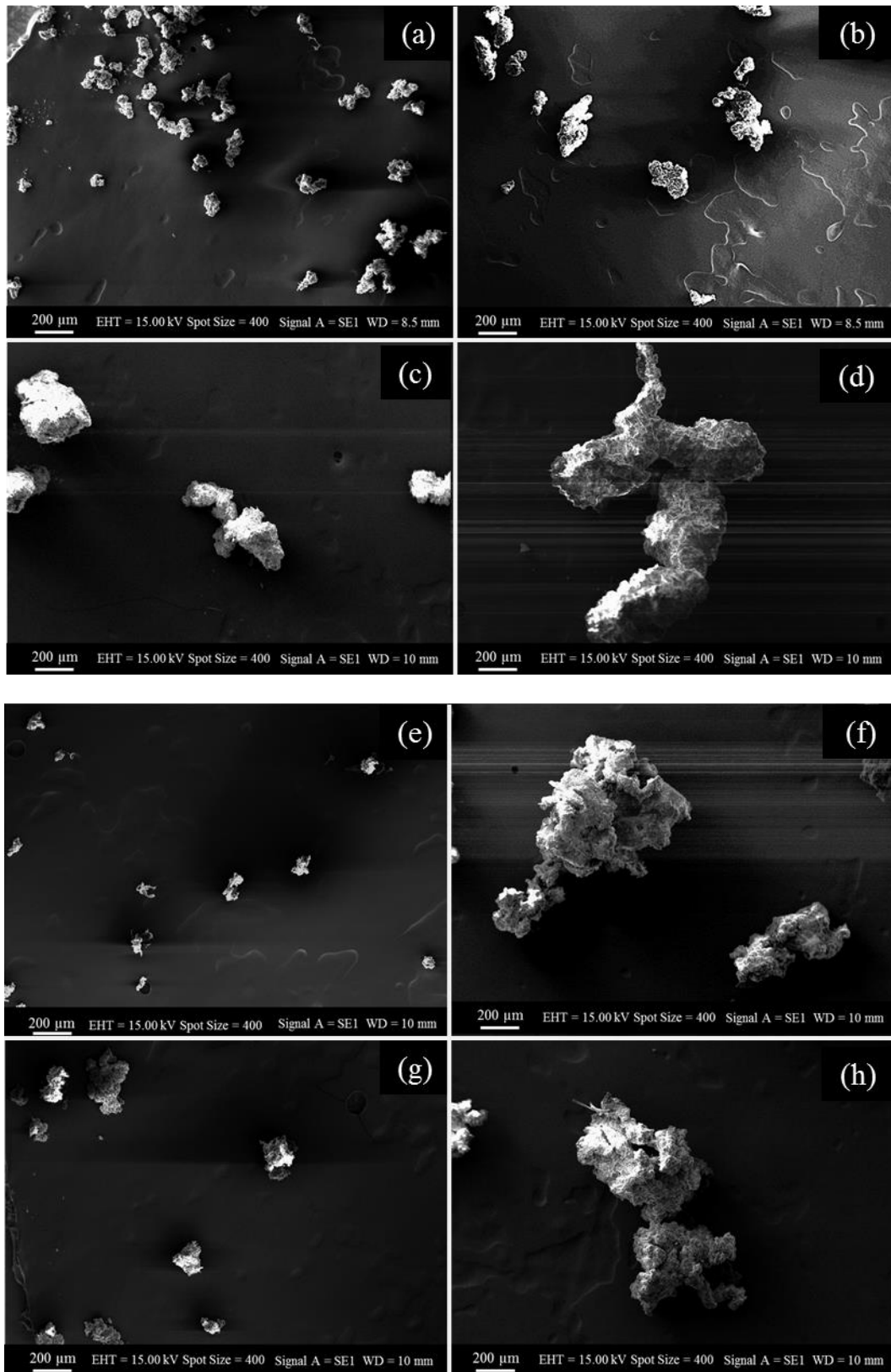
Fig. 5. 12. SEM images of wear debris after abrasion test with 125 µm and 425 µm abrasive particles size: (a) and (b) NR1, (c) and (d) NR2, (e) and (f) NR4, (g) and (h) NR6.
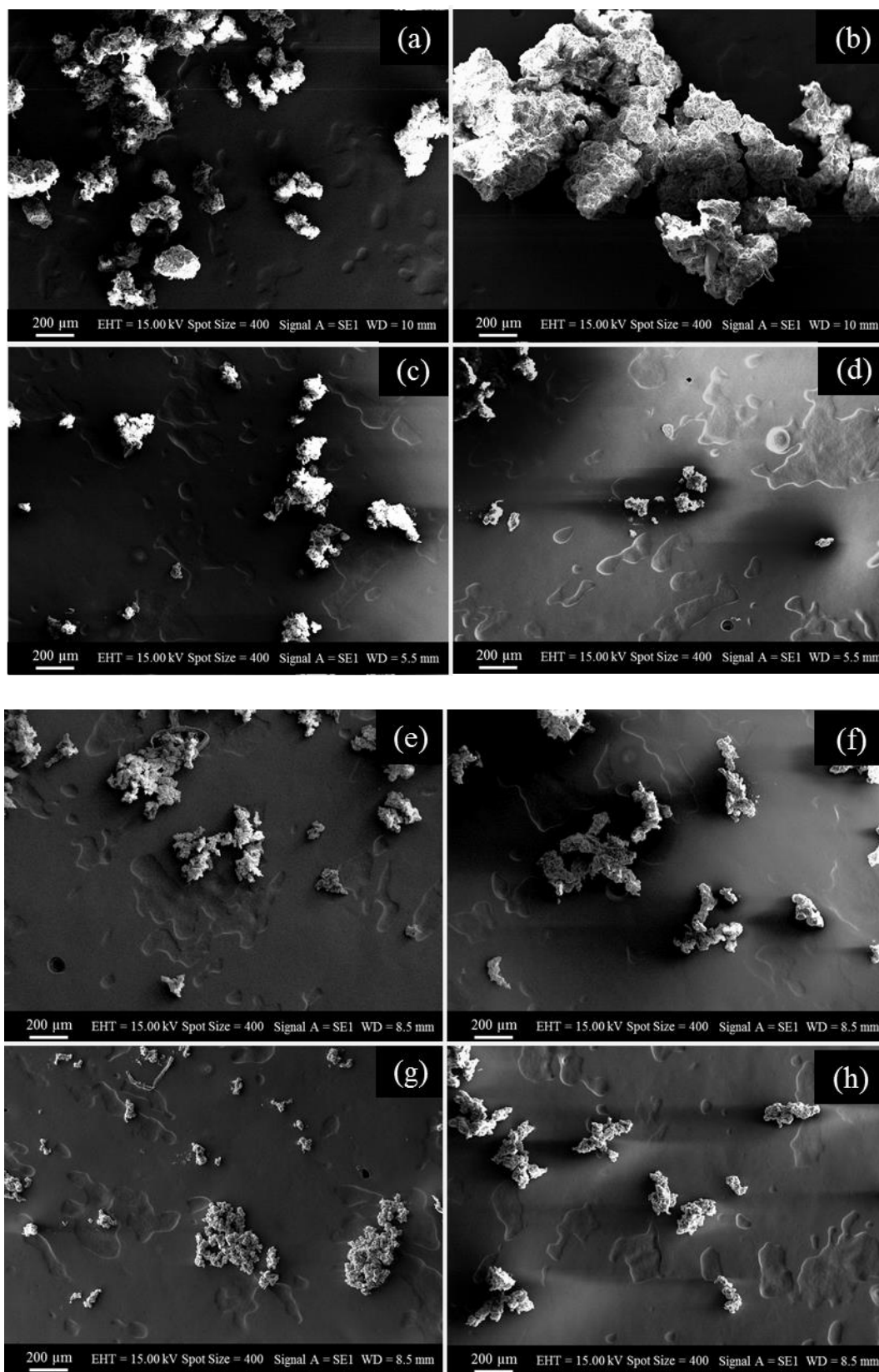
Fig. 5. 13. SEM images of wear debris after abrasion test with 125 µm and 425 µm abrasive particles size: (a) and (b) NR7, (c) and (d) NR8, (e) and (f) SBR, (g) and (h) NBR.

Fig. 5. 14, Fig. 5. 15, and Fig. 5. 16 illustrate the coefficient of friction as a function of abrasive particle size when the sliding speed is 0.25, 0.5 and 1 m/min, respectively. It is seen that mostly COF increases with different rates when the abrasive particle size increases, at different sliding speed. Fig. 5. 17 shows the variation of COF at different sliding speeds and abrasive particle size. The COF of elastomers as a function of WR at different abrasive particle size is shown in Fig. 5. 18, which is ascending with an increase of wear rate.
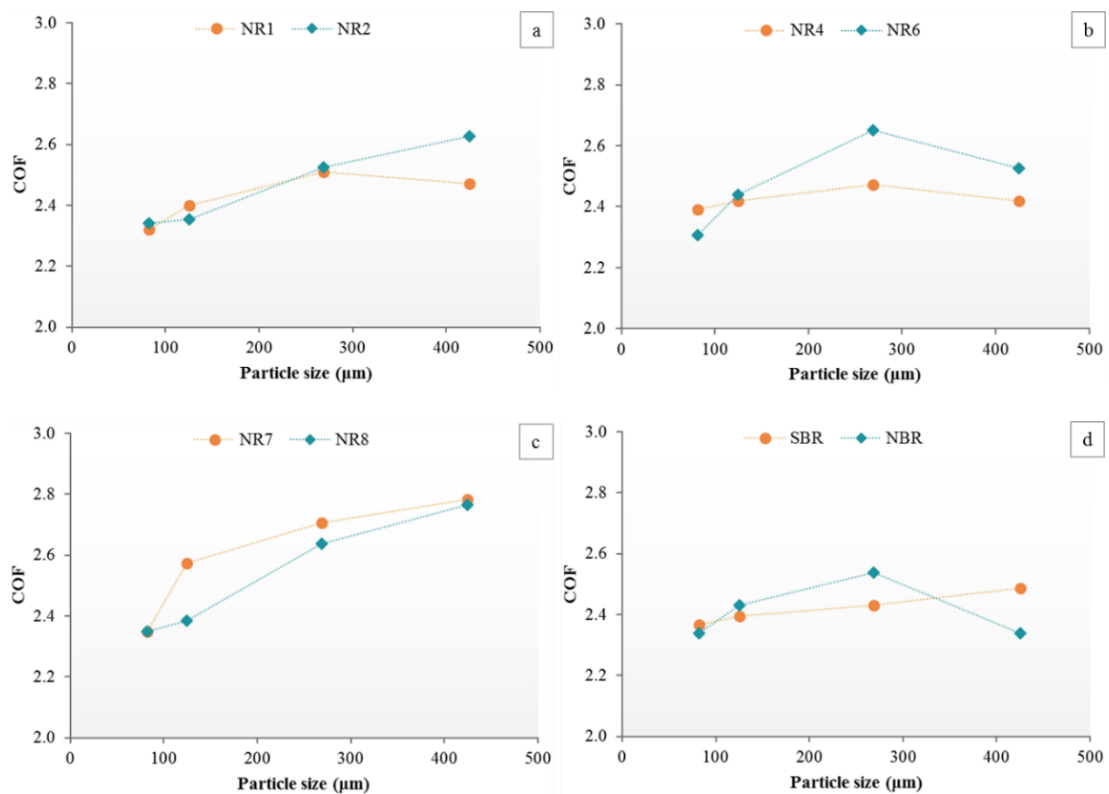
Fig. 5. 14. Variation of COF as a function of abrasive size (sliding speed of 0.25 m/min).
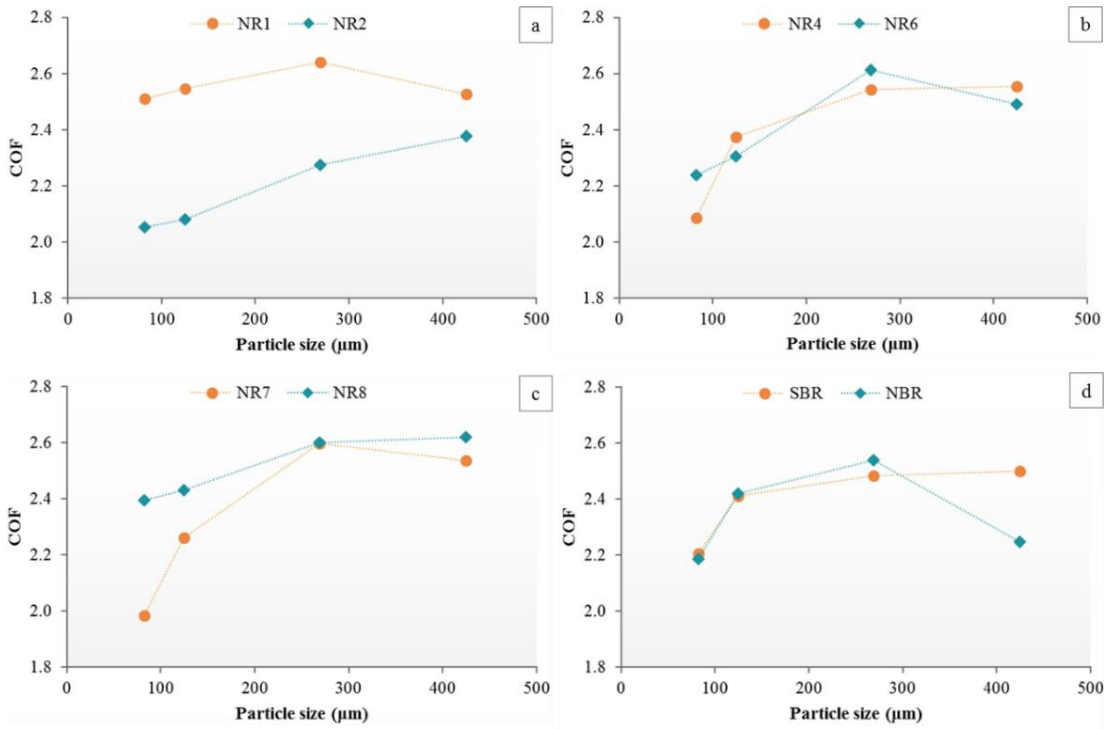
Fig. 5. 15. Variation of COF as a function of abrasive size (sliding speed of 0. 5 m/min).
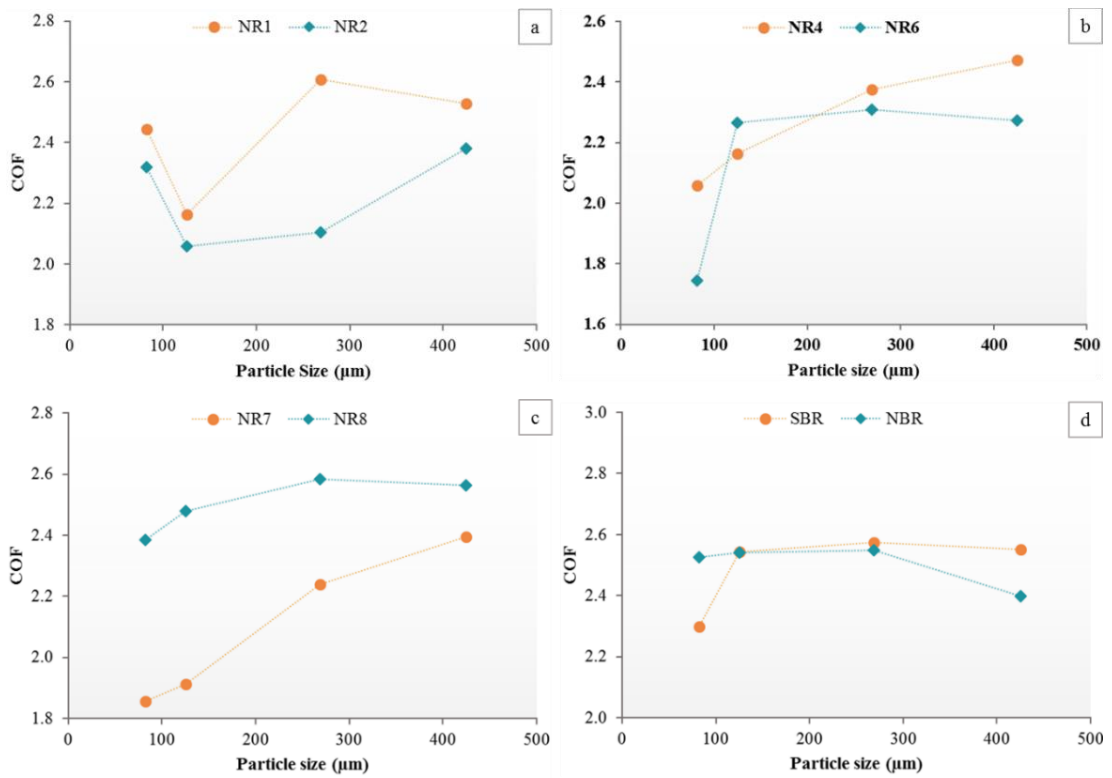
Fig. 5. 16. Variation of COF as a function of abrasive size (sliding speed of 1 m/min).
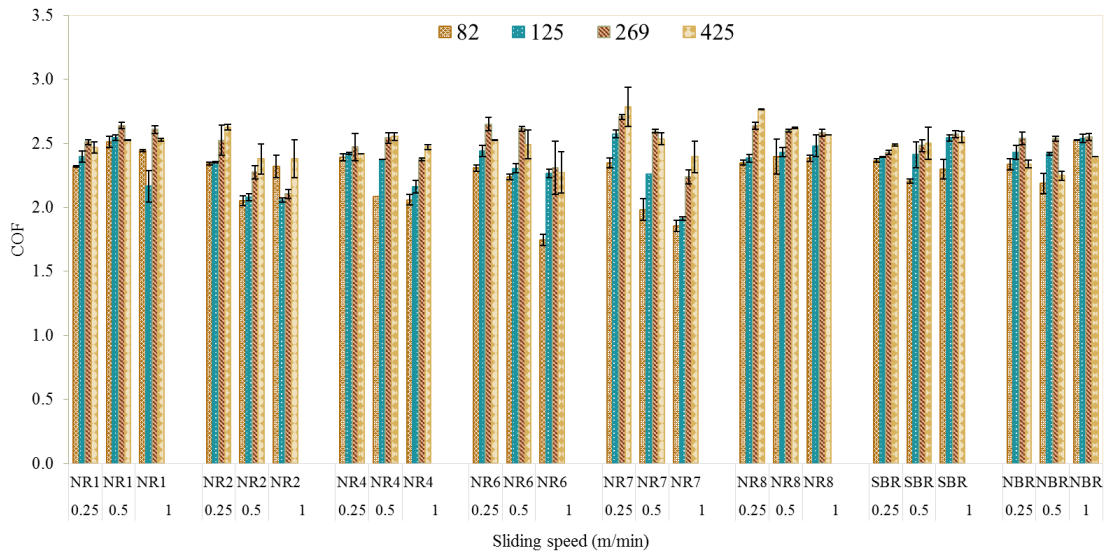
Fig. 5. 17. Average values of COF as a function of sliding speed and abrasive particle.
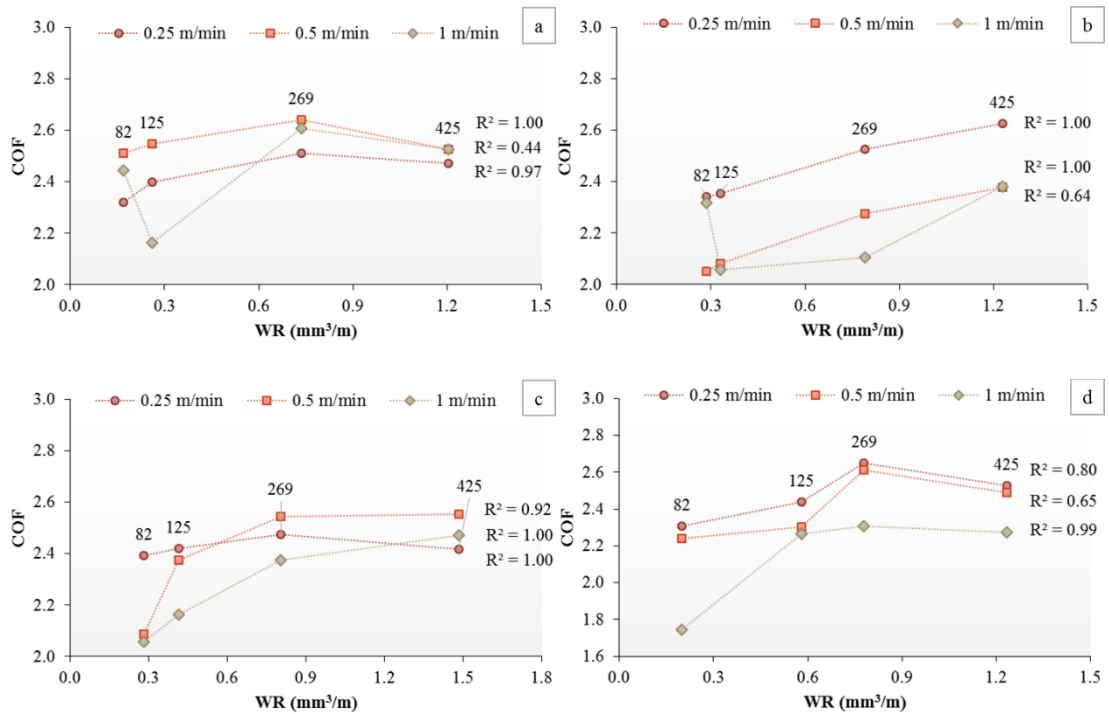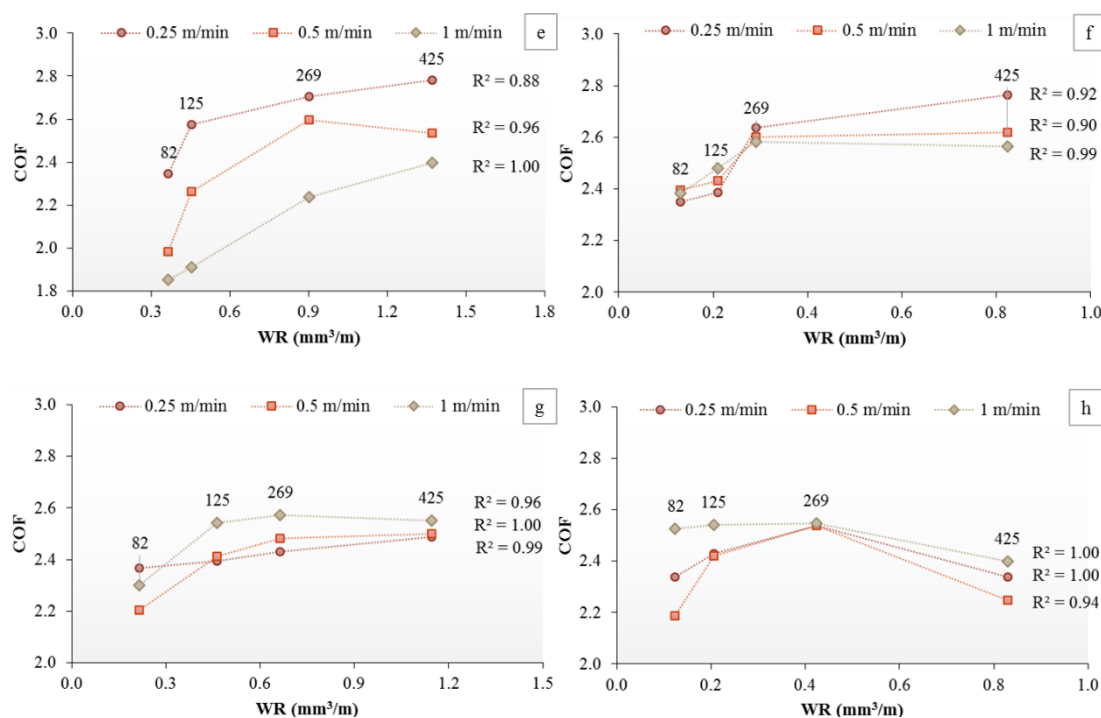
Fig. 5. 18. COF as a function of WR: (a) NR1, (b) NR2, (c) NR4, (d) NR6, (e) NR7, (f) NR8, (g) SBR, (h) NBR.

5.4. Discussion

5.4.1. Effect of the abrasive particle size on wear

5.4.1.1. Wear rate

The increase of wear rate with increasing of the abrasive particle size (Fig. 5. 1) is due to the higher protuberance of the abrasives into the softer material (rubber) resulting in a higher depth of penetration, larger contact area, ploughing, and cutting. Additionally, the number of abrasives on the specified surface area decreases (see Fig. 3. 2), so the stress on individual abrasive particles increases. Consequently, during the sliding, fracture and deformation increase at the counter face, which leads to the severe abrasion (Singh et al., 2002, Tangudom et al., 2014, Shen et al., 2016).

Because the wear mechanism varies with increase of the abrasive particle size, a slight change is observed in wear rate's graph (slope of the graph) (see Fig. 5. 1. d) (Lancaster, 1969, Thavamani et al., 1993, Bhattacharya and Bhowmick, 2010), which will be discussed in detail in section 5.4.1.2.

As mentioned in chapter 2 and 4, the mechanical properties of material influence the wear behaviour; wear volume is inversely proportional to the mechanical properties (Lancaster, 1969, Briscoe et al., 1986, Shipway and Ngao, 2003). Wear rate as a function of mechanical properties is plotted in Fig. 5. 19. The polynomial regressions are applied, and both fitted lines and coefficient of determination are illustrated. The correlation between wear rate and product of tensile strength and elongation at break at different abrasive particle size increase with increase of the abrasive particle size until reaching 269 μm. Under the normal load, at low abrasive particle size, the particles are not detached from the surface and the rubber mostly deforms. Therefore, elongation at break and tensile strength of the elastomers affect the wear resistant of them.

On the other hand, tear strength does not have any effect on wear behaviour at low abrasive particle size ($R^2 < 0.3$). At the highest abrasive particle size due to the severe abrasive, the particles are torn off from the surface, in addition to deformation, tearing also takes place in wear. It is seen, simultaneously, with decrease of the coefficient of determination for $(\sigma\varepsilon)^{-1}$, R^2 raises to above 0.8 for $(HT)^{-1}$. Put it differently, tear strength has more impact on wear rate at high abrasive particle size.
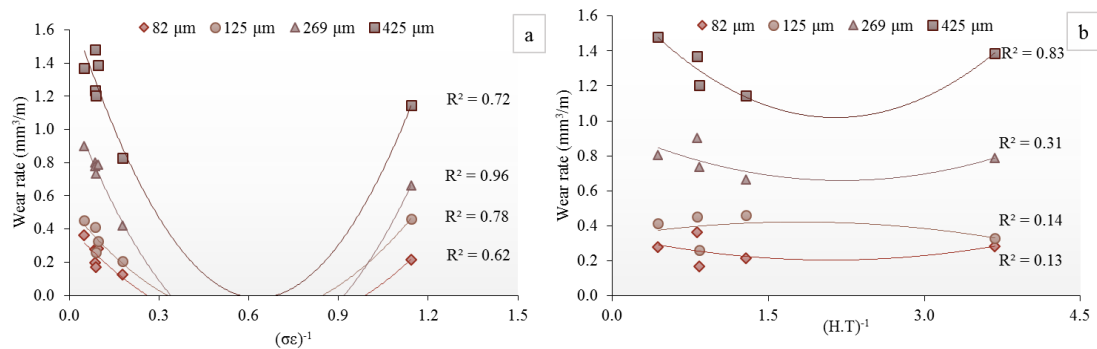
Fig. 5. 19. Wear rate as a function of mechanical properties at different abrasive particle size: (a) $(\sigma\varepsilon)^{-1}$, (b) $(HT)^{-1}$.

Among these three elastomer types, the molecular chain of NBR and SBR have an attached bulky group, which restricts the chain movement, they show high resistance against deformation. Compare to the NRs with a linear molecular chain that deforms more easily, they show higher wear durability.

At low abrasive particle size (82 μm), the difference between the wear rates is insignificant (see Fig. 5. 2). It could be attributed to clogging effect by embedded wear debris on the abrasive paper. It is known that fine abrasives clog easier than the coarse ones, which leads to the smoother counter face and reduction of abrasives' penetration into the softer material and wear (Sin et al., 1979, De Pellegrin et al., 2009b, Shen et al., 2016).

Since the stress is not enough to detach the particles from the surface, deformation and crack initiation followed by propagation dominate the wear behaviour while sliding against small abrasives. For NBR and SBR with high hardness (65 shore A), deformation slowly happens, thus the wear rate is lower compared to NRs. Among the NRs, NR7 has the highest wear rate since it has the highest elongation at break, leading to higher adhesive friction by increase of the real contact area. As the wear rate is directly proportional to the friction coefficient (Vaziri et al., 1988, Harsha et al., 2003).

As the number of particles decreases on the specific surface area, with increase of the abrasive particle size, the pressure on each particle increases, too. Thus, the plastic deformation and material removal dominate the wear. As a result, the tear strength of the rubber plays a significant role. On one hand, the increasing rate of wear of NR7 (with high tear strength) slows down, under severe stress since rubbers with high elongation at break deform heavily before particles' detachment (see Fig. 5. 4. d and Fig. 5. 7. d). On the other hand, the accelerating rate of wear of NR2, NR1, and SBR (rubbers with low tear strength) enhances, with increase of the abrasive particle size. The difference between the wear rate of NR4, NR6, and NR8, which have similar mechanical properties, is discussed in detail in section 4.4.1.1.

Finally, with increase of the abrasive particle size, the abrasives become rounded and duller (see Fig. 3. 2) thus the particles do not penetrate deeply, particularly when the hardness of the elastomer is high, the friction drops and the contact surfaces slide at ease, hence, NBR shows lower wear rate.

5.4.1.2. Wear mechanism

Under the applied load, NRs abraded against abrasives owing to the nucleation and development of microcracks, a series of ridges are formed on the worn surface as seen

in Fig. 5. 3- 5. 8. These well-defined and equally spaced ridges are characteristic of the frictional wear. With increase of the abrasive particle size, the real contact area increases, abrasives became rounded and blunt resulting in the transfer of wear mechanism from frictional wear to fatigue wear, which is confirmed by the presence of dimples and pitting marks on the worn surface (Thavamani et al., 1993). In comparison with other rubbers, on the abraded surface of NR1 with low tear strength, the wear particles are formed (see Fig. 5. 3. d). Additionally, the stretched particles are observed on the surface of NR2 and NR7, rubbers with a higher elongation at break, they plastically deform before material removal. The measured average ridge's space of wear patterns are shown in Table 5. 1 and plotted as a function of wear rate demonstrated in Fig. 5. 20, which has a good agreement with wear resistance of the rubbers. Those with higher wear rate have greater ridge's space. Besides, the ridges' space correlates linearly with the abrasive particle size (see Fig. 5. 11). It increases with increase of the abrasives' size, which also results in higher wear rate. As seen in Fig. 5. 20, there is also a linear relationship between the ridge space and wear rate.
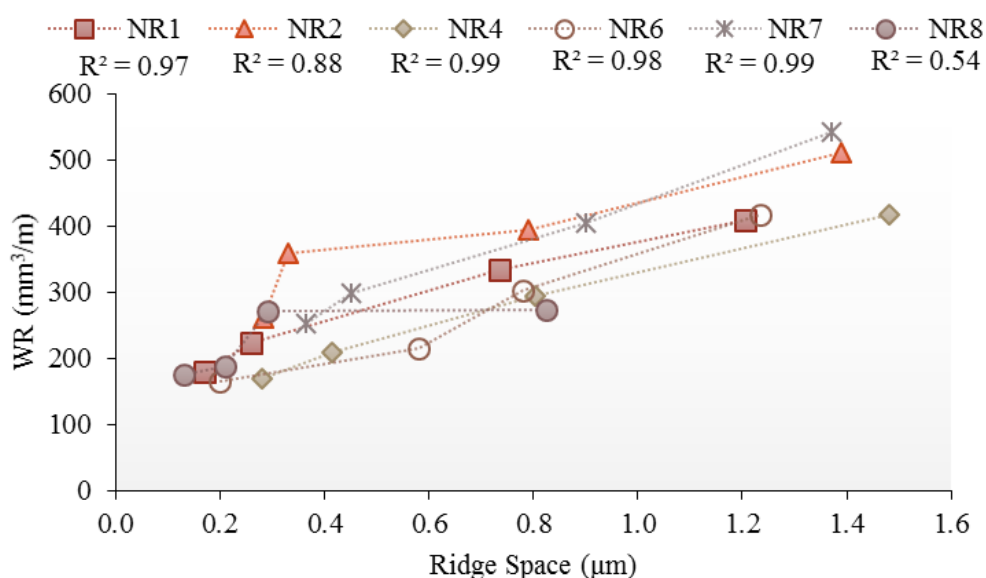
Fig. 5. 20. Wear rate vs ridge space.

SEM image of abraded SBR (see Fig. 5. 9) shows the formation of the ridges alongside with score line on the surface during abrading by fine abrasives. With the

increase of the abrasive particle size, the pressure on the real contact area increases leading to the fracture of the ridges and generation of the rolled debris. With looming of the ridges, the wear mechanism also varies from frictional wear to the abrasion by roll formation, which is mostly seen at materials with low tear strength (Moore, 1980, El-Tayeb and Nasir, 2007, Shen et al., 2016). The formed wear debris act as a third body in the system and change two-body abrasive wear to three-body abrasive.

NBR shows a different wear behaviour, in contrast with NRs when it is abraded against fine abrasives, scratches and grooves are observed on the surface caused by cutting, ploughing or plastic flow of the material (Lancaster, 1969, Muhr and Roberts, 1992, Junkong et al., 2015). The wear mechanism is abrasion wear by micro cutting (small abrasives) and micro ploughing (large abrasives).

5.4.1.3. Wear debris

Two types of the wear debris are formed when the elastomer is abrading by low and high abrasive particle size: intrinsic and aggregates (see Fig. 5. 12 and Fig. 5. 13). The low abrasive particle size's shape is angular (see Fig. 3. 2. a and b) causing micro cutting on the surface, thus the formed debris is continuous. With the increase of the grit size, the abrasives become rounded resulting in ploughing on the surface, so the generated wear particles are discontinuous and deformed. The wear debris of SBR and NBR is loose and granular at 125 μm, whereas the wear debris of SBR is rolled and elongated at 425 μm (see Fig. 5. 13. f).

The average size of generated wear debris increases with the increase of the abrasive particle size (see Table 5. 2). NR2 and NR7 have the longest wear debris since the deformability of the elastomer is high and its frictional work increases, resulting in the formation of the aggregate particles. The smallest wear debris is belonged to the NBR and SBR, because of their high hardness.

5.4.2. Effect of the abrasive particle size on the friction

During sliding of the elastomers against a rough surface adhesive friction and deformation contribute to friction behavior (Persson et al., 2008, Braun et al., 2016). Adhesive friction and deformation are caused by the adhesion between the elastomer

and the abrasive, and the energy loss resulted from plastic deformation and wear particles' formation, respectively (Liang, 2007, Coronado, 2015).

The COF mostly increases with the growing of the abrasive particle size (see Fig. 5. 14- 5. 15), attributed to deeper penetration of the abrasives into the softer material that requires higher tangential force to slide on the rough surface, larger real contact area, and higher plastic deformation (Coronado, 2015, Feng et al., 2016, Shen et al., 2016). The formed ridges' space grows (see Table 5. 1) with increase of the grit size, so the contact spots also increases. The COF of NBR also raises with an increase of the abrasive particle size until reaching the critical size, and then above this value, it drops. As the wear mechanism of NBR is abrasion by micro-cutting and micro-ploughing, the generated fine particles act as a transfer film leading to rising of adhesive friction (dominant friction at fine grits) since the friction occurs between elastomers with same atomic composition and molecular structure. At coarser abrasives, plastic deformation controls the friction, the applied stress on contact spots increases and abrasion happens by micro ploughing (deformation) (see Fig. 5. 10). Thus, the thickness of the produced thin film reduces and loose particles detach from the surface (Coronado, 2015), as a result, the COF decreases. The critical size is determined where COF is independent of the abrasive particle size (De Pellegrin et al., 2009b).

The rubbers almost display a similar trend at different sliding speed with a change of the abrasive particle size with some exceptions. For instance, while sliding velocity is 1 m/min initially, the COF of NR1 and NR2 decreases with the increase of the abrasive particle size from 82 μm to 125 μm, then with further increase of the abrasive size, it increases (see Fig. 5. 16. a). It might be due to the growth of the real contact area because of embedded particles on the abrasive paper. It has been known that fine abrasives clog faster than coarse ones (Sin et al., 1979, Hamid et al., 2013). With the increase of the abrasive size, applied stress at the counter face increases, thus the loose particles detaches from the surface of the abrasive paper and COF reduces. A similar trend is observed for COF of NBR investigated by Shen et al. (Shen et al., 2016), with increase of the grit size, firstly COF drops to a minimum value at 20 μm grit size and then raises, the sliding speed is 0.08 m/s.

As mentioned in chapter 2, the sliding velocity affects the friction of the polymers. Additionally, at high velocities (V > 0.01 m/s), the generated frictional heat leads to temperature rise at the counter face, which also influences the friction behavior (Lorenz et al., 2015). In current work, though, the sliding velocity is under 0.01m/s, thus the generated heat and its contribution to the friction is negligible.

By comparing the COF at various sliding velocities (see Fig. 5. 17), it is seen with increase of the sliding speed, at various particle size, COF behaves differently; it decreases or increases. The former is due to the short contact time and reduction of the effective contact area. The latter is attributed to the increase of viscous resistant of the rubber leading to the higher strain rate, causing higher friction (Myshkin et al., 2005, Lorenz et al., 2015). For some rubbers, the minimum COF is observed at 0.5 m/min, which could be explained by the transfer of adhesive (elastic contact) to the deformation (plastic contact).

Similar to wear, when the abrasive particle size and sliding speed change the mechanical properties of the elastomers also affect the friction of elastomers. The adhesive friction dominates while sliding speed and the abrasive particle size are low, 0.25 m/min and 82 μm, respectively. The elastomers with low hardness, high tensile strength, and elongation at break (such as NR2) have higher COF since the real contact area grows under pressure leading to increase of adhesive friction. The deformation is the dominant parameter when rubber slides on the coarser abrasives (Mofidi, 2009, Coronado, 2015). The elastomers with low tear strength, which means low energy consumption, and high amount of formed wear particles acting as a third party and reducing the real contact area smoothen the counter face, consequently elastomer slides at ease and COF of those rubbers is less than others.

Moreover, with increase of the velocity, COF of NRs declines slightly when sliding against coarser abrasive size that the dominant factor is deformation. Since their linear molecular chain deforms easier, thus the contribution of hysteresis to friction decreases. Inversely, the attached bulky group of SBR and NBR makes the sliding harder and prohibits the movement of the molecular chain and deformation resulting in raise of hysteresis friction.

The relation between the wear rate and COF demonstrated in Fig. 5. 18. The regressions are applied and the coefficients of determinations are above 0.9, in other words, there is a good correlation between COF and wear rate of the elastomers. The coefficient of friction depends on wear rate, which varies with the variation of the wear mechanism.

5.5. Summary

In this chapter, the effect of abrasive particle size on the tribological behavior of elastomers is studied.

- With a variation of the abrasive size of the rough surface (from fine to coarse), the wear rate and COF of elastomers increase, owing to the greater contact area and deeper protuberance of abrasives into the elastomer that causes the higher depth of penetration, deformation, and material removal.

- Wear mechanism of NRs and SBR varies from frictional wear to fatigue and roll formation, respectively. NBR's wear mechanism is abrasion by micro cutting and micro ploughing.

- The mechanical properties such as elongation at break and tensile strength on wear play a pivotal role at small abrasive particle size whereas hardness and tear strength are more pronounced at the bigger abrasive size.

- Considering the variation of COF with abrasive particle size and sliding speed, it is concluded that the abrasive particle size, the mechanical properties of the elastomer, and sliding velocity shift the maximum and minimum value of COF by affecting the adhesive and deformation contribution to the friction.

Chapter 6. Statistical analysis

6.1. Introduction

Catastrophic failure can happen in systems, due to the weakening of the main structure of the component. The wear and friction are important output parameters that control the life of elastomer components and affect design considerations. The surface roughness is an important indicator of the wear mechanism. The temperature rise in interfaces as a result of frictional heating also needs to be considered in relation to abradibility (Muhr and Roberts, 1992). In practice friction, roughness, and wear are the results of many interactions caused by operating parameter, material properties, and the abrasives' properties.

To analyze the influence of effective parameter and their contribution to the process there are different statistical methods such as the traditional method, Pareto ANOVA, and Design of the experiment (Taguchi's design).

The traditional method uses the mean value of the outputs to represent the associations between output and input parameters. Since it does not usually take account of data on the variation of responses, a comprehensive study is not possible for this method (Pramanik, 2013). In Pareto ANOVA, the average response values are applied to monitor the trends of the variable and the interaction of each input variable with output quality variable is determined. In the design of experiment (DOE), an analytical method is used to do the minimum work, time, and energy to obtain the maximum information. This technique is based on orthogonal array experiments with the optimum control parameter that saves time, material and cost in addition to eliminating the need for repeating the experiments. Furthermore, it recognizes and determines interactions and influence of different control factors. It has been applied successfully for statistical analysis of wear of polymer and their composites (Pasha et al., 2012, Rajashekaraiah et al., 2014). To optimize the strength of the process data, Taguchi statistical analysis is utilized by including signal-to-noise (S/N) ratio in the data.

The S/N ratio is calculated by equation (6.1).

$$\frac{S}{N} = -10 \log \frac{1}{n} \left(\sum_{i=1}^{n} y_i^2 \right) \qquad (6.1)$$

Where n and y are the number of observations and observed data, respectively. The equation (6.1) is suitable for parameters where the adage 'the smaller the better' is true. All output parameters considered in this investigation fall into this group. The higher the magnitude of S/N ratio, results in the better outcome because it assures the best quality with the least variance. Further details of Taguchi's design and ANOVA can be found in the literature by Park and Cho et al. (Park, 1996, Cho and Lee, 2000).

It has been observed that the applied load, abrasive particle size, and product of tensile strength and elongation at break ($\sigma.\varepsilon$) have a significant effect on the tribological behaviour of the elastomers (see chapters 4 and 5). In this chapter, with the help of statistical methods, the contribution of these parameters on the wear process is studied to establish a relationship between these parameters with wear and friction. Since the variation of the surface roughness is one of the consequences of the material removal due to the wear (Myshkin et al., 2005), the wear mechanism is presented by the surface roughness.

The temperature build-up (TBU) represents the friction. As the frictional work provides the required energy for tearing and removal of debris from the surface of the elastomer, that part of it converts to heat energy leading to the increase of the temperature on the abraded surface (Bhattacharya and Bhowmick, 2010). The temperature rise influences dependence of the rubber friction to the normal load stress, in addition to affecting friction and wear (Myshkin et al., 2005, Persson, 2006, Lorenz et al., 2011, Persson, 2011, Selig et al., 2014).

The outcomes will be beneficial to the researchers and professionals in this area to select the proper type of rubber according to their applications.

6.2. Method

Three different elastomers NR (8), SBR, and NBR as specimen, wear test machine, profilometer, and infrared thermometer described in chapter 3 are used. The parameters for the wear test are: sliding speed 0.32 m/s, sliding distance 40 m, abrasive particle size 82,125, and 269 µm, and applied load 5, 10, and 15N.

Pareto ANOVA and Taguchi analysis arranged by L_{27} (3^3) orthogonal array (Taguchi, 1987) and all the parameters are examined. Overall, 81 specimens are tested, namely nine specimens (replicates) for each rubber. Table 6. 1 and 6. 2 show the control parameters and their levels considered in this investigation with respect to input parameters, respectively.

To analyze the experimental outcomes of traditional analysis, Pareto analysis of variation (ANOVA), and Taguchi's signal-to-noise (S/N) ratio analysis are used.

Table 6. 1. Input parameters with their levels.

Input parameter	Symbol	Level 0	Level 1	Level 2
Applied load (N)	A	5	10	15
Particle size (µm)	B	82	125	269
$(\sigma.\varepsilon)^{-1} \times 10^{-3}$ (mm^2/N)	C	0.08	0.18	1.14

Table 6. 2. Experiments details.

Exp. No.	Applied force (N)	Particle size (μm)	$(\sigma.\varepsilon)^{-1} \times 10^{-3}$ (mm²/N)
1	5	82	0.08
2	5	82	0.18
3	5	82	1.14
4	5	125	0.08
5	5	125	0.18
6	5	125	1.14
7	5	269	0.08
8	5	269	0.18
9	5	269	1.14
10	10	82	0.08
11	10	82	0.18
12	10	82	1.14
13	10	125	0.08
14	10	125	0.18
15	10	125	1.14
16	10	269	0.08
17	10	269	0.18
18	10	269	1.14
19	15	82	0.08
20	15	82	0.18
21	15	82	1.14
22	15	125	0.08
23	15	125	0.18
24	15	125	1.14
25	15	269	0.08
26	15	269	0.18
27	15	269	1.14

6.3. Results

Due to multi-variability nature of data, there are different ways to present them. A large volume of data is acquired and analyzed. Only a few data are presented, nevertheless, all of the interactions are reflected in different phases.

6.3.1. Wear rate

Table 6. 3 exhibits the Pareto ANOVA analysis of elastomers' wear rate. It shows the abrasive particle size (B) with the contribution of 39.78 % has the most substantial effect on the wear rate, followed by the applied load (A) that has an almost similar contribution to that of particle size (33.10 %), and $(\sigma.\varepsilon)^{-1}$ (19.40 %).

Table 6. 3. Pareto ANOVA analysis for wear rate.

Sum at factor level	Factor and interaction								
	A	B	A×B	A×B	C	A×C	A×C	B×C	B×C
0	158.54	158.41	127.38	124.26	136.86	116.43	122.17	106.91	122.32
1	113.90	121.72	116.27	107.23	133.84	123.39	116.25	120.61	120.77
2	83.84	76.15	112.63	124.79	85.57	116.46	117.85	128.75	113.18
Sum of squares of difference (S)	8477.55	10188.52	354.23	598.85	4968.64	96.60	56.26	731.18	143.50
Contribution ratio (%)	33.10	39.78	1.38	2.34	19.40	0.38	0.22	2.85	0.56

	39.78 B	33.10 A	19.40 C	2.85 B×C	2.34 A×B	1.38 A×B	0.56 B×C	0.38 A×C	0.22 A×C
Cumulative contribution	39.78	72.88	92.28	95.13	97.47	98.85	99.41	99.79	100.00
Check on significant interaction	B×C two-way table								
Optimum combination of significant factor level	A0B0C0								

The response table and graphs of mean S/N ratio for the wear rate are demonstrated in Table 6. 4 and Fig. 6. 1, respectively. The term "Max-Min" denotes to subtraction of minimum value from the maximum value of levels.

As shown in Table 6. 4, the lowest load parameter (A0) is the best option to achieve a low wear rate. The average variation in wear rate as presented in Fig. 6. 2 shows that the lowest $(\sigma.\varepsilon)^{-1}$, the smallest particle size, and the lowest applied load offer the lowest wear rate. Fig. 6. 2. also shows wear rate increases with the increase of the load, abrasive particle size, and $(\sigma.\varepsilon)^{-1}$.

Table 6. 4. Response table of mean S/N ratio for wear rate and significant interaction.

Input parameters	Symbol	Mean S/N ratio			
		Level 0	Level 1	Level 2	max-min
Applied load	A	17.62	12.66	9.32	8.30
Particle size	B	17.60	13.52	8.46	9.14
$(\sigma.\varepsilon)^{-1}$	C	15.21	14.87	9.51	5.70
Interaction B×C	B×C	11.88	13.40	14.31	2.43
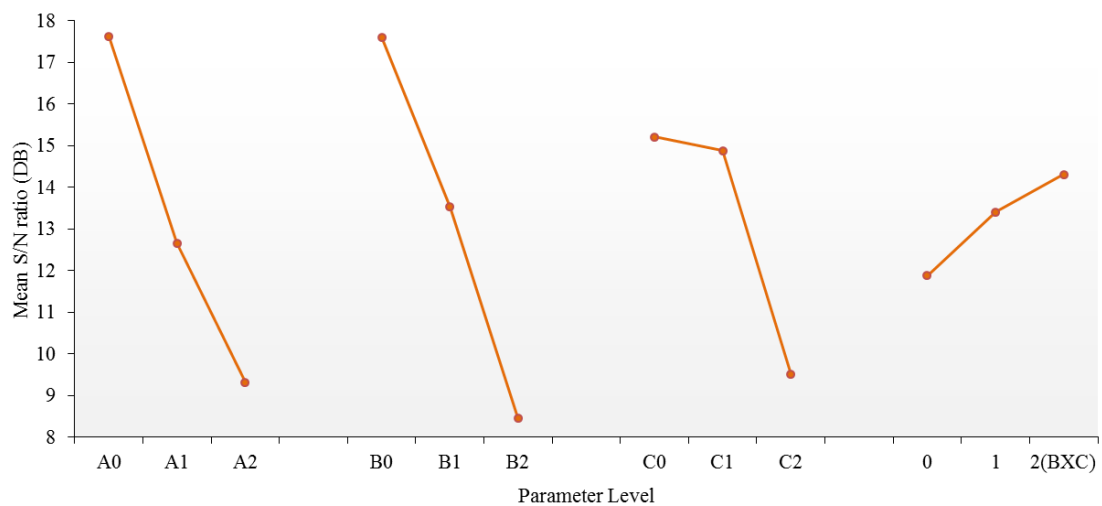
Fig. 6. 1. Response graph of S/N ratio for wear rate.
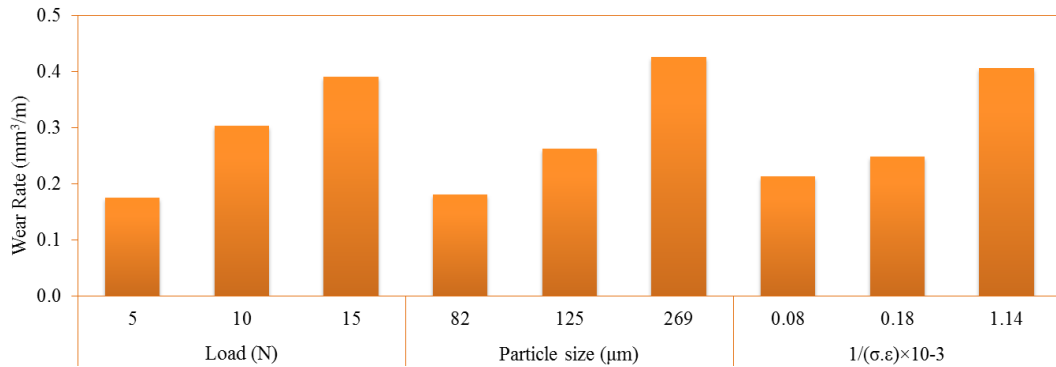
Fig. 6. 2. Average wear rate of three parameters.

6.3.2. Surface roughness

Table 6. 5 displays Pareto ANOVA analysis for the surface roughness. The abrasive particle size (B) has the most significant effect on the roughness with 78.49 % contribution followed by $(\sigma.\varepsilon)^{-1}$ (7.55 %), and applied load (5.49 %).

Table 6. 5. Pareto ANOVA analysis of surface roughness.

Sum at factor level	Factor and interaction								
	A	**B**	**A×B**	**A×B**	**C**	**A×C**	**A×C**	**B×C**	**B×C**
0	-101.02	-80.34	-113.35	-115.04	-126.04	-102.92	-109.31	-116.87	-111.03
1	-117.50	-99.73	-112.55	-113.72	-100.13	-115.57	-118.90	-111.55	-107.51
2	-122.07	-160.52	-114.69	-111.82	-114.42	-122.09	-112.38	-112.17	-122.05
Sum of squares of difference (S)	734.95	10502.10	6.99	15.71	1010.41	569.97	144.00	50.78	345.25
Contribution ratio (%)	5.49	78.49	0.05	0.12	7.55	4.26	1.08	0.38	2.58

	B	C	A	A×C	B×C	A×C	B×C	A×B	A×B
	78.49	7.55	5.49	4.26	2.58	1.08	0.38	0.12	0.05
Cumulative contribution	78.49	86.04	91.53	95.79	98.37	99.45	99.83	99.95	100.00
Check on significant interaction	A×C two-way table								
Optimum combination of significant factor level	A0B0C1								

Table 6. 6 and Fig. 6. 3 illustrate the response table and a graph of mean S/N ratio of the surface roughness, respectively. It is clear that the smallest abrasive particle size (B0) results in the lowest surface roughness. The strength of the parameters' effect is represented by the slope of the response graph, which is confirmed by ANOVA analysis as shown in Table 6. 5. The obtained results by Pareto ANOVA and Taguchi S/N response are verified by the traditional analysis shown in Fig. 6. 4. It shows the surface roughness increases with the increase of the normal load and abrasive size. Though, with increase of $(\sigma.\varepsilon)^{-1}$, it decreases initially and then increases.

Table 6. 6. Response table of mean S/N ratio for surface roughness and significant interaction.

		Mean S/N ratio			
Input parameters	**Symbol**	**Level 0**	**Level 1**	**Level 2**	**max-min**
Applied load	A	-11.22	-13.06	-13.56	2.34
Particle size	B	-8.93	-11.08	-17.84	8.91
$(\sigma.\varepsilon)^{-1}$	C	-14.00	-11.13	-12.71	2.88
Interaction A×C	A×C	-11.44	-12.84	-13.57	2.13
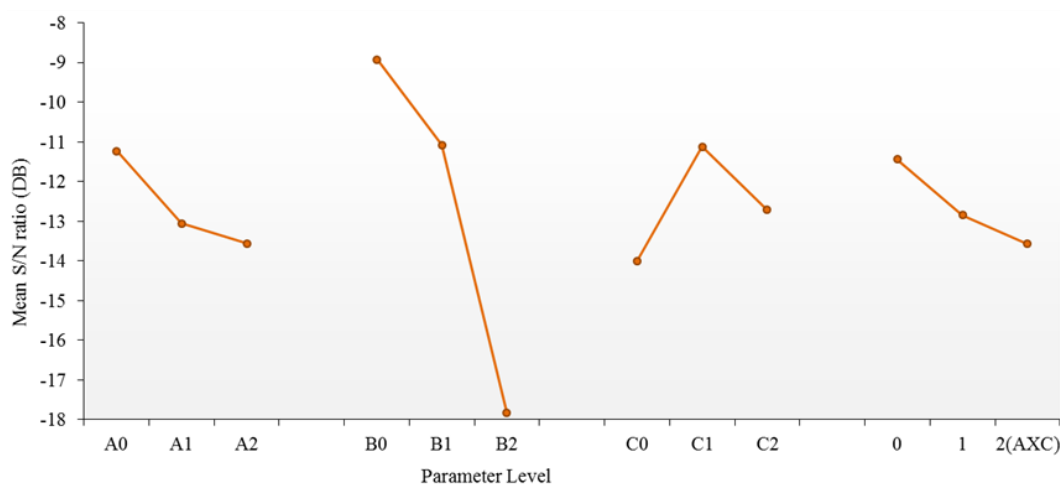
Fig. 6. 3. Response graph of S/N ratio for surface roughness.
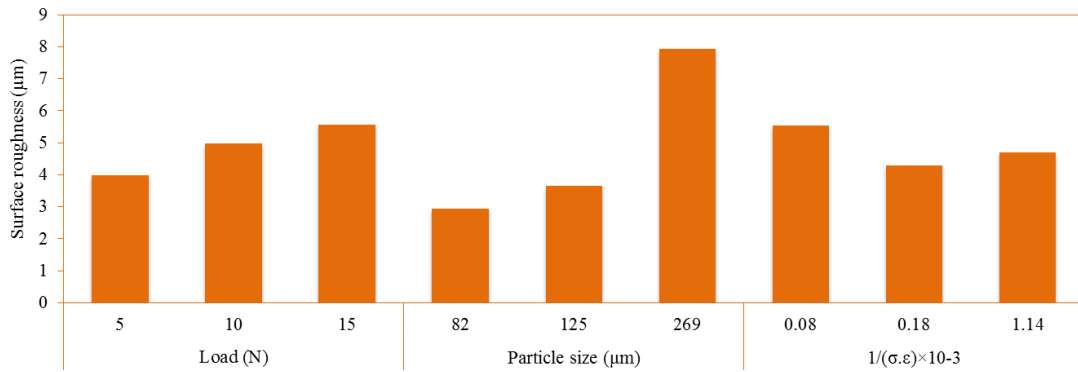
Fig. 6. 4. The average surface roughness of three parameters.

6.3.3. Temperature build-up (TBU)

Pareto ANOVA analysis of TBU presented in Table 6. 7. shows the abrasive particle size (B) has the most significant effect with 52.35 % participation followed by $(\sigma.\varepsilon)^{-1}$ of 14.05 % and applied load of 0.86 %. The applied load and mechanical properties' interaction (A×C) also plays a role in TBU (13.44 %).

Table 6. 7. Pareto ANOVA analysis for temperature build-up.

Sum at factor level	Factor and interaction								
	A	**B**	**A×B**	**A×B**	**C**	**A×C**	**A×C**	**B×C**	**B×C**
0	-86.90	-74.09	-81.66	-85.82	-94.60	-88.37	-78.53	-94.58	-87.56
1	-91.66	-83.92	-90.99	-96.87	-95.53	-88.91	-95.77	-88.02	-87.01
2	-89.82	-110.37	-95.73	-85.69	-78.25	-91.10	-94.08	-85.78	-93.82
Sum of squares of difference (S)	34.59	2111.57	307.46	247.29	566.53	12.58	542.26	125.38	86.00
Contribution ratio (%)	0.86	52.35	7.62	6.13	14.05	0.31	13.44	3.11	2.13

B	C	A×C	A×B	A×B	B×C	B×C	A	A×C
52.35	14.05	13.44	7.62	6.13	3.11	2.13	0.86	0.31

Cumulative contribution	52.35	66.40	79.84	87.46	93.59	96.70		98.83	99.69	100.00
Check on significant interaction	A×C two-way table									
Optimum combination of significant factor level	A0B0C2									

The response table and graph of mean S/N ratio are presented in Table 6. 8 and Fig. 6. 5, respectively. The generated TBU at low applied load, small abrasive particle size (B), and high $(\sigma.\varepsilon)^{-1}$ (C2) is the minimum one, which is verified by the traditional method's result shown in Fig. 6. 6. The variation of TBU is negligible with respect to the variation of applied load. The TBU escalates with the decrease of $(\sigma.\varepsilon)^{-1}$ and the increase of abrasive particle size.

Table 6. 8. Response table of mean S/N ratio for (TBU) and significant interaction.

		Mean S/N ratio			
Input parameters	Symbol	Level 0	Level 1	Level 2	max-min
Applied load	A	-9.66	-10.18	-9.98	0.53
Particle size	B	-8.23	-9.32	-12.26	4.03
$(\sigma.\varepsilon)^{-1}$	C	-10.51	-10.61	-8.69	1.92
Interaction A×C	A×C	-8.73	-10.64	-10.45	1.92
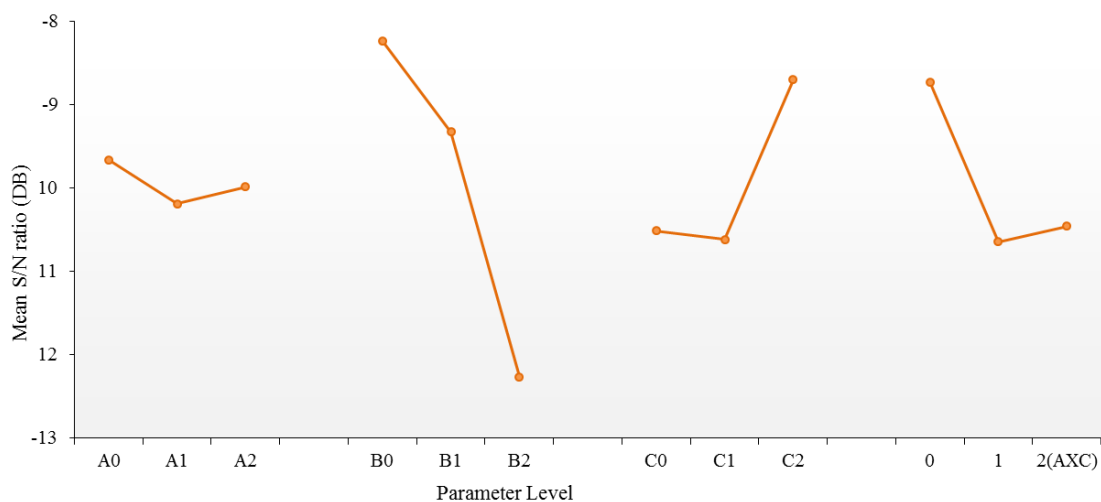
Fig. 6. 5. Response graph of S/N ratio for TBU.
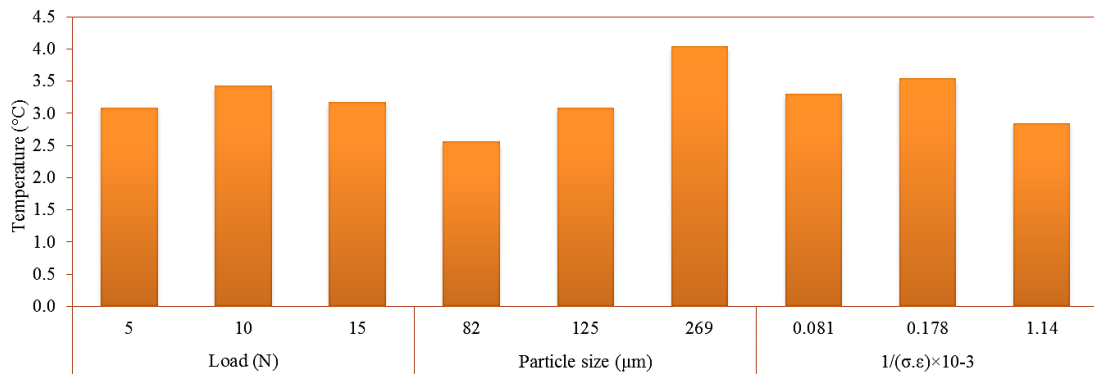
Fig. 6. 6. Average TBU of three parameters.

6.4. Discussion

The traditional method, Pareto ANOVA, and Taguchi's design are performed to identify the significance of the control factors on wear rate, surface roughness, and TBU, statistically.

The analysis of the wear rate's results demonstrates that the contribution of interaction is negligible compared to the total contribution of the main factors (92.28 %) (see Table 6. 3). In other words, the main factors mostly have effect on the wear rate and it is possible to reduce the wear rate by selecting the optimum input parameters.

The interaction of B×C is noteworthy, thus a two-way table is applied (see appendix 1) to select an optimum level of B and C, and it is defined as B0C0. To achieve the lowest wear rate, A0B0C0 is determined as the best combination of input factors, which is based on the low level of applied load, abrasive particle size, and $(\sigma.\varepsilon)^{-1}$. The average variation in wear rate shown in Fig. 6. 2 also confirms this.

There is a combination of the applied load and abrasive particle size that the stress concentration is maximum on the surface. The material removal is facilitated by the increase of $(\sigma.\varepsilon)^{-1}$, which means low tensile strength and elongation at break resulting hence the elastomer shows less resistant against deformation.

Table 6. 5 indicates that the main parameters contribution is about 91.03 % for the surface roughness of the worn elastomers. Consequently, optimization of the surface

roughness is possible by proper selection of input parameters. A two-way analysis of A×C interactions (see appendix 1) indicates A0B0C1 is the optimum combination of factors that offers the lowest surface roughness. It indicates the minimum surface roughness is achieved at the low level of applied load, abrasive particle size, and medium $(\sigma.\varepsilon)^{-1}$. Fig. 6. 4 shows the surface roughness increases with the increase of normal load and abrasive size. In other words, under higher loading, the large abrasive particles generate deeper ploughing marks and scratches on the surface of the rubber leading to an increase of the surface roughness, when the wear mechanism is abrasion. While the wear mechanism is friction wear it points to the ridges' formation on the worn surface. However, with the increase of $(\sigma.\varepsilon)^{-1}$ the surface roughness decreases initially and then increases again. There is a critical value of $(\sigma.\varepsilon)^{-1}$ that minimum surface roughness is achieved. It is known that the tensile strength and elongation at break affect the wear mechanism and as a result the surface roughness by forming the ridges, scratches, and grooves. Their height, depth, and space influence the surface roughness.

For TBU, on the contrary with results of the wear rate and surface roughness, the contribution of interactions (32.74 %) in comparison with the main factors (67.26 %) is high (see Table 6. 7), therefore, it is difficult to optimize temperature build-up by selecting input parameters. To achieve minimum TBU, a two-way table of A×C interaction (see appendix 1) is applied, the lowest TBU is achieved at A0C2. Consequently, A0B0C2 is the optimum combination of parameters. TBU increases due to the larger abrasives and higher $(\sigma.\varepsilon)^{-1}$, as they increase the adhesive friction and deformation, respectively. Accordingly, the friction increases, which leads to increase of the frictional heat, thus the surface temperature (TBU) raises.

Compared to two other factors, the effect of the applied load is negligible on TBU since elastomers deform more easily under the applying load compare to the other materials (metals, composites, and ceramics). Furthermore, the variation of $(\sigma.\varepsilon)^{-1}$ with applied load leads to variation of friction by changing the resistance of material to the deformation and affecting the contribution of it, which is the dominant factor on wear. The interaction between the applied load and abrasive particle size influences the friction, as a result, the generated heat on the surface. It is confirmed by the obtained

results that investigated the effect of load and the abrasive particle size on friction, individually (see Fig. 4. 20 and Fig. 5. 14 – 5.16).

6. 5. Summary

The presented results show that the operating variables such as the applied load and abrasive particle size, and mechanical properties of rubber (tensile strength and elongation at break) have effect on the wear rate, surface roughness, and TBU. The following conclusions are drawn based on the above investigation:

- With the Taguchi method and ANOVA analysis, the optimal combination of effective parameters on two body abrasive wear parameters is predicted to an acceptable level of accuracy.

- The wear rate depends on the effect of individual parameters considered in this investigation. The abrasive particle size has the highest contribution (39.78 %) on the wear rate followed by the normal load and $(\sigma.\varepsilon)^{-1}$. It is likely that the wear rate can be optimized by controlling these parameters. The minimum wear rate is obtained at the smallest abrasive size, and the lowest $(\sigma.\varepsilon)^{-1}$ and applied load.

- The abrasive particle size has the highest contribution (78.49 %) towards the surface roughness followed by $(\sigma.\varepsilon)^{-1}$ and normal load. Thus, the surface roughness can be optimized by selecting the proper values of input parameters.

- Temperature build-up is also affected prominently by the abrasive particle size followed by $(\sigma.\varepsilon)^{-1}$ and the interaction between applied load and abrasive particle size.

- The abrasive particle size (B) is the main contributor to the wear rate, surface roughness, and TBU.

Chapter 7. Development of a model

7.1. Introduction

Predicting the wear behavior of materials by considering the effect of operating parameters, mechanical, and physical properties is one of the most studied areas. There are a limited number of papers (see chapter 2), which developed a wear equation considering various factors for elastomers and polymers. For example, Lancaster et al. (Lancaster, 1968) suggested a relation between hardness, elastic modulus, breaking strength, elongation at break, and the wear rate. However, the previous studies by Budinski (Budinski, 1997), Fukahori (Fukahori and Yamazaki, 1995), and the obtained result in chapter 4 show that this equation correlates poorly for polymers and elastomers and the relationship between wear volume and load is not linear. Rhee (Rhee, 1970) proposed a nonlinear relation between the wear rate and pressure, velocity, and time. Few studies used the dimensional analysis, which is a mathematical tool, used in all the branches of science and engineering, to find a relation between the wear volume and the affecting parameters (Kar and Bahadur, 1974, Viswanath and Bellow, 1995). Nevertheless, most of these equations did not include the effect of mechanical properties on the wear rate. Moreover, they mostly focused on the wear of polymers and composites sliding on the metallic surface, not elastomers. On the other hand, an important operating parameter that affects the wear behavior is the abrasive particle and the counter face roughness. Its effect (shape and size) has been widely studied for the metallic materials (Stachowiak and Stachowiak, 2001, De Pellegrin and Stachowiak, 2002, Coronado, 2015); however, there is a limited study that includes the parameter of abrasive particle as the operating variable the wear equation (Rajesh and Bijwe, 2005).

A basic knowledge is needed to understand and control the material removal during the wear. However, the review of previous studies shows because of the complexities involved in wear there are few efforts to model it, particularly for elastomers. Due to the growing usage of the elastomers in different industries, it is desirable to predict the elastomers' wear durability. Considering these aspects, in this chapter an experimental wear model is presented to provide a better understanding of the elastomers' wear rate's relationship with operating variables and the material properties that dominate

the wear of elastomer sliding against abrasives, and expressing them in the form of an equation to determine wear rate.

7.2. Model development

To quantify the contribution of effective variables, a dimensional analysis method is used, which uses a dimensionally homogeneous equation in terms of the relationships among dimensionless variables (DV). The result of multiplying or dividing of combinations of physical variables, parameters, and constants of any particular system is a unit-less value called dimensionless variable. The Buckingham's Theorem explains that the difference between the variables and fundamental dimensions' number defines the independent DVs' number. It is used to characterize the relationships between the dimensionless variables and the original physical variables and qualitatively predict the mathematical relationship (Viswanath and Bellow, 1995, Rajesh and Bijwe, 2005).

A review of different studies and the obtained results from Taguchi's method (see chapters 2 and 6, respectively) shows the effective parameters on wear of elastomers are the combination of operating variables such as applied load, sliding velocity, time, and abrasive particle size, and the elastomers' mechanical properties including hardness, tensile strength, and elongation at break. Mechanical properties play an important role on wear behavior of elastomers, particularly before material detachment. These variables' relationship with the wear rate is considered to predict the wear rate by the dimensional analysis.

Wear volume (V) is used as the main dependent variable. Abrasive particle size (d), applied load/force (F), and hardness (H) are used as independent variables. Velocity (v), time (t), and ($\sigma.\varepsilon$) are considered as repeating variables. The three primary dimensions are mass (M), length (L), and time (T). Table 7. 1 shows the details of the wear process variables, their symbols, and dimensions. To obtain an expression for the wear of the elastomers, the dimensional analysis is used to connect the variables.

The Eq. 7.1 expresses the dependent variable wear volume (V). There are seven variables including the dependent one, thus there are four dimensionless groups

according to Pi-theorem, which each group has only one variable, and the rest is constant for a particular material.

Table 7. 1. Variables in a wear process, their symbols, and dimensions.

Variable	Symbol	Dimension
Wear volume	V	$[L^3]$
Load	F	$[MLT^{-2}]$
Abrasive particle size	d	$[L]$
Sliding velocity	v	$[LT^{-1}]$
Time	t	$[T]$
Sliding distance	S	$[L]$
Hardness	H	$[ML^{-1}T^{-2}]$
Tensile strength* Elongation at break	(σε)	$[ML^{-1}T^{-2}]$

$$f\{V, F, d, H, v, t, (\sigma.\varepsilon)\} = 0 \qquad (7.1)$$

$$\Pi_1 = v^a.t^b.(\sigma.\varepsilon)^c.V \qquad (7.2)$$

$$[LT^{-1}]^a[T]^b[ML^{-1}t^{-2}]^C[L^3] = [M^0L^0T^0] \qquad (7.3)$$

Exponents are calculated:

$$a = -3, \qquad b = -3, \qquad c = 0$$

Thus,

$$\Pi_1 = v^{-3}.t^{-3}.(\sigma.\varepsilon)^0.V = \frac{V}{(v.t)^3} = \frac{V}{S^3} \qquad (7.4)$$

$$\Pi_2 = v^a.t^b.(\sigma.\varepsilon)^c.F \qquad (7.5)$$

$$[LT^{-1}]^a[T]^b[ML^{-1}t^{-2}]^c[MLT^{-2}] = [M^0L^0T^0] \qquad (7.6)$$

Exponents are calculated:

$$a = -2, \qquad b = -2, \qquad c = -1$$

Thus,

$$\Pi_2 = v^{-2}.t^{-2}.(\sigma.\varepsilon)^{-1}.F = \frac{F}{(v.t)^2.(\sigma.\varepsilon)} = \frac{F}{S^2.(\sigma.\varepsilon)} \qquad (7.7)$$

$$\Pi_3 = v^a.t^b.(\sigma.\varepsilon)^c.d \qquad (7.8)$$

$$[LT^{-1}]^a[T]^b[ML^{-1}t^{-2}]^c[L] = [M^0L^0T^0] \qquad (7.9)$$

Exponents are calculated:

$$a = -1, \qquad b = -1, \qquad c = 0$$

Thus

$$\Pi_3 = v^{-1}.t^{-1}.(\sigma.\varepsilon)^0.d = \frac{d}{v.t} = \frac{d}{S} \qquad (7.10)$$

$$\Pi_4 = v^a.t^b.(\sigma.\varepsilon)^c.H \qquad (7.11)$$

$$[LT^{-1}]^a[T]^b[ML^{-1}t^{-2}]^c[ML^{-1}T^{-2}] = [M^0L^0T^0] \qquad (7.12)$$

Exponents are calculated:

$$a = 0, \qquad b = 0, \qquad c = -1$$

Thus,

$$\prod_4 = v^0 . t^0 . (\sigma.\varepsilon)^{-1} . H = \frac{H}{(\sigma.\varepsilon)} \qquad (7.13)$$

There are four groups and the physical significance of each group is as follows:

- The first and main dependent group (Eq. 7.4) illustrates the wear volume as a dependent variable during the abrasion.

- The second group (Eq. 7.7) involves load, sliding distance, tensile strength, and elongation at break represents the effect of normal load on deformation at the abrading interface.

- The third group (Eq. 7.10) includes the abrasive particle size along with the distance and illustrates the real contact area during the abrasion and applied stress.

- The last group (Eq. 7.13) consists of hardness, tensile strength, and elongation at break represents the resistance of the elastomer against deformation and crack formation. Furthermore, the material's distribution at the contact surface that equals the amount of work ($\sigma.\varepsilon$) per unit volume.

The main dependant group is combined in terms of an arbitrary function (f) that contains the other three groups, represented by Eq. 7.15 and 7.16.

$$\prod_1 = f(\prod_2, \prod_3, \prod_4) \qquad (7.15)$$

$$\left(\frac{V}{S^3}\right) = f\left(\frac{F}{S^2.(\sigma.\varepsilon)}, \frac{d}{S}, \frac{H}{(\sigma.\varepsilon)}\right) \qquad (7.16)$$

Eq. 7.16 is written in a generalized form as Eq. 7.17.

$$\left(\frac{V}{S^3}\right) = K\left(\frac{F}{S^2.(\sigma.\varepsilon)}\right)^x \left(\frac{d}{S}\right)^y \left(\frac{H}{(\sigma.\varepsilon)}\right)^z \qquad (7.17)$$

where K is wear coefficient and x, y, and z are unknown exponents that will be determined experimentally. Eq. 7.17 is simplified as

$$\frac{V}{S} = K \frac{F^x d^y H^z}{S^{2x+Y-2}.(\sigma.\varepsilon)^{x+z}} \qquad (7.18)$$

The Eq. 7.18 is rewritten as

$$WR = K \frac{F^x d^y H^z}{S^{2x+Y-2}.(\sigma.\varepsilon)^{x+z}} \qquad (7.19)$$

where WR is the wear rate (mm^3/m). In Eq. (7.19), the wear rate is expressed in terms of the operating variables (normal load, sliding distance, and abrasive particle size), which are controlled during the experiments, and material properties (hardness, tensile strength, and elongation at break).

7.3. Derivation of the exponents

To obtain the exponents in Eq. 7.19, the wear rate as a function of one of the three variables (normal load, abrasive particle size, and hardness) is calculated experimentally when one parameter varies and the other two are constant. The test method and obtained results are fully discussed in chapters 4 and 5. Then, here the wear rate is plotted as a function of the variable on logarithmic coordinates. Therefore, the exponents can be calculated from the logarithmic plots. The wear rate of different elastomers as a function of the normal load, abrasive particle size, and hardness is shown in Fig. 7. 1, Fig. 7. 2, and Fig. 7. 3, respectively.
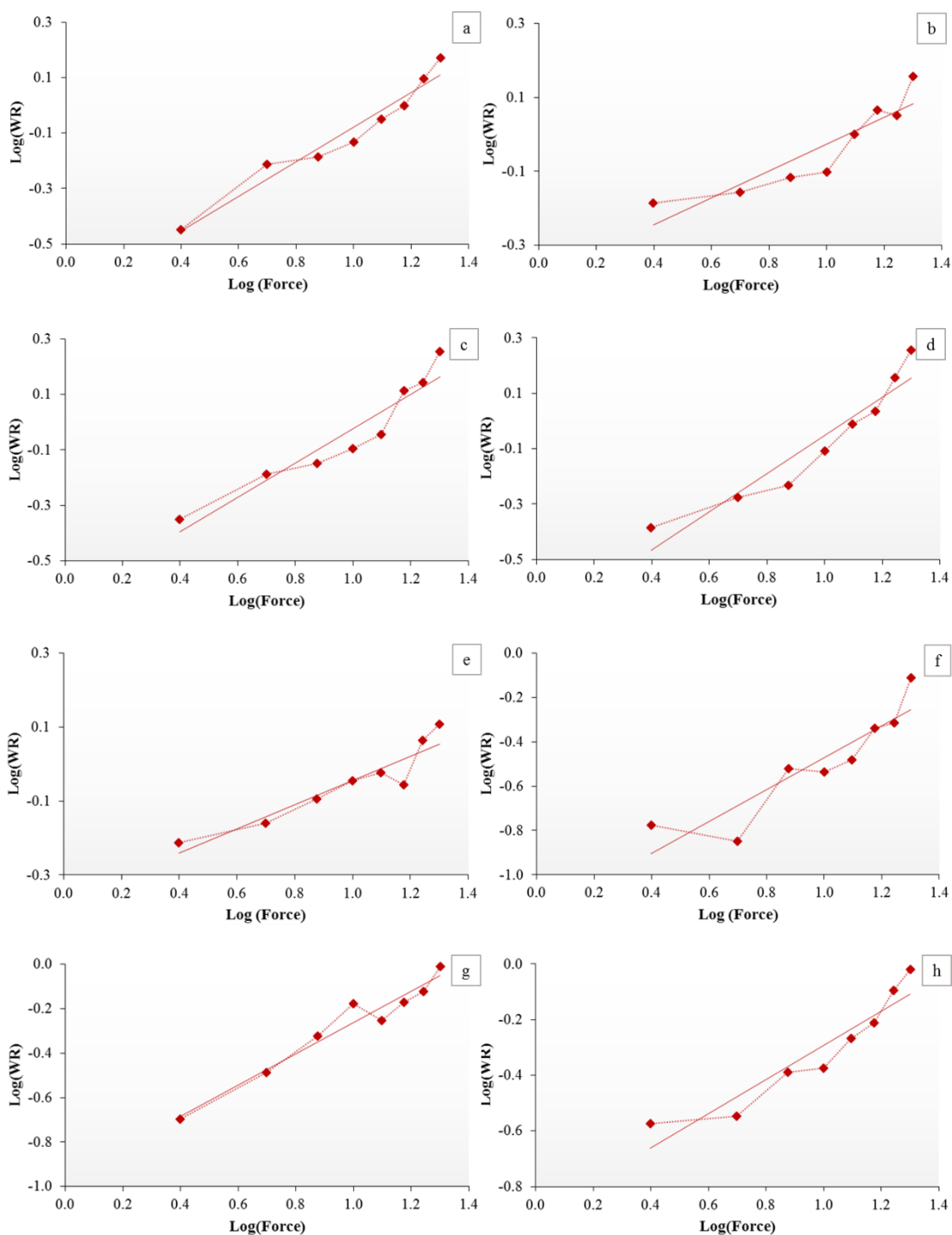
Fig. 7. 1. WR vs Load: (a) NR1, (b) NR2, (c) NR4, (d) NR6, (e) NR7, (f) NR8, (g) SBR, (h) NBR.
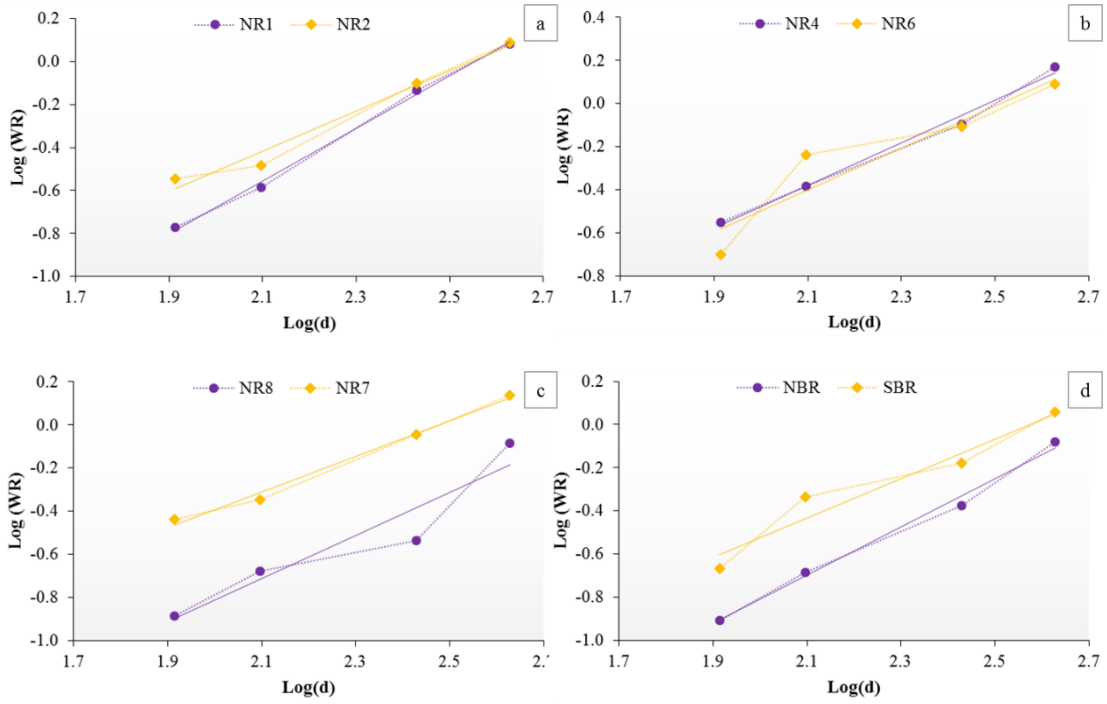
Fig. 7. 2. WR vs Abrasive particle size: (a) NR1 & NR2, (b) NR4 & NR6, (c) NR7 & NR8, (d) SBR & NBR.
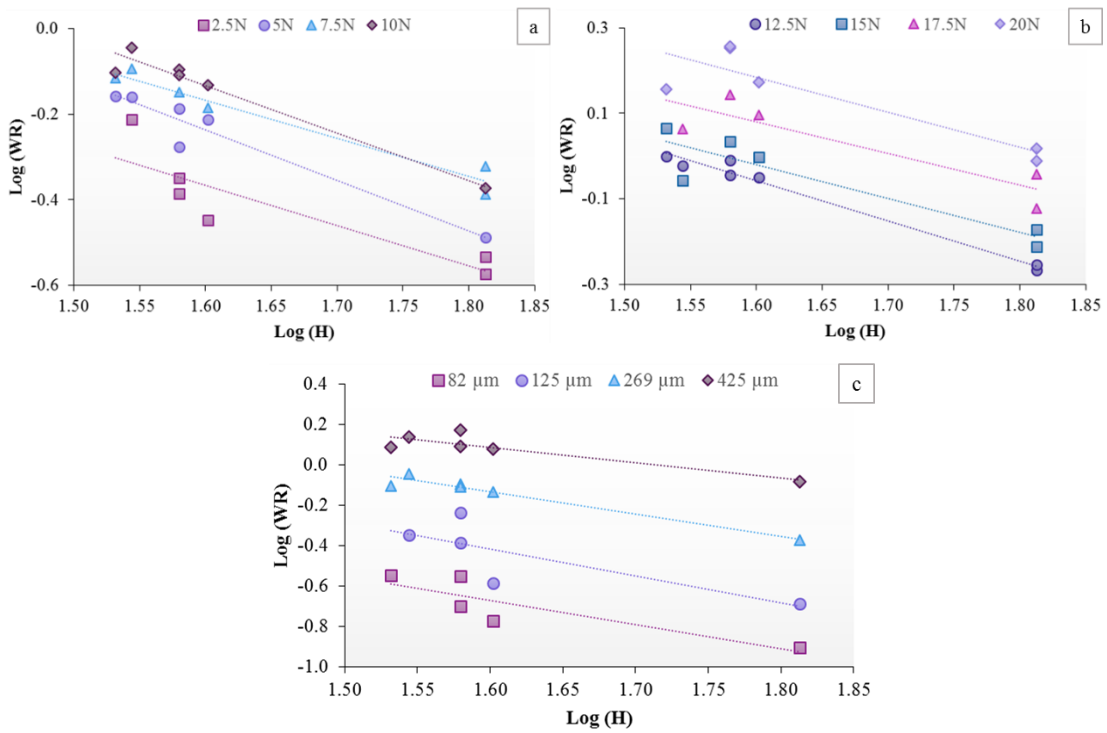
Fig. 7. 3. WR vs Hardness: (a) & (b) applied load, (c) particle size.

The data points fit a straight line, which implies that wear rate $\propto F^x, d^y, H^z$, where the slope of the straight line gives the exponents. Hence, the undetermined constants x, y, and z are evaluated by an empirical fit of abrasion wear data and the mean value is reported. Table 7. 2 represents x, y, and z values for each elastomer.

Table 7. 2. The x, y, and z values for NR, SBR, and NBR.

Elastomer	x	y	z
NR	0.662	1.037	-0.957
SBR	0.704	0.915	-0.957
NBR	0.613	1.117	-0.957

The x, y, and z values for each elastomer are substituted in Eq. 7.19. The final form of wear equations for NRs, SBR, and NBR are presented in Eqs. 7.20, 7.21, and 7.22, respectively.

$$WR_{NR} = K \frac{F^{0.662} d^{1.037} (\sigma . \varepsilon)^{0.295}}{S^{0.361} . H^{0.957}} \qquad (7.20)$$

$$WR_{SBR} = K \frac{F^{0.704} d^{0.915} (\sigma . \varepsilon)^{0.253}}{S^{0.323} . H^{0.957}} \qquad (7.21)$$

$$WR_{NBR} = K \frac{F^{0.613} d^{1.117} (\sigma . \varepsilon)^{0.344}}{S^{0.343} . H^{0.957}} \qquad (7.22)$$

To calculate the wear constant (K), Eqs. 7.20, 7.21, and 7.22 are rewritten. The obtained wear rate from the experimental tests, operating parameters (F, d, and S), and the material properties (H, σ, and ε) (see Table 3. 2) are substituted in Eqs. 7.23, 7.24, and 7.25.

$$K_{NR} = WR \frac{S^{361} H^{0.957}}{F^{0.662}. d^{1.037} (\sigma. \varepsilon)^{0.295}} \qquad (7.23)$$

$$K_{SBR} = WR \frac{S^{0.323} H^{0.957}}{F^{0.704}. d^{0.915} (\sigma. \varepsilon)^{0.253}} \qquad (7.24)$$

$$K_{NBR} = WR \frac{S^{0.343} H^{0.957}}{F^{0.613}. d^{1.117} (\sigma. \varepsilon)^{0.344}} \qquad (7.25)$$

The calculated wear coefficient for different loads, abrasive particle sizes, and elastomers do not show any significant change with varying the operating parameters. In other words, it is independent of operating parameters, thus the mean value is reported. The mean value of K for NRs, SBR, and NBR is $2.78 \times 10^{-5} \pm 0.06$, $2.35 \times 10^{-5} \pm 0.11$, and $5.30 \times 10^{-5} \pm 0.11$, respectively.

The calculated wear coefficients (K) are substituted in Eqs. 7.20, 7.21, and 7.22. The Eqs. 7.26, 7.27, and 7.28 represent the final form of wear rate's equation for NR, SBR, and NBR, respectively.

$$WR_{NR} = 2.78 \times 10^{-5} \frac{F^{0.662} d^{1.037} (\sigma. \varepsilon)^{0.295}}{S^{0.361}. H^{0.957}} \qquad (7.26)$$

$$WR_{SBR} = 2.35 \times 10^{-5} \frac{F^{0.704} d^{0.915} (\sigma. \varepsilon)^{0.253}}{S^{0.323}. H^{0.957}} \qquad (7.27)$$

$$WR_{NBR} = 5.30 \times 10^{-5} \frac{F^{0.613} d^{1.117} (\sigma. \varepsilon)^{0.344}}{S^{0.343}. H^{0.957}} \qquad (7.28)$$

7.4. Model verification

To validate the formulation, the wear rate is calculated by Eqs. 7.26, 7.27, and 7.28. Then, the calculated wear rate and experimental wear rate are plotted as a function of the applied load and the abrasive particle size, as shown in Fig. 7. 4 and Fig. 7. 5, respectively, while the other parameters are constant. The experimental results are obtained by running tests with eight different elastomers as the specimen and the wear test machine, described in chapter 3. The parameters for the wear test are: sliding speed 0.32 m/s, sliding distance 40 m. While the applied load is 10N, the abrasive particle size varies from fine to coarse: 82, 125, 269, and 425 µm. Different loads (2.5, 5, 7.5, 10, 12.5, 15, 17.5, and 20N) are applied, while the abrasive size is 269 µm.
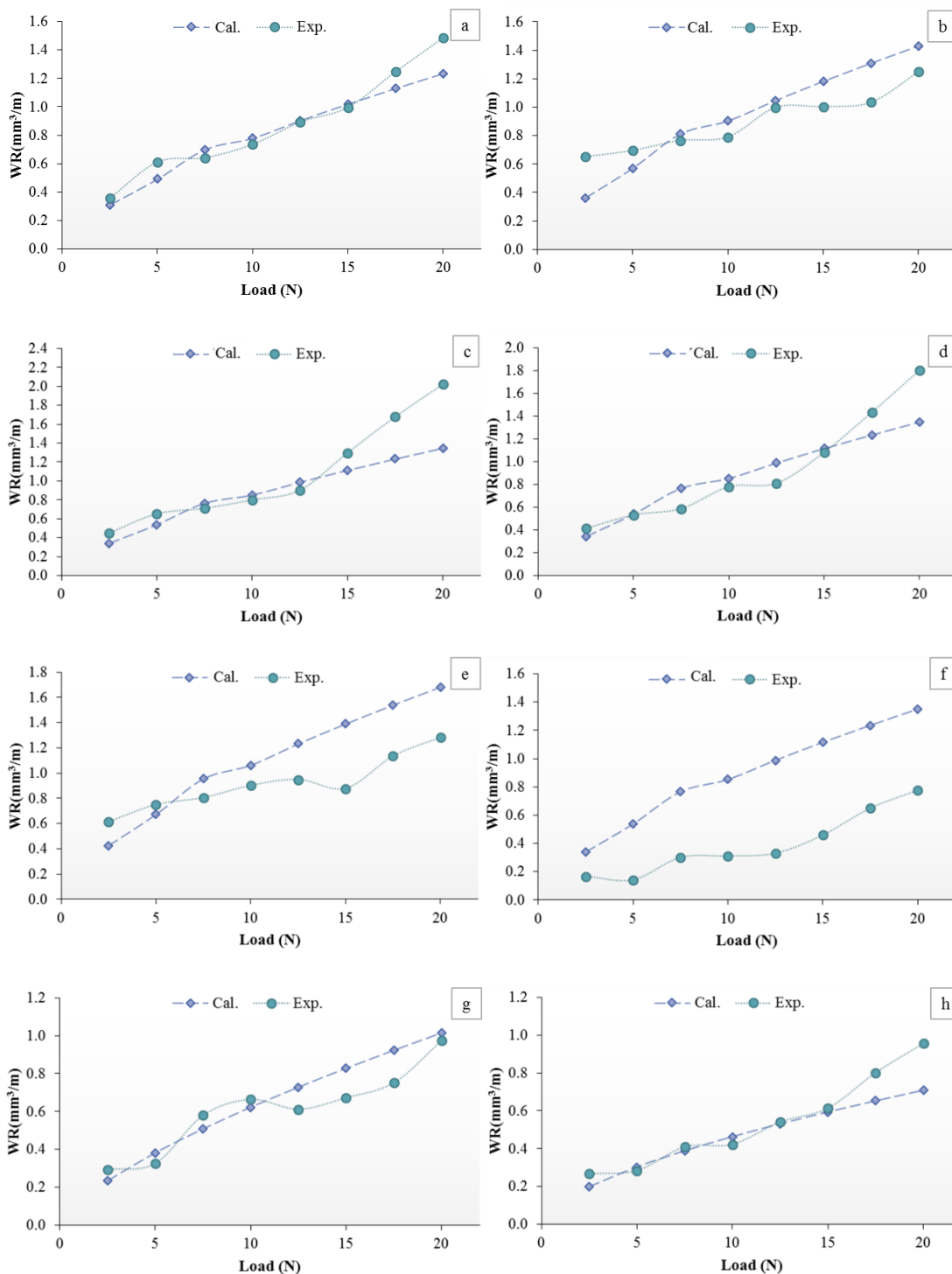
Fig. 7. 4. Calculated and experimental wear rate vs. applied load: (a) NR1, (b) NR2, (c) NR4, (d) NR6, (e) NR7, (f) NR8, (g) SBR, (h) NBR, abrasive particle size 269 µm.
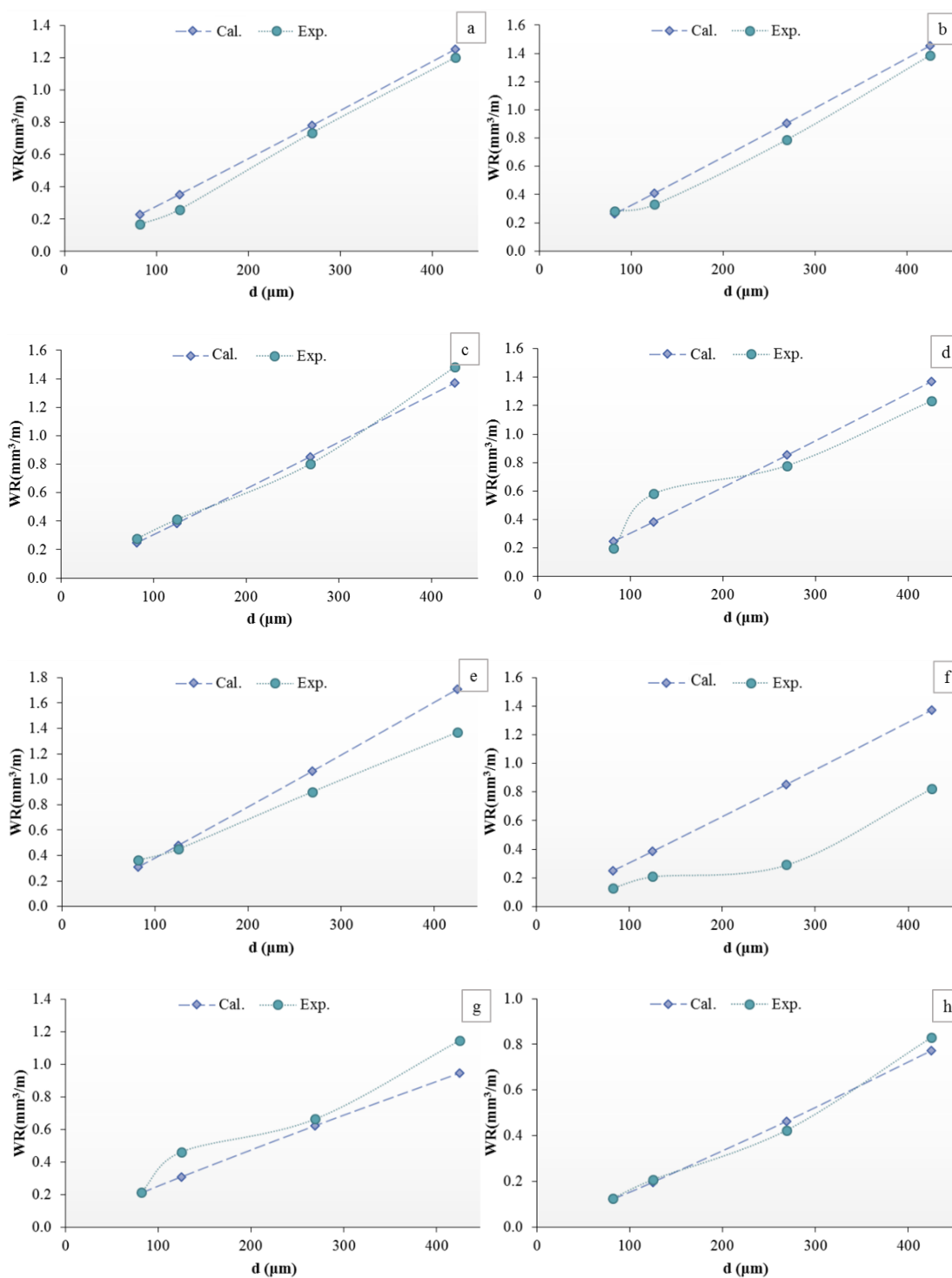
Fig. 7. 5. Calculated and experimental wear rate vs. abrasive particle size: (a) NR1, (b) NR2, (c) NR4, (d) NR6, (e) NR7, (f) NR8, (g) SBR, (h) NBR, applied load 10N.
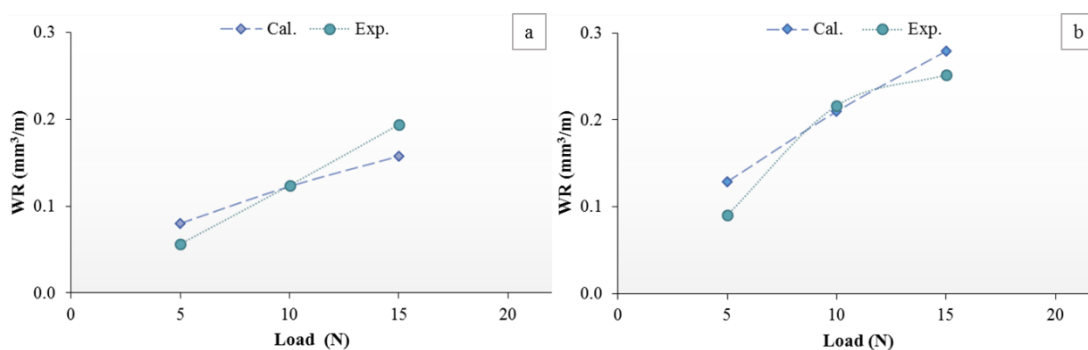
Fig. 7. 6. Calculated and experimental wear rate vs. applied load: (a) NBR, (b) SBR, abrasive particle size 125 µm.

7.5. Discussion

An equation is developed to predict the wear rate of elastomers by identifying and considering dominant properties of the material and operating variables that control the wear. The exponents and coefficients are obtained experimentally. The x, y, and z value (see Table 7. 2) show that the wear rate is directly proportioned to the applied load and abrasive particle size, and inversely to the hardness. It means the wear rate increases with the increase of the applied load and the abrasive particle size (see chapters 4 and 5) and decreases with the increase of the hardness. The exponent "y" with abrasive particle size is significant and the highest for each elastomer, which defines it, as the most critical operating variable. The results of Pareto ANOVA analysis also confirm (see Table 6. 3) that the abrasive particle size is the most effective parameter on the wear rate.

Under different test conditions, the exponents and the calculated wear coefficient are different for each elastomer and approximately the same for the NRs. It could be concluded that at least for these elastomers x, y, z, and K depend on the molecular structure and are independent of physical and chemical properties, and the operating parameters. The obtained results by Viswanath et. al. (Viswanath and Bellow, 1995) also approves this hypothesis, which is an important and desirable feature for the equation.

Comparison of theory and experimental results is a significant benchmark for any theory validation process. For each specimen, the calculated wear rate with varying

applied load (illustrated in Fig. 7. 4) shows a similar trend as the experimental ones with the excellent qualitative agreement. The elastomers fit the theoretical curves reasonably well, especially at low applied loads. However, it does not show the wear mechanism's change (change of wear rate trend).

The relationship between the abrasive particle size as a function of wear rate (demonstrated in Fig. 7. 5) indicates excellent qualitative and quantitative agreement between the calculated and experimental wear rate.

With increase of the applied load the formation of wear debris, their movement within the contact area, and being embedded into micro-pits, grooves, and the abrasive paper influence the contribution of abrasive particle size and the real contact area during the experimental test resulting in a difference between the calculated and experimental wear rate. For instance, wear debris of NR2 and NR7, which are the largest generated debris (see Table 4.2), acts as a third body between the specimen and rough surface, and decreases the contribution of the abrasive particle size and real contact area. On the contrary, the real contact area of other specimens with smaller abrasives is increased, thus the wear rate is higher than the calculated ones. In addition, the friction's variation with increase of the load (see Fig. 4. 22) affects the elastomers' wear rate. The difference between calculated and experimental wear rate for NR8 is more than the expected. This could be due to the specimen's geometry (CN bonding with 2mm thickness at the bottom), which leads to change in the contribution of the mechanical properties such as strain rate with increase of the applied load, and abrasive size that can affect wear behavior. It is discussed more in details in chapter 4.

7. 6. Summary

A review of researches on the wear behavior of polymers and elastomers showed there is no generally accepted equation for the prediction of wear of them, thus to provide a better characteristic expression of the parameters affecting the wear rate, a wear equation is developed.

- A non-linear wear equation is developed by quantifying the contribution of the operating variables and mechanical properties, based on the abrasive

wear studies and analysis using Buckingham's dimensional analysis approach on various elastomers.

- Abrasive particle size is included in the equation since it has a significant effect on the wear behavior of elastomers.

- The obtained exponents show the significance of each parameter on the wear rate.

- A good correlation is observed between the calculated and experimental wear rates.

Summary

8.1. Conclusion

The reported investigations on the wear and friction of the materials (metals, polymers, and composites) show that the applied load, the abrasive particle size, and mechanical properties of the material affect the tribological behaviour of the material.

The present work investigated the effect of these parameters on wear and friction behaviour of the elastomers using analytical and experimental methods. The following conclusions are drawn based on the obtained results.

From the applied load's effect on wear, it is concluded that the greater applied load results in the higher wear rate. Although, the rate of the ascending depends on the wear mechanism. While abrading under varying applied load, the wear mechanism changes according to the elastomer's properties. When the applied load is low, the wear mechanism is frictional wear, which is mixed with the fatigue wear for the NRs and is transferred to the abrasion wear for the NBR and SBR, with increase of the applied load. The wear rate's variation and wear mechanism depend on the mechanical properties, molecular chain's structure, and the chemical composition of the elastomer.

The increase of the applied load also affects the wear debris' formation, size, and shape that lead to the change of wear rate, and the adhesive and deformation contribution to the friction.

In addition to the wear, the friction is affected by the formation of the applied load. It is decreased and increased for the NRs and NBR, respectively. The participation of the adhesive and deformation changes due to the variation of the real contact area, third body formation, and deformability of elastomers, which results in decrease or increase of COF.

The wear rate's variation with the abrasive particle size is similar to the applied load. The wear rate increases with the increase of the grit size, however, the wear mechanism changes for each type of elastomer; as a result, the variations' rate changes, too.

A relationship is observed between the formed ridge's space of NRs with the applied load and the abrasive particle size. It increases with increase of wear until reaching a constant value. Similar to the case for the ridge's space, wear debris size also increases with increase of the applied load and the abrasive particle size. Their variation's rate depends on the elastomers' mechanical properties.

Generally, the COF raises with the change of the abrasive size from fine to coarse until reaching a critical value. It drops with further increase of the grit size. The maximum value of COF shifts with variation of the abrasive particle size, sliding velocity, and mechanical properties of the elastomer.

From the analytical investigation, it is found that the abrasive particle size is the most effective parameter on wear (rate and mechanism), followed by the applied load.

Considering these parameters, a non-linear wear equation is developed to predict the wear rate by quantifying the contribution of the operating variables and mechanical properties. There is a good correlation between the calculated and experimental wear rates for each elastomer type.

8.2. Future works

In the investigation of the wear behaviour in this thesis, it is focused on the two-body wear of the elastomers, and sand paper is used as an abrasive. However, in some industrial applications, such as conveyor belt systems that the rubber is exposed to the various abrasives and three-body abrasive wear occurs between the belt and pulley. Since the applied stress is different at three-body wear, to deal with this issue a test rig is designed (see Appendix 2), by modifying the ASTM G65 test equipment to simulate the wear process that happens in conveyor belt's system. In addition to running test with different abrasive particle size, abrasives with different shapes and types also can be used as the abrasive medium.

The tear strength is not considered in the developed model to calculate the wear rate. As tear strength plays significant role with increase of the applied load and abrasive particle size in the wear process, it would be good to take into account the tear strength's contribution. Thus, the wear rate would be predicted more accurately.

Wear has a significant impact on the friction coefficient; hence running the friction experiments at higher sliding distance to further study is required.

It would be interesting to investigate wear of more elastomers with different mechanical properties to validate the developed model.

References

ABDELBARY, A. 2014. *Wear of polymers and composites*, Elsevier.

ALAJMI, M. & SHALWAN, A. 2015. Correlation between Mechanical Properties with Specific Wear Rate and the Coefficient of Friction of Graphite/Epoxy Composites. *Materials,* 8**,** 4162-4175.

ARCHARD, J. F. 1953. Contact and rubbing of flat surfaces. *Journal of Applied Physics,* 24**,** 981-988.

BARQUINS, M. & ROBERTS, A. D. 1986. Rubber friction variation with rate and temperature: some new observations. *Journal of Physics D: Applied Physics,* 19**,** 547.

BASAK, A. K., CELIS, J. P., VARDAVOULIAS, M. & MATTEAZZI, P. 2014. Coefficient of friction measured from nano-to macro-normal loads on plasma sprayed nanostructured cermet coatings. *Metallurgical and Materials Transactions A,* 45**,** 1049-1056.

BASAK, A. K., ZEIN EDDINE, W., CELIS, J.-P. & MATTEAZZI, P. 2010. Characterisation and tribological investigation on thermally processed nanostructured Fe-based and Cu-based cermet materials. *Journal of nanoscience and nanotechnology,* 10**,** 1179-1184.

BHATTACHARYA, M. & BHOWMICK, A. K. 2010. Analysis of wear characteristics of natural rubber nanocomposites. *Wear,* 269**,** 152-166.

BOISSONNET, L., DUFFAU, B. E. & MONTMITONNET, P. 2012. A wear particle-based model of friction in a polymer–metal high pressure contact. *Wear,* 286–287**,** 55-65.

BRAUN, O. M., STEENWYK, B., WARHADPANDE, A. & PERSSON, B. N. J. 2016. On the dependency of friction on load: Theory and experiment. *EPL (Europhysics Letters),* 113**,** 56002.

BRISCOE, B. J., LIN HENG, Y. & STOLARSKI, T. A. 1986. The friction and wear of poly(tetrafluoroethylene)-poly (etheretherketone) composites: An initial appraisal of the optimum composition. *Wear,* 108**,** 357-374.

BRISCOE, B. J. & SINHA, S. K. 2002. Wear of polymers. *Proceedings of the Institution of Mechanical Engineers, Part J: Journal of Engineering Tribology,* 216**,** 401-413.

BUDINSKI, K. G. 1997. Resistance to particle abrasion of selected plastics. *Wear,* 203–204**,** 302-309.

BURR, B. H. & MARSHEK, K. M. 1982. An equation for the abrasive wear of elastomeric O-ring materials. *Wear,* 81**,** 347-356.

CHO, K. & LEE, D. 2000. Effect of molecular weight between cross-links on the abrasion behavior of rubber by a blade abrader. *Polymer,* 41**,** 133-140.

CORONADO, J. J. 2015. Abrasive size effect on friction coefficient of AISI 1045 steel and 6061-T6 Aluminium alloy in two-body abrasive wear. *Tribology Letters,* 60**,** 40.

CORONADO, J. J. & SINATORA, A. 2011. Effect of abrasive size on wear of metallic materials and its relationship with microchips morphology and wear micromechanisms: Part 1. *Wear,* 271**,** 1794-1803.

COVENEY, V. & MENGER, C. 1999. Initiation and development of wear of an elastomeric surface by a blade abrader. *Wear,* 233–235**,** 702-711.

DE PELLEGRIN, D. V., CORBIN, N. D., BALDONI, G. & TORRANCE, A. A. 2009a. Diamond particle shape: Its measurement and influence in abrasive wear. *Tribology International,* 42**,** 160-168.

DE PELLEGRIN, D. V. & STACHOWIAK, G. W. 2002. Assessing the role of particle shape and scale in abrasion using 'sharpness analysis': Part I. Technique development. *Wear,* 253**,** 1016-1025.

DE PELLEGRIN, D. V., TORRANCE, A. A. & HARAN, E. 2009b. Wear mechanisms and scale effects in two-body abrasion. *Wear,* 266**,** 13-20.

EL-TAYEB, N. S. M. & NASIR, R. M. 2007. Effect of soft carbon black on tribology of deproteinised and polyisoprene rubbers. *Wear,* 262**,** 350-361.

FELHÖS, D. 2008. *Dry Sliding and Rolling Tribotests of Carbon Black Filled EPDM Elastomers and Their FE Simulations* Ph.D., Technical University of Kaiserslautern.

FENG, D., SHEN, M. X., PENG, X. D. & MENG, X. K. 2016. Surface Roughness Effect on the Friction and Wear Behaviour of Acrylonitrile–Butadiene Rubber (NBR) Under Oil Lubrication. *Tribology Letters,* 65**,** 10.

FUKAHORI, Y. & YAMAZAKI, H. 1994. Mechanism of rubber abrasion. Part 1: Abrasion pattern formation in natural rubber vulcanizate. *Wear,* 171**,** 195-202.

FUKAHORI, Y. & YAMAZAKI, H. 1995. Mechanism of rubber abrasion part 3: How is friction linked to fracture in rubber abrasion? *Wear,* 188**,** 19-26.

GABRIEL, P. 2010. *Investigation and modelling of rubber friction.* Ph.D., Queen Mary of London.

GÅHLIN, R. & JACOBSON, S. 1999. The particle size effect in abrasion studied by controlled abrasive surfaces. *Wear,* 224**,** 118-125.

GATOS, K. G., KAMEO, K. & KARGER-KOCSIS, J. 2007. On the friction and sliding wear of rubber/layered silicate nanocomposites. *EXPRESS Polymer Letters,* 1**,** 27-31.

GENT, A. N. & PULFORD, C. T. R. 1983. Mechanisms of rubber abrasion. *Journal of Applied Polymer Science,* 28**,** 943-960.

GROSCH, K. A. 1963. The relation between the friction and visco-elastic properties of rubber. *Proceedings of the Royal Society of London. Series A. Mathematical and Physical Sciences,* 274**,** 21-39.

GUSTAFSSON, E. 2013. *Investigation of friction between plastic parts.* Master's, Chalmers University of Technology.

HAKAMI, F., PRAMANIK, A., RIDGWAY, N. & BASAK, A. K. 2017. Developments of rubber material wear in conveyor belt system. *Tribology International,* 111**,** 148-158.

HAMID, M. K. A., STACHOWIAK, G. W. & SYAHRULLAIL, S. 2013. The effect of external grit particle size on friction coefficients and grit embedment of brake friction material. *Procedia Engineering,* 68**,** 7-11.

HARSHA, A. P. & TEWARI, U. S. 2003. Two-body and three-body abrasive wear behaviour of polyaryletherketone composites. *Polymer Testing,* 22**,** 403-418.

HARSHA, A. P., TEWARI, U. S. & VENKATRAMAN, B. 2003. Three-body abrasive wear behaviour of polyaryletherketone composites. *Wear,* 254**,** 680-692.

JUNKONG, P., KUESENG, P., WIRASATE, S., HUYNH, C. & RATTANASOM, N. 2015. Cut growth and abrasion behaviour, and morphology of natural rubber filled with MWCNT and MWCNT/carbon black. *Polymer Testing,* 41, 172-183.

KAR, M. K. & BAHADUR, S. 1974. The wear equation for unfilled and filled polyoxymethylene. *Wear,* 30, 337-348.

KHAN, M. S. 2008. *Friction, wear and mechanical properties of electron beam modified PTFE-based rubber compounds.* Ph.D., Technical Universität Dresden.

LANCASTER, J. K. 1968. Relationships between the wear of polymers and their mechanical properties. *Proceedings of the Institution of Mechanical Engineers, Conference Proceedings,* 183, 98-106.

LANCASTER, J. K. 1969. Abrasive wear of polymers. *Wear,* 14, 223-239.

LIANG, H. 2007. *Investigating the mechanism of elastomer abrasion* Ph.D., University of London.

LIANG, H., FUKAHORI, Y., THOMAS, A. G. & BUSFIELD, J. J. C. 2010. The steady state abrasion of rubber: Why are the weakest rubber compounds so good in abrasion? *Wear,* 268, 756-762.

LORENZ, B., OH, Y., NAM, S. K., JEON, S. H. & PERSSON, B. N. J. 2015. Rubber friction on road surfaces: Experiment and theory for low sliding speeds. *The Journal of chemical physics,* 142, 194701-12.

LORENZ, B., PERSSON, B. N. J., DIELUWEIT, S. & TADA, T. 2011. Rubber friction: Comparison of theory with experiment. *The European Physical Journal E,* 34, 129.

LV, X. R., WANG, H. M. & WANG, S. J. 2015. Effect of swelling nitrile rubber in cyclohexane on its aging, friction and wear characteristics. *Wear,* 328–329, 414-421.

MEDALIA, A. I., ALESI, A. L. & MEAD, J. L. 1992. Pattern abrasion and other mechanisms of wear of tank track pads. *Rubber Chemistry and Technology,* 65, 154-175.

MENG, H. C. & LUDEMA, K. C. 1995. Wear models and predictive equations: their form and content. *Wear,* 181–183, Part 2, 443-457.

MOFIDI, M. 2009. *Tribology of elastomeric seal materials.* Ph.D., Luleå University of Technology.

MOLNAR, W., VARGA, M., BRAUN, P., ADAM, K. & BADISCH, E. 2014. Correlation of rubber based conveyor belt properties and abrasive wear rates under 2- and 3-body conditions. *Wear,* 320, 1-6.

MOORE, D. F. 1980. Friction and wear in rubbers and tyres. *Wear,* 61, 273-282.

MOORE, M. A. 1978. Abrasive wear. *International Journal of Materials in Engineering Applications,* 1, 97-111.

MUHR, A. H. & ROBERTS, A. D. 1992. Rubber abrasion and wear. *Wear,* 158, 213-228.

MYSHKIN, N. K., PETROKOVETS, M. I. & KOVALEV, A. V. 2005. Tribology of polymers: Adhesion, friction, wear, and mass-transfer. *Tribology International,* 38, 910-921.

PADENKO, E., BERKI, P., WETZEL, W. & KARGER-KOCSIS, J. 2016. Mechanical and abrasion wear properties of hydrogenated nitrile butadiene rubber of identical hardness filled with carbon black and silica. *Journal of Reinforced Plastics and Composites,* 35, 81-91.

PAL, K., DAS, T., RAJASEKAR, R., PAL, S. K. & DAS, C. K. 2009. Wear characteristics of styrene butadiene rubber/natural rubber blends with varying carbon blacks by DIN abrader and mining rock surfaces. *Journal of Applied Polymer Science,* 111**,** 348-357.

PAL, K., PAL, S. K., DAS, C. K. & KIM, J. K. 2010a. Influence of fillers on NR/SBR/XNBR blends. Morphology and wear. *Tribology International,* 43**,** 1542-1550.

PAL, K., PAL, S. K., DAS, C. K. & KIM, J. K. 2010b. Relationship between normal load and dynamic co-efficient of friction on rock-rubber wear mechanism. *Materials & Design,* 31**,** 4792-4799.

PARK, S. 1996. *Robust design and analysis for quality engineering,* USA: Springer, Boom Koninklijke Uitgevers.

PASHA, B. A. M., BUDAN, D. A., BASAVARAJAPPA, S., YADAV, S. M. & NIZAMUDDIN, B. A. 2012. Studies on wear resistance of PTFE filled with glass and bronze particles based on Taguchi technique. *Journal of Thermoplastic Composite Materials,* 26**,** 243-259.

PERSSON, B. N. J. 2001. Theory of rubber friction and contact mechanics. *The Journal of Chemical Physics,* 115**,** 3840-3861.

PERSSON, B. N. J. 2006. Rubber friction: role of the flash temperature. *Journal of Physics: Condensed Matter,* 18**,** 7789.

PERSSON, B. N. J. 2011. Rubber friction and tire dynamics. *Journal of Physics: Condensed Matter,* 23**,** 015003.

PERSSON, B. N. J., SIVEBAEK, I. M., SAMOILOV, V. N., ZHAO, K., VOLOKITIN, A. I. & ZHANG, Z. 2008. On the origin of Amonton's friction law. *Journal of Physics: Condensed Matter,* 20**,** 395006-11.

PETRICA, M., BADISCH, E. & PEINSITT, T. 2013. Abrasive wear mechanisms and their relation to rock properties. *Wear,* 308**,** 86-94.

POPOV, V. L., VOLL, L., KUSCHE, S., LI, Q. & ROZHKOVA, S. V. 2018. Generalized master curve procedure for elastomer friction taking into account dependencies on velocity, temperature and normal force. *Tribology International,* 120**,** 376-380.

PRAMANIK, A. I., M.N. 2013. Technology tools and approaches to improve undergraduate education. *International Journal of Research in Education Methodology,* 4**,** 390-400.

QUAGLINI, V., DUBINI, P., FERRONI, D. & POGGI, C. 2009. Influence of counterface roughness on friction properties of engineering plastics for bearing applications. *Materials & Design,* 30**,** 1650-1658.

RAJASHEKARAIAH, H., MOHAN, S., PALLATHADKA, P. K. & BHIMAPPA, S. 2014. Dynamic mechanical analysis and three-body abrasive wear behaviour of thermoplastic copolyester elastomer composites. *Advances in Tribology,* 2014**,** 14.

RAJESH, J. J. & BIJWE, J. 2005. Dimensional analysis for abrasive wear behaviour of various polyamides. *Tribology Letters,* 18**,** 331-340.

RATIA, V., HEINO, V., VALTONEN, K., VIPPOLA, M., KEMPPAINEN, A., SIITONEN, P. & KUOKKALA, V. T. 2014. Effect of abrasive properties on the high-stress three-body abrasion of steels and hard metals. *Tribologia,* 32**,** 3-18.

RAVI KUMAR, B. N., SURESHA, B. & VENKATARAMAREDDY, M. 2009. Effect of particulate fillers on mechanical and abrasive wear behaviour of polyamide 66/polypropylene nanocomposites. *Materials & Design,* 30**,** 3852-3858.

RHEE, S. K. 1970. Wear equation for polymers sliding against metal surfaces. *Wear,* 16**,** 431-445.

SCHALLAMACH, A. 1952. The load dependence of rubber friction. *Proceedings of the Physical Society. Section B,* 65**,** 657.

SCHALLAMACH, A. 1953. The velocity and temperature dependence of rubber friction. *Proceedings of the Physical Society. Section B,* 66**,** 386.

SCHALLAMACH, A. 1954. On the abrasion of rubber. *Proceedings of the Physical Society. Section B,* 67**,** 883-891.

SCHALLAMACH, A. 1958. Friction and abrasion of rubber. *Wear,* 1**,** 384-417.

SCHALLAMACH, A. 1963. A theory of dynamic rubber friction. *Wear,* 6**,** 375-382.

SCHALLAMACH, A. 1968. Abrasion, fatigue, and smearing of rubber. *Applied Polymer Science,* 12**,** 281-293.

SELIG, M., LORENZ, B., HENRICHMOLLER, D., SCHMIDT, K., BALL, A. & PERSSON, B. N. J. 2014. Rubber friction and tire dynamics: A comparison of theory with experimental data. *Tire Science and Technology, TSTCA,* 42**,** 216–262.

SHEN, M. X., DONG, F., ZHANG, Z. X., MENG, X. K. & PENG, X. D. 2016. Effect of abrasive size on friction and wear characteristics of nitrile butadiene rubber (NBR) in two-body abrasion. *Tribology International,* 103**,** 1-11.

SHIPWAY, P. H. & NGAO, N. K. 2003. Microscale abrasive wear of polymeric materials. *Wear,* 255**,** 742-750.

SIN, H., SAKA, N. & SUH, N. P. 1979. Abrasive wear mechanisms and the grit size effect. *Wear,* 55**,** 163-190.

SINGH, M., MONDAL, D. P., MODI, O. P. & JHA, A. K. 2002. Two-body abrasive wear behaviour of aluminium alloy–sillimanite particle reinforced composite. *Wear,* 253**,** 357-368.

STACHOWIAK, G. B. & STACHOWIAK, G. W. 2001. The effects of particle characteristics on three-body abrasive wear. *Wear,* 249**,** 201-207.

STACHOWIAK, G. W. & BATCHELOR, A. 2002. *Engineering tribology,* London, Elsevier.

STACHOWIAK, G. W. & PODSIADLO, P. 2001. Characterization and classification of wear particles and surfaces. *Wear,* 249**,** 194-200.

SURESHA, B., CHANDRAMOHAN, G., JAWAHAR, M. A. & MOHANRAJ, S. 2008. Three-body abrasive wear behavior of filled epoxy composite systems. *Journal of Reinforced Plastics and Composites,* 28**,** 225-233.

SURESHA, B., KUMAR, K. & SHIVA, N. 2009. Investigations on mechanical and two-body abrasive wear behaviour of glass/carbon fabric reinforced vinyl ester composites. *Materials & Design,* 30**,** 2056-2060.

TAGUCHI, G. 1987. *System of experimental design; engineering methods to optimize quality and minimize cost,* White Plains, New York, UNIPUB/Kraus International Publications.

TANGUDOM, P., THONGSANG, S. & SOMBATSOMPOP, N. 2014. Cure and mechanical properties and abrasive wear behavior of natural rubber, styrene–butadiene rubber and their blends reinforced with silica hybrid fillers. *Materials & Design,* 53**,** 856-864.

TEWARI, U. S. & BIJWE, J. 1991. On the abrasive wear of some polyimides and their composites. *Tribology International,* 24**,** 247-254.

THAVAMANI, P., KHASTGIR, D. & BHOWMICK, A. K. 1993. Microscopic studies on the mechanisms of wear of NR, SBR and HNBR vulcanizates under different conditions. *Journal of Materials Science,* 28**,** 6318-6322.

THONGSANG, S., VORAKHAN, W., WIMOLMALA, E. & SOMBATSOMPOP, N. 2012. Dynamic mechanical analysis and tribological properties of NR vulcanizates with fly ash/precipitated silica hybrid filler. *Tribology International,* 53**,** 134-141.

UNAL, H. & MIMAROGLU, A. 2003. Friction and wear behaviour of unfilled engineering thermoplastics. *Materials & Design,* 24**,** 183-187.

UNAL, H., MIMAROGLU, A., KADıOGLU, U. & EKIZ, H. 2004. Sliding friction and wear behaviour of polytetrafluoroethylene and its composites under dry conditions. *Materials & Design,* 25**,** 239-245.

UNAL, H., SEN, U. & MIMAROGLU, A. 2005. Abrasive wear behaviour of polymeric materials. *Materials & Design,* 26**,** 705-710.

VAZIRI, M., SPURR, R. T. & STOTT, F. H. 1988. An investigation of the wear of polymeric materials. *Wear,* 122**,** 329-342.

VISWANATH, N. & BELLOW, D. G. 1995. Development of an equation for the wear of polymers. *Wear,* 181–183, Part 1**,** 42-49.

VOSS, H. & FRIEDRICH, K. 1987. On the wear behaviour of short-fibre-reinforced peek composites. *Wear,* 116**,** 1-18.

WILLIAMS, J. A. 2005. Wear and wear particles-some fundamentals. *Tribology International,* 38**,** 863-870.

WOLDMAN, M., VAN DER HEIDE, E., TINGA, T. & MASEN, M. A. 2013. The influence of abrasive body dimensions on single asperity wear. *Wear,* 301**,** 76-81.

WU, G. 2016. *The mechanisms of rubber abrasion.* Ph.D., Queen Mary University of London.

WU, Y. P., ZHOU, Y., LI, J. L., ZHOU, H. D., CHEN, J. M. & ZHAO, H. C. 2016. A comparative study on wear behavior and mechanism of styrene butadiene rubber under dry and wet conditions. *Wear,* 356-357**,** 1-8.

XIE, Y. & BHUSHAN, B. 1996. Effects of particle size, polishing pad and contact pressure in free abrasive polishing. *Wear,* 200**,** 281-295.

ZSIDAI, L., DE BAETS, P., SAMYN, P., KALACSKA, G., VAN PETEGHEM, A. P. & VAN PARYS, F. 2002. The tribological behaviour of engineering plastics during sliding friction investigated with small-scale specimens. *Wear,* 253**,** 673-688.

ZUM GAHR, K. H. 1987. *Microstructure and wear of materials,* Amsterdam; New York, Elsevier.

Appendix

9.1. Appendix 1

BC two-way table for wear rate

	C0				C1				C2				
B0	22.143	19.528	14.401	**56.072**	27.778	18.875	12.467	**59.120**	20.848	13.959	8.41	**43.21**	**158.406**
B1	19.371	15.164	10.830	**45.364**	18.458	16.409	15.253	**50.119**	0.327	7.169	7.73	**15.23**	**110.713**
B2	17.726	10.549	7.144	**35.419**	12.348	8.079	4.176	**24.603**	8.539	4.163	3.43	**16.13**	**76.150**
Total				**136.86**				**133.84**				**74.57**	**345.270**

AC two-way table for surface roughness

	A0				A1				A2				
C0	-6.639	-9.686	-16.577	**-32.902**	-10.487	-14.611	-18.533	**-43.631**	-14.102	-15.295	-20.11	**-49.50**	**-126.036**
C1	-6.783	-8.570	-16.327	**-31.679**	-6.899	-10.871	-18.377	**-36.148**	-5.965	-8.046	-18.29	**-32.30**	**-100.128**
C2	-9.635	-10.555	-16.254	**-36.443**	-9.821	-9.974	-17.926	**-37.720**	-10.008	-12.119	-18.13	**-40.26**	**-114.425**
Total				**-101.02**				**-117.50**				**-122.07**	**-340.589**

AC two-way table for TBU

	A0				A1				A2				
C0	-7.191	-8.193	-11.288	**-26.672**	-9.767	-10.793	-13.066	**-33.625**	-10.526	-11.676	-12.10	**-34.31**	**-94.603**
C1	-7.166	-11.497	-14.247	**-32.910**	-7.531	-9.258	-12.690	**-29.479**	-10.725	-7.380	-15.03	**-33.14**	**-95.526**
C2	-5.674	-10.413	-11.232	**-27.319**	-7.388	-9.533	-11.638	**-28.558**	-8.127	-5.181	-9.07	**-22.38**	**-78.253**
Total				**-86.90**				**-91.66**				**-89.82**	**-268.383**

9.2. Appendix 2

CASE

1000
262.88
250
Ø 40
TOP PLATE
SCALE 1:20

125.86
3

1000
3
500
250 Ø 50 200
15°
UPPER BACK PLATE
SCALE 1:20

1.60 40
40
342.14
LEG X 4
SCALE 1:10

3
50
75
BOTTOM PLATE X 2
SCALE 1:5

540
3 250
SIDE PLATE X 2
SCALE 1:20

247
492 3
BOTTOM SLANTED PLATE X 2
SCALE 1:10

1.60 40
40
15°
250
MIDDLE LEG X 2
SCALE 1:10

347 347
1000
CASE FRONT VIEW

1000
3
37
164.28
50 15°
LOWER BACK PLATE
SCALE 1:10

	NAME	SIGNATURE	DATE			TITLE:	
DRAWN							
CHK'D							
APPV'D							
MFG							
Q.A				MATERIAL:	DWG NO.		A3
				STEEL METAL	CASE		
				WEIGHT:	SCALE:1:20	SHEET 1 OF 1	

UNLESS OTHERWISE SPECIFIED:
DIMENSIONS ARE IN MILLIMETERS
SURFACE FINISH:
TOLERANCES:
  LINEAR: ±3mm
  ANGULAR:

FINISH:
DEBUR AND BREAK SHARP EDGES
DO NOT SCALE DRAWING
REVISION

CERAMIC LAGGING SPECIMEN

SPECIMEN HOLDER

LEVER ARM (1)

LEVER ARM (2)

LEVER ARM (3)

Ø15 THRU

Ø12 THRU

30

28.20

638

30

1.60

LEVER ARM (1)
SCALE 1 : 10

211

202

PIVOT IN LINE WITH SURFACE OF WHEEL LINING

LEVER ARM
SCALE 1 : 5

25

40

3

40

Ø12 THRU

103

PIVOT
SCALE 1 : 10

267

30

1.60

30

30

LEVER ARM (2)
SCALE 1 : 10

5

2X Ø9 THRU

Ø9

16.80

20

55

140

HOLDING LUG
SCALE 1 : 2

25

30

2X Ø9 THRU

65

BACK PLATE
SCALE 1 : 2

320

45°

224.02

LEVER ARM (3)
SCALE 1 : 10

Ø10

Ø176

8

25

RUBBER BACKED CERAMIC LINING

SPECIMEN
SCALE 1 : 5

PART NUMBER	DESCRIPTION	Default/QTY.
ASTM G65_CASE_SLANTED BOTTOM		2
ASTM G65_LEG		4
ASTM G65_LEVER ARM		1
MOTOR_SUPPORT		1

UNLESS OTHERWISE SPECIFIED:
DIMENSIONS ARE IN MILLIMETERS
SURFACE FINISH:
TOLERANCES:
   LINEAR: ±3mm
   ANGULAR:

FINISH:

DEBUR AND BREAK SHARP EDGES

DO NOT SCALE DRAWING

REVISION

	NAME	SIGNATURE	DATE		TITLE:
DRAWN					
CHK'D					
APPV'D					
MFG					
Q.A		MATERIAL:			

DWG NO.

LEVER ARM & SPECIMEN HOLDER

A3

SCALE:1:20

WEIGHT:

SHEET 1 OF 1

12.70 +0.00 / -0.25

10

Rubber Lining

12.70

3.30

Steel Wheel

PROJECTED VIEW OF
WHEEL ASSEMBLY TO SHAFT

Ø 228.60 +0.00 / -0.25

Ø 35.00 +0.039 / -0.000

WHEEL WITH LINING
SCALE 1 : 2

190

290

330

40

45

18

A

A

R1

SHAFT (SIDE VIEW)
SCALE 1 : 2

M33x2.0 Machine Threads

10

4.70

Ø 45
Ø 35

L

10

R0.50

8

10

30
THREADING

SHAFT (TOP VIEW)
SCALE 1 : 2

SECTION A-A   SCALE 1 : 2
SCALE 1 : 2

KEY
SCALE 1 : 1

SolidWorks Student Edition.
For Academic Use Only.

NOTE:
-THE LENGTH OF THE KEY, *L* FOR THE WHEEL IS 13mm.
 FOR THE GEARBOX HUB *L* IS 35mm.

	NAME	SIGNATURE	DATE		TITLE:
DRAWN					
CHK'D					**WHEEL AND SHAFT**
APPVD					
MFG					
Q.A		MATERIAL:		DWG NO.	A3

UNLESS OTHERWISE SPECIFIED:
DIMENSIONS ARE IN MILLIMETERS
SURFACE FINISH:
TOLERANCES:
 LINEAR: ±3mm
 ANGULAR:

FINISH:

DEBUR AND
BREAK SHARP
EDGES

DO NOT SCALE DRAWING

REVISION

WEIGHT:

SCALE:1:5

SHEET 1 OF 1

Ø21.30

120

UPPER PIPE
SCALE 1 : 2

Ø21.30

30

LOWER PIPE
SCALE 1 : 2

43°

200

46.71

30

30

.60

SUPPORTING TUBE
SCALE 1 : 2

Ø174

238

81

43°

Ø23.47

Ø18

SAND HOLDER
SCALE 1 : 5

150

15

1.59

7.41°

22

76.42

1.59

WELD 3 SIDES

SAND NOZZLE
SCALE 1 : 2

140

45°

30

3

30

BASE
SCALE 1 : 2

ITEM NO.	PART	DESCRIPTION	QTY.
1	UPPER PIPE	Steel pipe - Ø15mm inner diameter	1
2	SAND HOLDER	Sheet Steel Metal - 2mm thickness	1
3	SUPPORTING TUBE	RHS Steel - 1.6mm thickness	4
4	BASE	Steel Angle - 3mm thickness	4
5	VALVE		1
6	LOWER PIPE	Steel pipe - Ø15mm inner diameter	1

UNLESS OTHERWISE SPECIFIED:
DIMENSIONS ARE IN MILLIMETERS
SURFACE FINISH:
TOLERANCES:
  LINEAR: ±3mm
  ANGULAR:

FINISH:

DEBUR AND BREAK SHARP EDGES

DO NOT SCALE DRAWING

REVISION

	NAME	SIGNATURE	DATE			TITLE:
DRAWN						
CHK'D						
APPV'D						
MFG						
Q.A			MATERIAL:		DWG NO.	A3

SAND HOPPER AND SAND NOZZLE

WEIGHT:

SCALE:1:5

SHEET 1 OF 1

BRACING SHS TUBE

335

40

1.60

40

FRONT SHS TUBE X 2

415

40

1.60

40

LEG X 4

445

40

1.60

40

SIDE SHS TUBE X 4

70

40

1.60

40

SIDE SHS TUBE

FRONT SHS TUBE

BRACING SHS TUBE

LEG

48.5

SCALE 1 : 10

Notes:
- All joints are to be butt weld
- All tubes use 40 x 40 mm square hollow section tubes with 1.6mm thickness

UNLESS OTHERWISE SPECIFIED: DIMENSIONS ARE IN MILLIMETERS SURFACE FINISH: TOLERANCES: LINEAR: ±3mm ANGULAR:		FINISH:		DEBUR AND BREAK SHARP EDGES	DO NOT SCALE DRAWING		REVISION
	NAME	SIGNATURE	DATE		TITLE:		
DRAWN							
CHK'D					**MOTOR SUPPORT**		
APPV'D							
MFG							
Q.A		MATERIAL:			DWG NO.		A3
		WEIGHT:			SCALE AS SHOWN	SHEET 1 OF 1	

SITI

MI...FP

MI...F

MI...FBR

	C	C₂	M 17	M' 17	W₁ 17	N	N₂	Q₁	L₃	F₁	P₁	P₂	D₄	Q₃	Q₄	S₁	S₂	V₂	V₃	V₁	G	I	I₁	I₂	R	T	C	D/D	t	U
80	50	30	130	110	110	14	16	150	100	200	180	145	168	130	130	5	5	11,5	11,5	100	127	80	63	103	95	133	72	35	10	32,3
90	52	40	180	130	110	14	16	127	119	200	200	160	215	168	130	5	5	14	11	110	138	80	80	24	111	143	75	38	10	41,3
110	72,5	52,5	180	180	130	15	18	160	150	250	250	200	215	210	60	5	5	15	15	112	173	110	146	44	141	143	77,5	42	12	46,3
130	55	42,5	200	250	180	15	18	160	187,5	300	300	240	263	210	210	5	5	15	15	112	184	130	163	60	155	173	85	46	14	51,3
150	85	-	250	-	190	20	-	175	-	350	-	250	200	-	215	6	-	17		114	221	160	192	160	182	204	110	61	16	59,3
175	95	-	300	-	230	22	-	210	-	400	-	350	290	-	265	8	-	15		116	258	176	215	204	203	222	119	80	18	64,4

NOTE: P, X, Y, W - see table motori n. B5 - pag. 180.   See motor table B5, B14 page 180.   Siehe Motortabelle B5, B14 auf Seite 180.

9.3. Appendix 3

9.3.1. Attribution of research outputs

Paper #1: F. Hakami, A. Pramanik, N. Ridgway, A. K. Basak, "Developments of rubber material wear in conveyer belt system", *Tribology International*, 111, 2017, 148-158.

Paper #2: F. Hakami, A. Pramanik, N. Islam, A. K. Basak, N. Ridgway, "Study of effective parameters on wear behaviour of rubbers based on statistical methods", *Polymers for Advanced Technologies*, 2018.

Paper #3: F. Hakami, A. Pramanik, A. K. Basak, N. Ridgway, N. Islam, "Effect of abrasive particle size on tribological behavior of elastomers", *Part J: Journal of Engineering Tribology*, 2018.

Paper #4: F. Hakami, A. Pramanik, A. K. Basak, N. Ridgway, "Elastomers' wear: Comparison of theory with experiment", *Tribology International*, 2018.

Table. 9.1.

Alokesh Pramanik, Department of Mechanical Engineering, Curtin University, Bentley, Perth, Australia

	Paper #1	Paper #2	Paper #3	Paper #4
Conception and design		×		×
Acquisition of data and method		×	×	
Data conditioning and manipulation		×		
Analysis and stastical method		×		×
Interpretation and discussion	×	×	×	×
Paper drafting or revising	×	×	×	×
Final Approval	×	×	×	×

I acknowledge that these represent my contribution to the above research output.

Signed...

Date............19.112.2018

Table. 9.2.

Animesh Basak, Adelaide Microscopy, the University of Adelaide, South Australia, Australia

	Paper #1	Paper #2	Paper #3	Paper #4
Conception and design				
Acquisition of data and method				
Data conditioning and manipulation				
Analysis and stastical method		×	×	×
Interpretation and discussion	×	×	×	×
Paper drafting or revising	×	×	×	×
Final Approval	×	×	×	×

I acknowledge that these represent my contribution to the above research output.

Signed...*Animesh Kumar Basak*........

Date....18/12/2018.......

Table. 9.3.

Nazrul Islam, Department of Mechanical Engineering, Curtin University, Bentley, Perth, Australia

	Paper #1	Paper #2	Paper #3	Paper #4
Conception and design		×		
Acquisition of data and method		×		
Data conditioning and manipulation		×		
Analysis and stastical method		×		
Interpretation and discussion		×		
Paper drafting or revising		×	×	
Final Approval		×	×	

I acknowledge that these represent my contribution to the above research output.

Signed....................................

Date..........18/12/18..........

Table. 9.4.
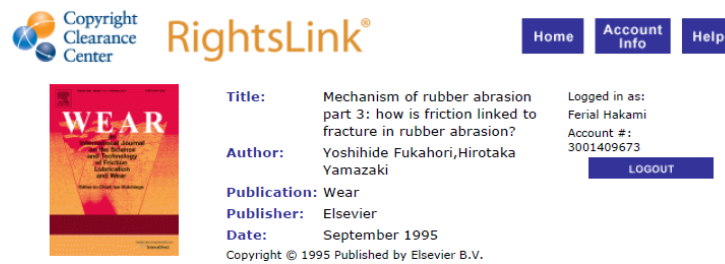
Nigel Ridgway, Department of Mechanical Engineering, Curtin University, Bentley, Perth, Australia

	Paper #1	Paper #2	Paper #3	Paper #4
Conception and design				
Acquisition of data and method				
Data conditioning and manipulation				
Analysis and stastical method				
Interpretation and discussion				
Paper drafting or revising	×	×	×	×
Final Approval				

I acknowledge that these represent my contribution to the above research output.

Signed............*N. Ridgway*............

Date............18/12/18..............

9.4. Appendix 4

9.4.1. Copyright permission

Fig. 2.7.

Fig. 2.9.

Fig. 6.1.-Fig. 6.6.

Table 6.2.-Table 6.8.